Electroweak Radiative Corrections to Gauge-Boson Pair Production in the High-Energy Regime of the LHC

Dissertation
zur
Erlangung der naturwissenschaftlichen Doktorwürde
(Dr. sc. nat.)

vorgelegt der
Mathematisch-naturwissenschaftlichen Fakultät
der
Universität Zürich
von
Andreas Kaiser
aus Deutschland

Promotionskomitee

Prof. Dr. Daniel Wyler	(Vorsitz)
PD. Dr. Ansgar Denner	(Leitung der Dissertation)
Prof. Dr. Thomas Gehrmann	

Zürich 2004

Zusammenfassung

Die vorliegende Arbeit beschäftigt sich mit der Analyse von elektroschwachen Strahlungskorrekturen bei hohen Energien. Ein besonderes Augenmerk liegt dabei auf den Effekten, die diese Korrekturen bei Prozessenverursachen, in denen massive Eichbosonpaare erzeugt werden. Am Large Hadron Collider (LHC), der momentan am CERN gebaut wird, wird aufgrund der hohen Luminosität und einer Schwerpunktsenergie von 14 TeV im Proton-Proton System, eine Vielzahl von Eichbosonpaaren erzeugt werden. Die hohe Statistik ermöglicht die Suche nach neuer Physik, d.h. nach Effekten die mit dem Standardmodell der Teilchenphysik nicht erklärt werden können. Um allerdings diese experimentellen Daten entsprechend auswerten zu können, müssen die theoretischen Vorhersagen die gleiche Präzision erreichen, wie der zu erwartende experimentelle Fehler. Es ist bekannt, dass elektroschwache Korrekturen bei höheren Energien ansteigen, da sie Logarithmen der elektroschwachen Skala über der Energieskala des zugrundeliegenden Prozesses enthalten. Solche Korrekturen können somit am LHC relevant werden.

Da massive Eichbosonen nur über die Rekonstruktion ihrer Zerfallsprodukte, d.h. die Rekonstruktion von Fermion-Antifermion-Paaren, nachgewiesen werden können, bestand der grösste Teil der Arbeit in dieser Dissertation im Erstellen eines Monte Carlo Programms zur Berechnung von Wirkungsquerschnitten für Streuprozesse von zwei nach vier Fermionen. In diesem Programm sind sowohl die führenden logarithmischen elektroschwachen Korrekturen, als auch anomale Drei- oder Viereichbosonkopplungen enthalten.

In dieser Arbeit wird die Konstruktion generischer Matrixelemente zur Berechnung der zugrundeliegenden Prozesse beschrieben. Es wird aufgezeigt, welche führenden elektroschwachen Korrekturen sich für diese Prozesse herleiten lassen und wie, mit Hilfe der Phase-Space-Slicing-Methode, die einzelnen Beiträge zu einer Vorhersage für physikalische Prozesse zusammengesetzt werden können. Weiterhin wird die Verwendung des Parton-Modells und die Renormierung der Partonverteilungen erklärt. Es werden zusätzlich die Methoden diskutiert, die bei der numerischen Auswertung benutzt wurden, sowie die Tests, mit denen das Monte Carlo Programm überprüft wurde. Schliesslich werden einige Observable für Prozesse mit WZ-, ZZ- oder WW-Produktion untersucht, wobei sich herausstellt, dass elektroschwache Korrekturen Änderungen von $10-25\%$ zu Vorhersagen in niedrigsten Störungsordnung hervorrufen können. Es werden die entsprechenden Verteilungen in physikalischen Observablen gezeigt, die für die Suche nach neuer Physik am LHC relevant sein werden.

Abstract

The present work is concerned with the analysis of one-loop electroweak corrections at high energies. Especially we are interested in the effects due to electroweak corrections in the production of massive gauge-boson pairs at the Large Hadron Collider (LHC) which is currently built at CERN. The high luminosity and therefore large statistics as well as a centre-of-mass energy of 14 TeV in the proton–proton rest frame of this new machine will provide us with the necessary data for new physics searches. However, the theoretical predictions for the cross sections of particle reactions observed at the LHC must reach the same accuracy as the expected experimental error. Since it is known that electroweak corrections increase with the energy due to logarithms of the electroweak scale over the energy scale of the investigated process, these corrections will become relevant for the data analysis at the LHC.

In this PhD thesis we investigate the leading-logarithmic electroweak corrections to massive gauge-boson pair production. Since massive gauge bosons are unstable they cannot be detected directly, but have to be reconstructed from the fermion–anti-fermion pairs they decay into. We have constructed a Monte Carlo program for two-to-four-fermion processes in which we included the leading-logarithmic corrections to massive gauge-boson production as well as the anomalous triple- and quartic-gauge-boson couplings.

We describe the construction of generic matrix elements for the processes we are interested in and explain how the leading electroweak radiative corrections must be applied in particular cases. Then we show how the different contributions are combined to obtain physical predictions in the framework of the phase-space slicing method. Furthermore the use of the parton model and the renormalization of parton-distribution functions is described. We also give a detailed view of the techniques we used for the numerical implementation and discuss the checks which were carried out to ensure the correctness of the program. Finally we investigate the effects of the electroweak corrections on some particular WZ-, ZZ-, and WW-production processes. We find that the corrections amount to $10-25\%$ of the lowest order cross sections for the investigated scenarios. We present the effects due to electroweak corrections in distributions of observables which will be of importance for new physics searches at the LHC.

Contents

Introduction

With the construction of the Large Hadron Collider (LHC) at CERN it will become possible to observe collisions of protons at centre-of-mass energies up to 14 TeV. These high-energy collisions hopefully directly produce unknown particles (e.g. supersymmetric particles) or show the existence of new physics by suppression or enhancement of processes that are already known in the standard model of particle physics. This high-energy regime also enables the production of more and more particles in the final state. Therefore it is necessary to have accurate predictions for many-particle final states in the standard model because such particle reactions are either signals for new physics themselves or appear as background to the so called new physics effects in the detectors.

One major class of processes which will be observed in the near future is the production of massive gauge-boson pairs. Amplitudes for gauge-boson pair production involve trilinear gauge-boson couplings. Therefore, the corresponding cross sections depend very sensitively on the non-abelian structure of the underlying theory. For this reason, vector-boson pair production has found continuous interest in the literature. In the last few years, gauge-boson self-interactions were directly measured at the Large Electron-Positron collider (LEP) and the Tevatron. Still, up to now the self-couplings have not been determined with the same precision as other gauge-boson properties, such as their masses and couplings to fermions. Despite of the high statistics reached at LEP2 in producing $\mathrm{W^+W^-}$ pairs, the resulting limits on possible anomalous couplings, which parameterize deviations from SM predictions due to new physics occurring at energy scales of order of tens of TeV, are not very stringent. The weakness of the LEP2 measurement is that W-pair-production events were generated at rather modest centre-of-mass (CM) energies. On the other hand, anomalous gauge-boson couplings cause strong enhancements in the gauge-boson pair-production cross section especially at large values of the di-boson invariant mass $M_{VV'}$ ($V, V' = \mathrm{W}, \mathrm{Z}$). A significant improvement in the bounds on triple gauge-boson couplings is expected from measurements at future colliders operating at high energies such as the

LHC. Therefore, in order to achieve a better precision in the determination of these couplings, it will be useful to analyse the di-boson production at hadron colliders at the highest possible CM energies.

The production of gauge-boson pairs already received a lot of attention at LEP. At the LHC the luminosity will be much higher and this will provide huge statistics in gauge-boson pair production [1]. With LHC approaching its goal of an integrated luminosity of $100\,\mathrm{fb}^{-1}$, a large data sample will be available to start a detailed investigation of the trilinear vertices.

The aim of this work is to give estimates for the electroweak radiative corrections to di-gauge-boson production processes one expects to observe at the LHC. Especially for high energies the electroweak corrections get enhanced due to correction terms which are proportional to logarithms of the electroweak scale over the energy scale. The fact that the electroweak (EW) corrections grow with increasing energy is well known, and analyses of the general behaviour of the EW corrections at high energies exist since long time (see for instance Refs. [2, 3]). But only rather recently, a process-independent recipe for the calculation of leading-logarithmic EW corrections has come out. This result is given in Refs. [4, 5, 6], where it has been shown that the leading-logarithmic one-loop corrections to arbitrary EW processes factorize into the tree-level amplitudes times universal correction factors. These corrections can reach up to 30% of the lowest-order cross section. Therefore such corrections have to be considered in precision experiments even if the leading contributions from radiative corrections clearly originate from QCD.

In order to match the experimental precision, theoretical predictions need to have an accuracy of the order of a few per cent to allow for a decent analysis of the data. At lowest order, this means taking into account all spin correlations and finite-width effects. The easiest way to fulfil this requirement is to go beyond the *production*$\times$*decay* approach by computing the full processes $\mathrm{PP} \to 4f$. The next step consists in a full understanding and control of higher-order QCD and EW corrections. In the past years, large effort has gone into accurate calculations of hadronic di-boson production (for a review on the subject see Ref. [1]). The $\mathcal{O}(\alpha_s)$ QCD corrections to gauge-boson pair production and decay have been extensively analysed by many authors. Several NLO Monte Carlo programs have been constructed and cross checked so that complete $\mathcal{O}(\alpha_s)$ corrections are now available [7, 8, 9, 10]. QCD corrections turn out to be quite significant at LHC energies. They can increase the lowest-order cross section by a factor of two if no cuts are applied and by one order of magnitude for large transverse momentum or large invariant mass of the vector bosons [11, 12]. By including a jet veto, their effects can be drastically reduced to the order of tens of per cent [8, 13], but in any case they have to be considered to get realistic and reliable estimates of total

cross sections and distributions.

In view of the envisaged precision of a few per cent at the LHC, also a discussion of EW corrections is in order. For single W- and Z-boson production, $\mathcal{O}(\alpha)$ corrections have been computed taking into account the full QED and weak contributions [14]. One loop weak corrections have been also investigated for $b\bar{b}$ and $\gamma/Z+$jet hadron-production [15]. By contrast, gauge-boson pair production at hadron colliders is commonly treated by including only universal radiative corrections such as the running of the electromagnetic coupling, and corrections to the ρ parameter. This approach is based on the belief that the remaining EW corrections (dominated by double-logarithmic contributions) are not relevant at the LHC just because physical cross sections decrease strongly with increasing invariant mass of the gauge-boson pairs, i.e. where EW corrections can be not negligible. However, a first analysis of the effect of one-loop logarithmic EW corrections on WZ and Wγ production processes at the LHC [16] has instead demonstrated that $\mathcal{O}(\alpha)$ corrections are of the same order or bigger than the statistical error, when exploring the large invariant-mass and rapidity region.

Using the method of Refs. [4, 5, 6], we investigate the effect of leading-logarithmic EW corrections to the hadronic production of $W^{\pm}Z$, ZZ, and $W^{\pm}W^{\mp}$ pairs in the large-invariant-mass region of the hard process at the LHC. The simplest experimental analyses of gauge-boson pair production will rely on purely leptonic final states. Semi-leptonic channels, where one of the vector bosons decays hadronically, have been analysed at the Tevatron [17] showing that these events suffer from the background due to the production of one vector boson plus jets via gluon exchange. For this reason, we show only results for di-boson production where both gauge bosons decay leptonically into electrons or muons.

Chapter 1

Overview

This work is focussed on the electroweak physics which is included in high-energy processes with gauge-boson pair production. In the proton–proton collisions at the LHC a large number of the massive electroweak gauge bosons Z and $W^{\pm}$ will be produced. Since these gauge bosons are unstable they decay into a pair of leptons or a pair of quarks. Hence, in the case of the production of two gauge bosons, a four-fermion final state is observed. In this work we always assume that this final state at least contains two leptons. In this way we exclude the pure QCD process with four quarks in the final state.

1.1 Calculations in the parton model

In the LHC experiments two protons P_1 and P_2 which carry the momenta $p_{\text{beam},1}$ and $p_{\text{beam},2}$ collide. Since protons are composite objects we use the parton model for our calculation. In the parton model we assume that only one parton (i.e. a quark or a gluon) from each proton is involved in the reaction that finally leads to the final state observed in the detector. The full process can be written as

$$P_1(p_{\text{beam},1})P_2(p_{\text{beam},2}) \to X_1 X_2 f_3 f_4 f_5 f_6(\gamma) \tag{1.1}$$

with X_1, X_2 denoting the fragments of the colliding protons, which are not considered in this calculation (see Figure 1.1). The final-state particles we are interested in are the fermions $f_3, \ldots, f_6$ and eventually an additional hard photon γ. The cross section for the production of these particles is calculated using the parton model. This means, that we consider the particles $f_3, \ldots, f_6(\gamma)$ being produced by an interaction of two partons q_1 and q_2 where q_1 is a quark originating from proton P_1 and q_2 is a quark originating from proton P_2.

These partons carry certain fractions $x_1, x_2 \in [0,1]$ of the momenta of the protons. Therefore the subprocess can be written as

$$q_1(p_1,\sigma_1)q_2(p_2,\sigma_2) \to f_3(p_3,\sigma_3)f_3(p_4,\sigma_4)f_5(p_5,\sigma_5)f_6(p_6,\sigma_6)\left(\gamma(p_\gamma,\lambda)\right). \quad (1.2)$$

Here $p_1,\ldots,p_6$ denote the momenta of the particles and $\sigma_1,\ldots,\sigma_6$ their helicities. The momenta of the incoming partons are $p_1 = x_1 p_{\text{beam},1}$ and $p_2 = x_2 p_{\text{beam},2}$.

The probability to find the quark q in the proton P_i with momentum fraction x is described by the parton distribution function $\Phi_{i,q}(Q,x)$. The distribution function depends on the factorization scale Q of the underlying process. The parton distribution functions cannot be calculated theoretically because in these functions all kinds of non-perturbative QCD effects appear. Especially for QCD interactions with small momentum transfer the QCD coupling constant g_s becomes large and perturbation theory is not valid any more. For this reason the parton distribution functions $\Phi_{i,q}(Q,x)$ must be measured in an experiment.

The origin of the scale dependence are the QCD corrections that are usually calculated in the $\overline{\text{MS}}$ scheme. We do not include virtual QCD corrections for the calculation of the partonic process. Nevertheless a part of the QCD corrections is included in the parton distribution functions. The details and our choice for the factorization scale Q are discussed in chapter 5.1. As we do not include QCD corrections we proceed here with the assumption that for the time being we can ignore the dependence on the factorization scale introduced by the parton distribution functions.

In order to get the cross section for the process $P_1P_2 \to 4f$ we have to convolute the partonic cross section $\mathrm{d}\sigma_{q_1q_2\to 4f}$ with the structure functions $\Phi_{1,q_1}(Q,x_1)$ and $\Phi_{2,q_2}(Q,x_2)$. For an anti-quark–quark initial state we have to take the sum over all anti-quarks $\bar{q}_1$ and all quarks q_2:

$$\begin{aligned}\mathrm{d}\sigma(s) \;=\; & \sum_{\bar{q}_1}\sum_{q_2}\int_0^1 \mathrm{d}x_1 \int_0^1 \mathrm{d}x_2 \big[\Phi_{1,\bar{q}_1}(Q,x_1)\Phi_{2,q_2}(Q,x_2)\mathrm{d}\sigma_{\bar{q}_1q_2\to 4f}(\hat{s}) \\ & + \Phi_{1,q_2}(Q,x_1)\Phi_{2,\bar{q}_1}(Q,x_2)\mathrm{d}\sigma_{q_2\bar{q}_1\to 4f}(\hat{s})\big]. \end{aligned} \quad (1.3)$$

In the case of two quarks or two anti-quarks in the inital state we sum over all quark or anti-quark pairs q_1, q_2:

$$\mathrm{d}\sigma(s) \;=\; \sum_{q_1,q_2}\int_0^1 \mathrm{d}x_1 \int_0^1 \mathrm{d}x_2 \big[\Phi_{1,q_1}(Q,x_1)\Phi_{2,q_2}(Q,x_2)\mathrm{d}\sigma_{q_1q_2\to 4f}(\hat{s})\big] \quad (1.4)$$

with the hadronic centre-of-mass energy $s = (p_{\text{beam},1} + p_{\text{beam},2})^2$ and the partonic centre-of-mass energy of the partonic system $\hat{s} = x_1x_2s$.

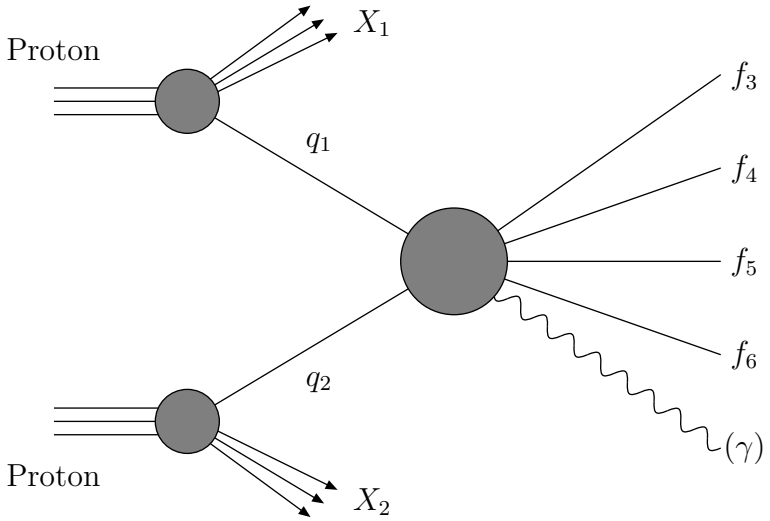

Figure 1.1: Decomposition of the full process in the parton picture

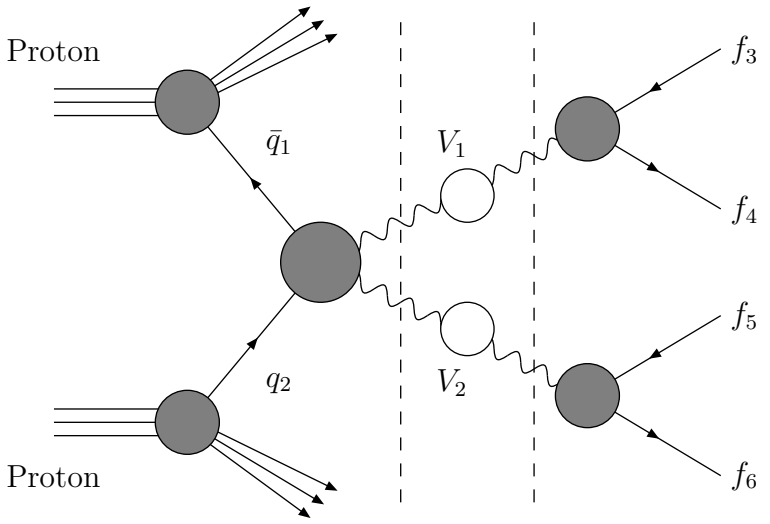

Figure 1.2: Full process in double-pole approximation

1.2 Inclusion of radiative corrections

The main aim of this work is the study of the effects of the electroweak radiative corrections to gauge-boson pair production at high energies. Therefore the leading-logarithmic corrections to the gauge-boson production subprocess have been implemented in a Monte Carlo program which calculates cross sections for proton–proton to four fermions. For a suitable choice of cuts on the momenta of the final-state fermions, the cross section is dominated by the production of a pair of on-shell gauge bosons as an intermediate state. In this way the process factorizes into gauge-boson production and gauge-boson decay as is shown in figure 1.2.

With leading order we denote the cross section which is obtained by the convolution of a tree-level partonic subprocess with the parton distribution functions. All fermions are assumed to be massless and hence we put the fermion masses to zero wherever this is possible. We only keep fermion masses if they appear in logarithms because here we need them to regularize mass divergences.

The virtual radiative corrections are calculated to the partonic cross section using the double-pole approximation (DPA). In this approximation we assume that the main contribution to the four fermion production process is due to diagrams in which two on-shell gauge bosons are produced. In this case we have two resonant gauge-boson propagators and cut the process into gauge-boson production and gauge-boson decay as it is indicated in figure 1.2 by the dashed lines. The contributions from Feynman diagrams with resonant gauge-boson propagators are enhanced by a factor of M_V/Γ_V for each resonance in comparison to the contributions with only non-resonant propagators. Contributions from radiative corrections originating from diagrams with non-resonant propagators are formally of order $(\alpha/\pi)(\Gamma_V/M_V)$ and should be well below 0.1% compared to the Born contributions. This argument is only true if we take care that the main contributions are really given by a the factorized process shown in figure 1.2. In order to stay in a regime where the DPA is valid we apply appropriate cuts on the phase space to ensure the presence of an almost on-shell gauge-boson pair. This is not a limitation to our prediction since the same kind of cuts must also be used in an experiment in order to identify a gauge-boson production process. The use of the DPA in the calculation has the advantage that we can calculate the virtual radiative corrections separately for the production and the decay process. For a process in DPA we use the momenta k_1, k_2 and the masses M_{V_1}, M_{V_2} for intermediate massive gauge bosons.

For the real radiative corrections we do not use the DPA because it is difficult to make a proper definition for the splitting into production and

decay as we have in the virtual case. In the case of the production of charged gauge bosons we here run into problems if we consider a soft photon emitted from these intermediate gauge bosons. In this case we might find a close to on-shell gauge boson which emits a photon and is still almost on-shell. So it is not clear if this photon should be considered as coming from the production or the decay process. Instead of the DPA we therefore use the exact matrix element for $2f \to 4f\gamma$ to determine the real corrections.

In addition we consider the high-energy limit which means that we make the following assumptions in the calculation of radiative corrections:

- For all invariants that are not identical to a gauge-boson mass we assume $(p_i \pm p_j)^2 \gg M_V^2$ or $(k_i \pm p_j)^2 \gg M_V^2$. In this limit we can do an expansion in terms of $m_i/\sqrt{s}$ where m_i denotes all the masses involved in the process and s is a shorthand for all large invariants that may occur.

- At one-loop level we only keep terms that are proportional to mass-singular logarithms. We denote all double or single logarithms of the form $\log(m_i^2/s)$ as mass-singular logarithms.

- We restrict ourselves to Born matrix elements that are not mass suppressed. This means that we omit all contributions of the matrix elements for gauge-boson production which include one longitudinal and one transverse gauge-boson.

1.3 Outline of the calculation

1.3.1 Splitting into subcontributions

Since we have to deal with different phase spaces the next-to-leading order cross section σ_1 was split into different subcontributions. In general we differentiate between virtual corrections and real corrections to the considered process

$$\sigma_{\text{total}} = \sigma_{\text{Born}} + \sigma_1 = \sigma_{\text{Born}} + \sigma_{\text{virt}} + \sigma_{\text{real}}. \tag{1.5}$$

The virtual corrections emerge from the exchange of virtual particles and the real corrections emerge from the production of additional photons in the final state. For the calculation of this subcontibutions different phase spaces are used. In the following we will denote a cross section σ which is the differential cross section $\mathrm{d}\sigma$ integrated over an n particle phase space Φ_n as

$$\sigma = \int_{\Phi_n} \mathrm{d}\sigma. \tag{1.6}$$

In the case of the Born contributions we take the full four-particle phase space, for the virtual corrections we use an on-shell projected phase space, and for the real corrections a five-particle phase space is needed:

$$\sigma_{\text{total}} = \int_{\Phi_4} \mathrm{d}\sigma_{\text{Born}} + \int_{\Phi_4^{\text{DPA}}} \mathrm{d}\sigma_{\text{virt}}^{\text{DPA}} + \int_{\Phi_5} \mathrm{d}\sigma_{\text{real}}. \tag{1.7}$$

An exact definition of the phase space integrals is given in chapter 1.4. The integration over the DPA phase space is somewhat more complicated than the other integrations because the projection on on-shell momenta may not be unique. If there is more than one possibility to perform an on-shell projection all these possibilities have to be taken into account. In general two possibilities exist to construct intermediate gauge bosons from the two fermions and anti-fermions in the final state. We denote these pairs with $(f_{i_3}, \bar{f}_{i_4})$ and $(f_{i_5}, \bar{f}_{i_6})$ and the corresponding gauge bosons with V_1 and V_2. Any matrix element $\mathcal{M}^{\text{DPA}}$ that uses DPA must be written as a sum over the possibilities to construct fermion pairs $(f_{i_3}, \bar{f}_{i_4})$. A correct expression for the DPA matrix element is given by

$$\mathcal{M}^{\text{DPA}} = \sum_{(f_{i_3}, \bar{f}_{i_4})} \mathcal{M}^{\text{DPA}}_{(f_{i_3}, \bar{f}_{i_4})} \tag{1.8}$$

in which it is implicitly understood that for the evaluation the corresponding momenta of the phase spaces $\Phi^{\text{DPA}}_{4,(f_{i_3}, \bar{f}_{i_4})}$ have to be used. Formula (1.7) still contains an inconsistency in the cancellation of infrared divergences due to the use of the DPA. A solution of this problem is given in the next section.

1.3.2 Treatment of infrared and collinear divergences

The virtual corrections to the process $PP \to 4f$ involve infrared divergences as well as so-called collinear divergences. Both kinds of divergences must be regularized in a proper way. Due to the Bloch-Nordsieck theorem [18] the infrared divergent parts of a cross section cancel if the additional production of soft photons is taken into account. We ensure this cancellation in this calculation by including the process $PP \to 4f + \gamma$ in leading order.

The virtual radiative corrections are treated in DPA to take advantage of the factorization into gauge-boson production and gauge-boson decay. In this way also the infrared divergent part of the corrections is calculated in DPA. Since the process $PP \to 4f + \gamma$ includes the full five-particle phase space we have to apply the following matching in order to cancel the divergent parts

in the virtual and real corrections

$$\begin{aligned}\sigma_{\text{total}} &= \int_{\Phi_4} \mathrm{d}\sigma_{\text{Born}} + \int_{\Phi_4^{\text{DPA}}} \left(\mathrm{d}\sigma_{\text{virt}}^{\text{DPA}} - \mathrm{d}\sigma_{\text{virt,sing}}^{\text{DPA}}\right) \\ &\quad + \int_{\Phi_4} \mathrm{d}\sigma_{\text{virt,sing}} + \int_{\Phi_5} \mathrm{d}\sigma_{\text{real}}. \end{aligned} \tag{1.9}$$

We subtract the infrared-singular part $\mathrm{d}\sigma_{\text{virt,sing}}^{\text{DPA}}$ of the virtual corrections taken in DPA and then add the infrared-singular part $\mathrm{d}\sigma_{\text{virt,sing}}$ of the virtual corrections to the full process $PP \to 4f$. The singular part of the virtual corrections is only defined up to constant parts so that our approach leads to an ambiguity within these constant parts, which are shifted from the virtual to the real corrections. As it is shown in Ref. [19] this ambiguity is of the order of the uncertainty of the DPA approach and hence can be neglected in the numerical evaluation. A detailed definition of the singular part $\mathrm{d}\sigma_{\text{virt,sing}}$ is given in chapter 4.2.

1.3.3 Implementation of the gauge-boson width

The width of the gauge bosons $\mathrm{W}^{\pm}$ and Z are formally higher-order contributions because these are obtained from a Dyson sum which includes radiative corrections up to infinite order. Anyhow we have to include a width for a gauge boson with s-channel propagator for a physical prediction. Our calculation of radiative corrections in DPA requires the fixed-width scheme. For tree-level processes we have implemented the gauge-boson width in three different ways. These are the fixed-width scheme, the running-width scheme and the complex-mass scheme:

- In the fixed-width scheme we use an s-channel propagator of the form

$$P_V(k^2) = \frac{1}{k^2 - M_V^2 + \mathrm{i} M_V \Gamma_V}. \tag{1.10}$$

  While in a t-channel (i.e. $P_V(k)$ with $k^2 < 0$) we set the width Γ_V of the gauge boson to zero.

- Also in the running width scheme we include only widths for s-channel propagators. But here the width depends on the particle momentum

$$P_V(k^2) = \frac{1}{k^2 - M_V^2 + \mathrm{i}\frac{k^2}{M_V^2} M_V \Gamma_V}. \tag{1.11}$$

- In the complex-mass scheme all gauge-boson masses M_V in the propagators and in the couplings are replaced by complex masses $\overline{M}_V = \sqrt{M_V^2 - \mathrm{i}M_V\Gamma_V}$. The propagator of V is defined as

$$P_V(k^2) = \frac{1}{k^2 - \overline{M}_V^2}, \tag{1.12}$$

  and all couplings have to be replaced with couplings that contain complex masses. Note that also the weak mixing angle θ_w becomes complex in this scheme. Therefore the cosine of θ_w must be defined as

$$\cos^2\theta_\mathrm{w} = 1 - \sin^2\theta_\mathrm{w} = \frac{\overline{M}_\mathrm{W}}{\overline{M}_\mathrm{Z}} = \frac{M_\mathrm{W}^2 - \mathrm{i}M_\mathrm{W}\Gamma_\mathrm{W}}{M_\mathrm{Z}^2 - \mathrm{i}M_\mathrm{Z}\Gamma_\mathrm{Z}}. \tag{1.13}$$

The main drawback of the fixed- and the running-width schemes is the violation of gauge invariance. The complex-mass scheme does not lead to such a violation, because it does not change any algebraic cancellations. But in this scheme also complex counterterms must be introduced due to the complex masses. A detailed description of the advantages and disadvantages of the different schemes can be found in Refs. [20, 21].

1.4 Construction of the phase space

To calculate the cross section the integration over the phase space has to be performed. The volume of the phase space for n particles in the final state with momenta k_i is given by

$$\Phi_n = \int \left(\prod_{l=1}^{n} \frac{\mathrm{d}^3\vec{k}_l}{(2\pi)^3 2k_l^0} \right) (2\pi)^4 \delta^4 \left(p_1 + p_2 - \sum_{l=1}^{n} k_l \right). \tag{1.14}$$

The cross section for the reaction $1 + 2 \to 3 + 4 + \cdots + n$ is then

$$\sigma = (2\pi)^4 \int \left(\prod_{l=3}^{n} \frac{\mathrm{d}^3\vec{p}_l}{(2\pi)^3 2p_l^0} \right) \delta^4 \left(p_1 + p_2 - \sum_{l=3}^{n} p_l \right) \mathrm{d}\sigma(p_1, \ldots, p_n). \tag{1.15}$$

To perform the phase-space integration for four or five particles in the final state special techniques must be used. Following the PhD thesis of Markus Roth [22] a multi-channel Monte Carlo integration is used. This technique allows to choose particular mappings for the different resonances in the contributing Feynman diagrams according to their special topology. In this way it is possible to integrate over the complex peaking structure of the integrand

in the phase space which is necessary to get numerically stable results. In the Monte Carlo program three different phase spaces are constructed

$$\begin{aligned}
\mathrm{d}\Phi_4 &= \left(\prod_{l=3}^{6}\frac{\mathrm{d}^3\vec{p}_l}{(2\pi)^3 2p_l^0}\right)(2\pi)^4\delta^4\left(p_1+p_2-\sum_{l=3}^{6}p_l\right), \quad (1.16)\\
\mathrm{d}\Phi^{\mathrm{DPA}}_{4,(f_{i_3},\bar{f}_{i_4})} &= \left(\prod_{l=3}^{6}\frac{\mathrm{d}^3\vec{p}_l}{(2\pi)^3 2p_l^0}\right)(2\pi)^4\delta^4\left(p_1+p_2-\sum_{l=3}^{6}p_l\right)\\
&\quad\times\delta\left((p_{i_3}+p_{i_4})^2-M_{V_1}^2\right)\delta\left((p_{i_5}+p_{i_6})^2-M_{V_2}^2\right), \quad (1.17)\\
\mathrm{d}\Phi_5 &= \left(\prod_{l=3}^{7}\frac{\mathrm{d}^3\vec{p}_l}{(2\pi)^3 2p_l^0}\right)(2\pi)^4\delta^4\left(p_1+p_2-\sum_{l=3}^{7}p_l\right). \quad (1.18)
\end{aligned}$$

The on-shell projected phase space $\Phi^{\mathrm{DPA}}_{4,(f_{i_3},\bar{f}_{i_4})}$ depends on the fermion pairs $(f_{i_3},\bar{f}_{i_4})$ and $(f_{i_5},\bar{f}_{i_6})$ which are the decay products of the gauge bosons V_1 and V_2, respectively. In general we can construct two different on-shell projected phase spaces $\Phi^{\mathrm{DPA}}_{4,(f_3,\bar{f}_4)}$ and $\Phi^{\mathrm{DPA}}_{4,(f_3,\bar{f}_6)}$ for the outgoing fermions $f_3,\bar{f}_4,f_5,\bar{f}_6$. If both fermion pairs $(f_3,\bar{f}_4)$, $(f_5,\bar{f}_6)$ and $(f_3,\bar{f}_6)$, $(f_5,\bar{f}_4)$ are possible physical decay products, a separate on-shell projection must be applied for each of these possibilities.

For example if the final state is given by $\mathrm{e}^-\mathrm{e}^+\nu_\mathrm{e}\bar{\nu}_\mathrm{e}$ there are two possible on-shell projections. If these particles were produced by the decay of two massive gauge bosons we find the gauge-boson pair $(\mathrm{W}^-,\mathrm{W}^+)$ for the fermion pairs $(\mathrm{e}^-,\bar{\nu}_\mathrm{e})$ and $(\nu_\mathrm{e},\mathrm{e}^+)$ and the gauge-boson pair (Z,Z) for the fermion pairs $(\mathrm{e}^-,\mathrm{e}^+)$ and $(\nu_\mathrm{e},\bar{\nu}_\mathrm{e})$.

The same is true for the final state $\mathrm{e}_3^-\mathrm{e}_4^+\mathrm{e}_5^-\mathrm{e}_6^+$ which only contains electrons and positrons. Here we have the decay products of two Z-bosons but still we have to use two different on shell projections because we can construct two Z-bosons from the fermion pairs $(\mathrm{e}_3^-,\mathrm{e}_4^+)$ and $(\mathrm{e}_5^-,\mathrm{e}_6^+)$ as well as from the fermion pairs $(\mathrm{e}_3^-,\mathrm{e}_6^+)$ and $(\mathrm{e}_5^-,\mathrm{e}_4^+)$.

1.4.1 Construction of momenta

The momenta for the phase-space integration are constructed using the multichannel Monte Carlo approach. In the Monte Carlo integration we replace the integral over the phase space by an averaged sum over the momenta in this phase space. The momenta are calculated from a set of random numbers $r_i \in [0.1]$ so that the integration over the phase space must be mapped into an integration over a unit hyper cube $r_1 \ldots r_n$. This mapping of a set of momenta to a set of random numbers can be done an many different ways. However, the integration error we get for the integration over the random

numbers $\mathrm{d}r_1 \ldots \mathrm{d}r_n$ is considerably lower if the integrand as a function of $r_1 \ldots r_n$ is almost a constant.

In the multi-channel Monte Carlo approach for each Feynman diagram contributing to a given process a different mapping is chosen. In this way all the known resonances in the particle propagators on the internal lines of the diagram can be taken into account. A mapping is essentially a substitution in the integration over the phase space. If we write the phase-space integration as an integration over invariants instead of momenta we get integrals for the total cross section of the form

$$\sigma = \int_{s_{\min}}^{s_{\max}} f(s)\mathrm{d}s, \tag{1.19}$$

with some function $f(s) = |\mathcal{M}|^2$ which is basically given by a squared matrix element and may have a complicated peaking structure in the invariant s. For the Monte Carlo integration we have to use random numbers $r \in [0, 1]$. Therefore we have to find a substitution (mapping) so that

$$\sigma = \int_{s_{\min}}^{s_{\max}} f(s)\mathrm{d}s = \int_0^1 \frac{f(s(r, s_{\min}, s_{\max}))}{g_s(s(r, s_{\min}, s_{\max}))}\mathrm{d}r, \tag{1.20}$$

with

$$g_s = \left(\frac{\mathrm{d}s(r, s_{\min}, s_{\max})}{\mathrm{d}r}\right)^{-1}. \tag{1.21}$$

If one knows the peaking structure of f it may be possible to choose a function $s(r, s_{\min}, s_{\max})$ in such a way that the probability density g_s mimics the behavior of f in the regions where f is large. In this way the integrand $f(s)/g_s$ in the second integral in (1.20) may become an almost constant function in r. This method is also known as importance sampling and reduces the numerical error in the Monte Carlo integration considerably. An example for such a mapping in one dimension is the Breit–Wigner propagator of a massive gauge boson V with mass M_V. A propagator of this type leads to a cross section $\sigma \propto 1/\left[(s - M_V^2) + M_V^2\Gamma_V^2\right]$. The invariant s in this example is the squared momentum of the gauge boson. If we use the function

$$s(r) = M_V^2 + M_V\Gamma_V \tan\left(y_{\min} + r(y_{\max} - y_{\min})\right) \tag{1.22}$$

with

$$y_{\min,\max} = \arctan\left(\frac{s_{\min,\max} - M_V^2}{M_V\Gamma_V}\right), \tag{1.23}$$

to map the integration over s on a random number r we find a corresponding density function

$$g_s(s, s_{\min}, s_{\max}) = \frac{M_V\Gamma_V}{(y_{\max} - y_{\min})\left[(s - M_V^2) + M_V^2\Gamma_V^2\right]}. \tag{1.24}$$

Thus the factor $1/\left[(s-M_V^2)+M_V^2\Gamma_V^2\right]$ in the cross section σ is exactly canceled by g_s. Due to the cancellation we effectively get an integration over the constant $(y_{\max}-y_{\min})/(M_V\Gamma_V)$.

In the multi-channel Monte Carlo method several of these mappings are used in parallel. This makes it possible to create an effective mapping for a complicated function like a differential cross section in which we know the peaking structure of contributions due to single Feynman diagrams, but do not know the complete peaking structure. In this case we construct mappings according to each Feynman diagram separately. Let n be the number of Feynman diagrams contributing to a given process. We can write the cross section σ which is the integral over the phase space Φ as

$$\sigma = \sum_{i=1}^{n} \alpha_i \int \frac{f(\mathbf{s}_i(\mathbf{r}))}{g_{\mathbf{s}_i}} \mathrm{d}\mathbf{r} \tag{1.25}$$

with a set of random numbers $\mathbf{r} = (r_1, \ldots, r_m) \in [0,1]^m$ and sets $\mathbf{s}_i$ of invariants that are functions of this random numbers. The α_i are a priori weights for the channels $i = 1, \ldots, n$ which satisfy $\sum_{i=1}^{n} \alpha_i = 1$ and $\alpha_i > 0$. Note that the actual set of invariants $\mathbf{s}_i$ may vary for different channels i. The density $g_{\mathbf{s}_i}$ is given by

$$\frac{1}{g_{\mathbf{s}_i}} = \left| \frac{\partial \mathbf{s}_i(\mathbf{r})}{\partial \mathbf{r}} \right|_{\mathbf{r}=\mathbf{r}(\mathbf{s}_i)} . \tag{1.26}$$

In the Monte Carlo program we introduce an additional random number $r_0 \in [0,1]$ to choose one of the n channels for each integration point:

$$\sigma = \int_0^1 \mathrm{d}r_0 \sum_{i=1}^{n} \alpha_i \theta(r_0 - \beta_{i-1}) \theta(\beta_i - r_0) \int \frac{f(\mathbf{s}_i(\mathbf{r}))}{g_{\mathrm{tot}}} \mathrm{d}\mathbf{r}, \tag{1.27}$$

with $\beta_0 = 0$, $\beta_i = \sum_{j=1}^{i} \alpha_j$ and the total density $g_{\mathrm{tot}} = \sum_{i=1}^{n} \alpha_i g_{\mathbf{s}_i}$ which gives the probability to generate the specific phase-space point determined by r_0 and $\mathbf{r}$. During the evaluation of this integral the weights α_i can be adjusted to the contributions of the single channels. In this way the calculation of the integral can be further optimized.

For the partonic process $q_1 q_2 \to 4f$ we introduce seven topologies from which all contributing Feynman diagrams can be constructed by the proper insertion of fields. The topologies are shown in figure 1.3 and can be assembled by taking the following building blocks:

- Internal propagators.
- Two-to-two processes with a t-channel propagator.

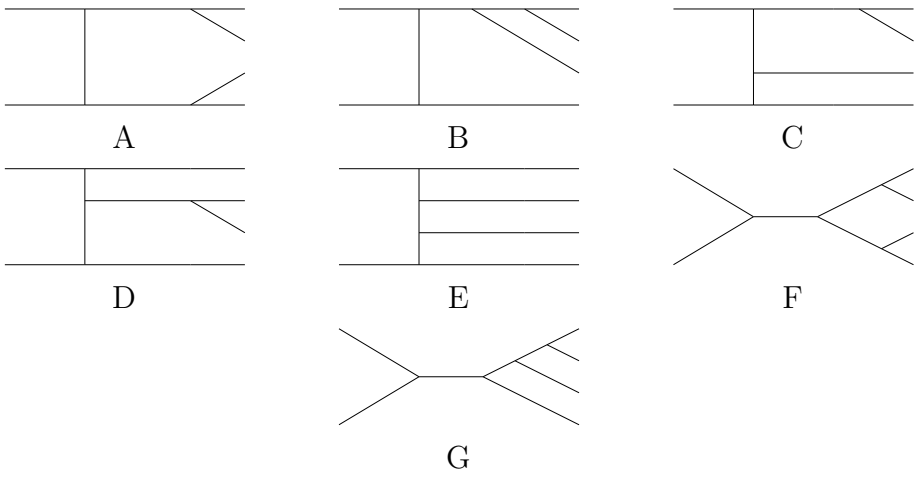

Figure 1.3: Topologies for a $2 \to 4$ particle process

- Decay of one particle into two particles.

Each of these three building blocks is mapped considering the particular invariants which occur.

In addition to this the parton distribution functions are mapped within the phase-space generator. This allows to choose suitable mappings for the topologies F and G in figure 1.3 with an s-channel propagator from the annihilation of the two incoming quarks. Usually this s-channel is not mapped because it does not play a role in the high-energy regime in which any particle propagating on this line is far off-shell. But in the case of tree-level calculations at low energies this propagator might become resonant and therefore a mapping might be necessary for a stable numerical integration.

In DPA we have to apply an on-shell projection on the generated momenta. In this case it is sufficient to take the topologies A and F from figure 1.3 into account. These are the only topologies in which two resonant gauge bosons can appear. In DPA we can restrict the calculation to these two topologies and thus we can take advantage in the numerical integration. By using just the topologies A and F we have a high probability to generate momenta that are already almost on-shell and the on-shell projection described in the next section only causes minor changes to these momenta. Further on we can use the fact that the two s-channel propagators on which we perform the on-shell projection are already mapped according to the Breit-Wigner resonance mapping (1.22). There is a cancellation of the propagators in the squared matrix element with the density functions of the mappings. In DPA the off-shell momenta must be inserted in the resonant propagators and the

rest of the matrix element must be evaluated using the on-shell projected momenta. For the topologies A and F the propagators with off-shell momenta cancel exactly the density functions of the mappings so that the integration over the phasespace $\Phi_4^{\rm DPA}$ becomes independent of the momenta inserted in these propagators. We use this effect to reduce the integration time for the integration by inserting only the on-shell projected momenta in these propagators. It is of particular importance here to emphasize that the integrals over Φ_4 and $\Phi_4^{\rm DPA}$ have the same measure. So the probability densities g_s used in the Monte-Carlo program are identical for these two integrations.

1.4.2 On-shell projection for double-pole approximation

The construction of on-shell momenta for the gauge bosons in DPA is done in the following way. In order to construct the process

$$\begin{aligned} f_1(p_1)f_2(p_2) &\to V_1(k_1)V_2(k_2), \\ V_1(k_1) &\to f_3(p_3)f_4(p_4), \\ V_2(k_2) &\to f_5(p_5)f_6(p_6) \end{aligned} \tag{1.28}$$

with $k_1^2 = M_{V_1}^2$ and $k_2^2 = M_{V_2}^2$, first a set of momenta $\tilde{p}_1, \tilde{p}_2, \tilde{p}_3, \tilde{p}_4, \tilde{p}_5, \tilde{p}_6$ is calculated by the phase-space generator. We keep the incoming momenta $p_1 = \tilde{p}_1, p_2 = \tilde{p}_2$ and hence the centre-of-mass $p = \tilde{p}_1 + \tilde{p}_2$ fixed. With $\beta = p^3/p^0$ we can boost to the centre-of-mass system (CMS) of the subprocess in which

$$\begin{aligned} p^{0\prime} &= \frac{p^0 - \beta p^3}{\sqrt{1-\beta^2}}, \quad \vec{p}' = 0, \\ \tilde{k}_1^{0\prime} &= \frac{\tilde{k}_1^0 - \beta \tilde{k}_1^3}{\sqrt{1-\beta^2}}, \quad \tilde{k}_1^{1\prime} = \tilde{k}_1^1, \quad \tilde{k}_1^{2\prime} = \tilde{k}_1^2, \quad \tilde{k}_1^{3\prime} = \frac{\tilde{k}_1^3 - \beta \tilde{k}_1^0}{\sqrt{1-\beta^2}}. \end{aligned} \tag{1.29}$$

The on-shell projected momentum k_1' in this system reads

$$\begin{aligned} k_1^{0\prime} &= \frac{p^2 + M_{V_1}^2 - M_{V_2}^2}{2p^{0\prime}} = \frac{p^2 + M_{V_1}^2 - M_{V_2}^2}{2\sqrt{p^2}}, \\ |\vec{k_1}'| &= \sqrt{k_1^{0\prime 2} - M_{V_1}^2}. \end{aligned} \tag{1.30}$$

If we keep the spatial direction of $\tilde{k}_1'$ in the CMS the on-shell projected momentum $\vec{k_1}'$ is fully determined

$$\vec{k_1}' = \vec{\tilde{k}}_1' \frac{|\vec{k_1}'|}{|\vec{\tilde{k}}_1'|}, \tag{1.31}$$

and in the laboratory frame we find by boosting back

$$k_1^0 = \frac{k_1^{0\prime} + \beta k_1^{3\prime}}{\sqrt{1-\beta^2}}, \quad k_1^1 = k_1^{1\prime}, \quad k_1^2 = k_1^{2\prime}, \quad k_1^3 = \frac{k_1^{3\prime} + \beta k_1^{0\prime}}{\sqrt{1-\beta^2}}. \tag{1.32}$$

The on-shell projected momentum of the gauge boson V_2 is $k_2 = p - k_1$. To calculate the momenta for the outgoing fermions p_3, p_4 and p_5, p_6 we fix the direction of $\tilde{p}_3$ and $\tilde{p}_5$ by keeping the cosines $\cos\theta_1, \cos\theta_2$ of the angles between $k_1, \tilde{p}_3$ and $k_2, \tilde{p}_5$ fixed:

$$\begin{aligned} p_3^0 &= \frac{M_{V_1}^2}{2(k_1^0 - |\vec{k_1}|\cos\theta_1)}, \qquad \vec{p_3} = \vec{\tilde{p}_3}\frac{p_3^0}{|\vec{\tilde{p}_3}|}, \qquad p_4 = k_1 - p_3, \\ p_5^0 &= \frac{M_{V_2}^2}{2(k_2^0 - |\vec{k_2}|\cos\theta_2)}, \qquad \vec{p_5} = \vec{\tilde{p}_5}\frac{p_5^0}{|\vec{\tilde{p}_5}|}, \qquad p_6 = k_2 - p_5. \end{aligned} \tag{1.33}$$

1.5 Features of the Monte Carlo program

At tree-level the Monte Carlo program can handle all standard-model processes with four leptons or two quarks and two leptons in the final state. Especially the cross sections for proton–proton to two quarks and a lepton anti-lepton pair and proton–proton to two anti-quarks and a lepton anti-lepton pair are included.

The calculations of tree-level cross sections include anomalous triple gauge-boson couplings for the process $PP \to 4f$ and anomalous quartic gauge couplings for the process $PP \to 4f\gamma$. A description of these couplings can be found in Refs. [23, 24, 25].

Radiative corrections are implemented using the high-energy limit and the DPA. In this case only fermion–anti-fermion initial states for the partonic process have to be considered because only here two resonant gauge-boson propagators can appear. The corrections include the leading electroweak logarithms which are defined in chapter 3.2. For the gauge-boson decays and the non-factorizable part of the corrections only photonic corrections contribute in the high-energy limit.

For the convolution over the parton densities various possibilities of mapping the parton distribution functions are supplied. This allows to choose a different mapping in the program if a cross section must be evaluated in an exclusive range for the partonic centre-of-mass energy $\hat{s}$. It is also possible to skip the convolution over parton densities and to use the Monte Carlo program for evaluating e^-e^+ or e^-e^- cross sections.

The possibility exists to define any function in the momenta as an observable for a histogram. This allows to generate plots for differential cross

sections like $\mathrm{d}\sigma/\mathrm{d}\sqrt{\hat{s}}$. These histograms are generated separately for subcontributions, like virtual and real corrections, providing a possibility to examine regions of the phase space in which the radiative corrections may become large.

Chapter 2

The matrix elements

There are two independent sets of matrix elements included in the Monte Carlo program. The first set is given by the generic matrix elements calculated by Denner, Dittmaier, Roth, and Wackeroth for $e^+e^- \to 4\,\text{fermions} + \gamma$ in Ref. [26]. For the production of four fermions there are only two fundamental topologies (see fig. 2.1) from which all Feynman diagrams contributing to a $2f \to 4f$ process can be constructed by permuting the external particles $f_1, \ldots, f_6$.

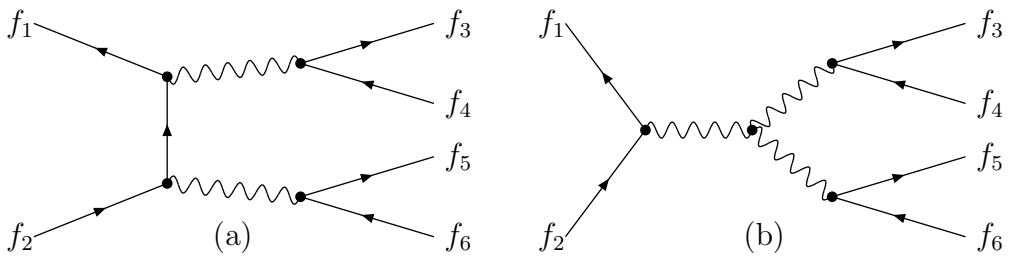

Figure 2.1: The fundamental topologies for $2 \to 4$ fermions

The second set was especially designed to implement the universal leading-logarithmic corrections. These matrix elements are only valid in the double-pole approximation, since they are factorized into gauge-boson pair production and gauge-boson decay. The approach chosen to calculate radiative corrections makes use of the Goldstone-Boson Equivalence Theorem (GBET) according to which matrix elements with two longitudinal gauge bosons are replaced by matrix elements with corresponding would-be Goldstone bosons.

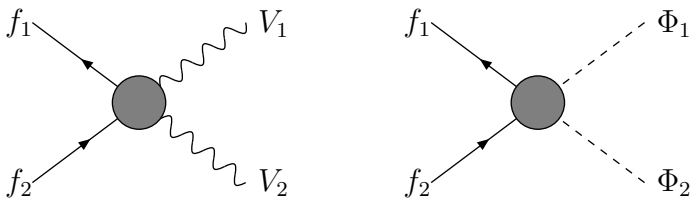

Figure 2.2: Production of gauge-boson pairs

2.1 The matrix elements for $f_1 f_2 \to f_3 f_4 f_5 f_6 (+\gamma)$

In the parton picture the we need amplitudes for two fermions to four fermions or two fermions to four fermions and an additional photon

$$f_1(p_1,\sigma_1) f_2(p_2,\sigma_2) \to f_3(p_3,\sigma_3) f_4(p_4,\sigma_4) f_5(p_5,\sigma_5) f_6(p_6,\sigma_6)\,(+\gamma(p_\gamma,\lambda))\,. \tag{2.1}$$

In the following section we explain how these amplitudes are constructed.

2.1.1 Four-fermion production

Each Feynman diagram for the process $f_1 f_2 \to f_3 f_4 f_5 f_6$ can be related to a Feynman diagram with six incoming fermions by crossing. In this way we can express every Feynman diagram by one of the two generic diagrams in figure 2.1. These generic diagrams are given by the functions

$$\mathcal{M}_{V_1V_2}^{\sigma'_{f_1},\sigma'_{f_2},\sigma'_{f_3},\sigma'_{f_4},\sigma'_{f_5},\sigma'_{f_6}}(p'_{f_1},p'_{f_2},p'_{f_3},p'_{f_4},p'_{f_5},p'_{f_6}) \quad = \tag{2.2}$$

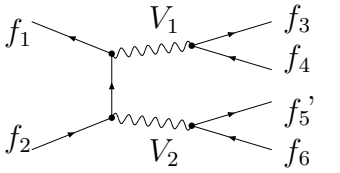

$$\mathcal{M}_{VWW}^{\sigma'_{f_1},\sigma'_{f_2},\sigma'_{f_3},\sigma'_{f_4},\sigma'_{f_5},\sigma'_{f_6}}(p'_{f_1},p'_{f_2},p'_{f_3},p'_{f_4},p'_{f_5},p'_{f_6}) \quad = \tag{2.3}$$

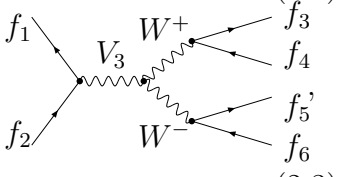

which were listed in Ref. [26]. Here $p'_{f_1},\ldots,p'_{f_6}$ are incoming momenta and $\sigma'_{f_1},\ldots,\sigma'_{f_6}$ are the helicities of the particles $f_1 \ldots f_2$, respectively. We extended the couplings used in these functions by the corresponding factors from the Cabibbo–Kobayaschi–Maskawa matrix. In this way the possible

mixing of quark generations is automatically included in the matrix elements constructed from this functions. Every Feynman diagram which occurs for a given $2f \to 4f$ process can be constructed from these two general functions. To describe outgoing particles the helicities must be inverted and the momenta p_i must be replaced by $-p_i$. This is automatically done by multiplying them with the particle direction $d_i \in \{-1, +1\}$ which is set to -1 for all outgoing particles. The momenta $p'_{f_1}, \ldots, p'_{f_6}$ and helicities $\sigma'_{f_1}, \ldots, \sigma'_{f_6}$ needed in the generic functions read

$$p'_i = d_i p_i, \qquad \sigma'_i = d_i \sigma_i. \tag{2.4}$$

In the following we use the particle number $i \in \{1, \ldots, 6\}$ as an abbreviation for the particle momentum p_i and the helicity σ_i. A particular Feynman diagram can then either be written as

$$\mathcal{M}^{\mathrm{a},V_1,V_2}(i_1, i_2, i_3, i_4, i_5, i_6) = \sum_{f'}$$

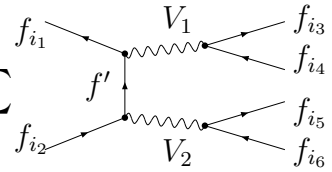

(2.5)

or

$$\mathcal{M}^{\mathrm{b},V_3}(i_1, i_2, i_3, i_4, i_5, i_6) =$$

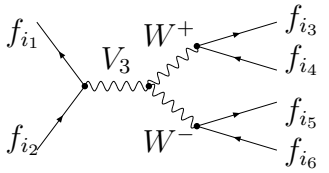

(2.6)

where the numbers $i_1, i_2, i_3, i_4, i_5, i_6$ are a permutation of $1, 2, 3, 4, 5, 6$. In this way it is possible to create all processes including six fermions on the external lines. The sum over the fermions on the internal line in formula (2.5) is only necessary if f_{i_1} and f_{i_2} are quarks and quark mixing via the Cabibbo–Kobayaschi–Maskawa matrix is taken into account. In all other cases only one possibility for the fermion f' exists. To build the Feynman diagrams to a given process it is completely sufficient to consider permutations of the fermions on the outgoing lines (i.e.$f_{i_1}, f_{i_3}, f_{i_5}$) and of the fermions on the incoming lines (i.e.$f_{i_2}, f_{i_4}, f_{i_6}$). For later use we define a polarization-dependent matrix element with polarizations $\sigma_1, \sigma_2, \sigma_3, \sigma_4, \sigma_5, \sigma_6$ as

$$\begin{aligned}\mathcal{M}^{\mathrm{weak}}_{\pm} = \sum_{\{i_1,i_3,i_5\}} \sum_{\{i_2,i_4,i_6\}} & \frac{\mathrm{sign}(\{i_1, i_3, i_5\})\mathrm{sign}(\{i_2, i_4, i_6\}) \pm 1}{2} \\ & \times \Bigg[\sum_{V_1=W^\pm,Z,\gamma} \sum_{V_2=W^\pm,Z,\gamma} \mathcal{M}^{\mathrm{a},V_1,V_2}(i_1, i_2, i_3, i_4, i_5, i_6) \\ & \qquad + \sum_{V_3=Z,\gamma} \mathcal{M}^{\mathrm{b},V_3}(i_1, i_2, i_3, i_4, i_5, i_6) \Bigg],\end{aligned} \tag{2.7}$$

where the two sums run over the permutations of the numbers of outgoing and incoming fermions. The functions sign($\{i_1, i_3, i_5\}$) and sign($\{i_2, i_4, i_6\}$) give the sign of the permutations. Note that in this definition $\mathcal{M}_+^{\text{weak}}$ contains all diagrams with a positive permutation of the fermion lines and $\mathcal{M}_-^{\text{weak}}$ all diagrams with a negative sign of the permutation. This will turn out to be a very useful definition as soon as we have to consider the various colour structures of these diagrams. All diagrams that are not physical, e.g. a diagram which would include a $e^-\bar{u}Z$ coupling, are not taken into account in these sums. As condition to decide whether a diagram is physical or not we use the existence of the couplings in the standard model. If within a diagram one coupling does not exist in the standard model the function $\mathcal{M}^{\text{a},V_1,V_2}$ or $\mathcal{M}^{\text{b},V_3}$ is set to zero.

The squared matrix element in the case of one pair of quarks or no quarks is

$$|\mathcal{M}_{2\,\text{quarks}}|^2 = \frac{1}{4}\frac{N_{\text{colour}}}{N_{\text{av}}N_{\text{perm}}}\sum_{\sigma_1,\ldots,\sigma_6}|\mathcal{M}_+^{\text{weak}} + \mathcal{M}_-^{\text{weak}}|^2 \tag{2.8}$$

with the colour factor $N_{\text{colour}} = 3$ for one quark pair or $N_{\text{colour}} = 1$ if there are no quarks. The factor $N_{\text{av}} = 9$ takes the average over all colour states in the case of incoming quarks and the factor $N_{\text{perm}} = 2^{N_{\text{id}}}$ is the symmetry factor in the case of N_{id} pairs of identical particles in the final state. If there are four quarks, two additional complications must be taken into account. First the exchange of gluons between two pairs of quarks becomes possible giving rise to additional Feynman diagrams with gluon exchange. Apart from the colour matrices in the strong couplings these diagrams can be calculated by substituting a photon with a gluon, i.e. by dividing out the weak coupling of the photon and replacing it by the strong coupling of the gluon

$$\mathcal{M}^{\text{gluon},V}(i_1,i_2,i_3,i_4,i_5,i_6) =$$

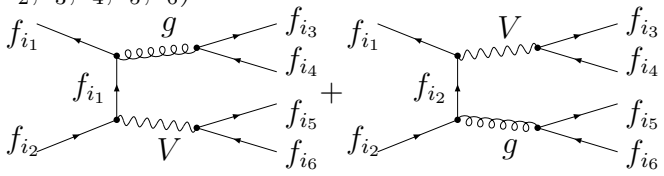

$$= \frac{\alpha_s}{\alpha Q(f_{i_1})Q(f_{i_3})}\mathcal{M}^{\text{a},\gamma,V}(i_1,i_2,i_3,i_4,i_5,i_6) + \frac{\alpha_s}{\alpha Q(f_{i_2})Q(f_{i_6})}\mathcal{M}^{\text{a},V,\gamma}(i_1,i_2,i_3,i_4,i_5,i_6). \tag{2.9}$$

Now we define

$$\mathcal{M}_{\pm}^{\text{gluon}} = \sum_{\{i_1,i_3,i_5\}} \sum_{\{i_2,i_4,i_6\}} \frac{\text{sign}(\{i_1,i_3,i_5\})\text{sign}(\{i_2,i_4,i_6\}) \pm 1}{2} \times \left[\sum_{V=W^{\pm},Z,\gamma} \mathcal{M}^{\text{gluon},V}(i_1,i_2,i_3,i_4,i_5,i_6) \right]. \quad (2.10)$$

Secondly the different colour matrices in the quark lines must be taken into account, because the diagrams contribute to different colour structures. Without loss of generality let the four quarks be the fermions f_1, f_2, f_3, f_4 with colour indices c_1, c_2, c_3, c_4 and f_5, f_6 be leptons without colour. Furthermore let f_1, f_3, f_5 denote the particles on the lines pointing out of the diagrams and f_2, f_4, f_6 denote the particles on the lines pointing into the diagrams. Now there are two possible ways to construct fermion pairs that couple to gauge bosons:

$$\begin{aligned} P_1 &:= (f_1,f_2)(f_3,f_4)(f_5,f_6) \\ P_2 &:= (f_1,f_4)(f_3,f_2)(f_5,f_6). \end{aligned} \quad (2.11)$$

These two can be distinguished by the signs of the permutations

$$\begin{aligned} \text{sign}(\{i_1,i_3,i_5\})\text{sign}(\{i_2,i_4,i_6\}) &= +1, \text{for pairs } (f_1,f_2)(f_3,f_4)(f_5,f_6) \\ \text{sign}(\{i_1,i_3,i_5\})\text{sign}(\{i_2,i_4,i_6\}) &= -1, \text{for pairs } (f_1,f_4)(f_3,f_2)(f_5,f_6). \end{aligned} \quad (2.12)$$

Depending on the pairing of the quarks and if these pairs are connected by an electroweak gauge boson or a gluon we get four different colour structures and hence we get four matrix elements

$$\begin{aligned} \mathcal{M}_{P_1}^{\text{weak}} &= \delta_{c_1c_2}\delta_{c_3c_4}\mathcal{M}_{+}^{\text{weak}} \\ \mathcal{M}_{P_2}^{\text{weak}} &= \delta_{c_1c_4}\delta_{c_2c_3}\mathcal{M}_{-}^{\text{weak}} \\ \mathcal{M}_{P_1}^{\text{gluon}} &= \frac{1}{4}\lambda^a_{c_1c_2}\lambda^a_{c_3c_4}\mathcal{M}_{+}^{\text{gluon}} \\ \mathcal{M}_{P_2}^{\text{gluon}} &= \frac{1}{4}\lambda^b_{c_1c_4}\lambda^b_{c_2c_3}\mathcal{M}_{-}^{\text{gluon}}. \end{aligned} \quad (2.13)$$

Here λ^a_{ij} are the Gell-Mann matrices which appear in the couplings of the gluons. If we average over the colours and spins of the incoming particles and sum over the different colour and spin states of the outgoing particles the squared matrix element reads

$$|\mathcal{M}_{4\,\text{quarks}}|^2 = \frac{1}{4N_{\text{av}}N_{\text{perm}}} \sum_{\sigma_1,\ldots,\sigma_6} \sum_{c_1,c_2,c_3,c_4} \left| \mathcal{M}_{P_1}^{\text{weak}} + \mathcal{M}_{P_2}^{\text{weak}} + \mathcal{M}_{P_1}^{\text{gluon}} + \mathcal{M}_{P_2}^{\text{gluon}} \right|^2. \quad (2.14)$$

We can use the completeness relations

$$\lambda^a_{ij}\lambda^a_{kl} = -\frac{2}{3}\delta_{ij}\delta_{kl} + 2\delta_{il}\delta_{jk} \tag{2.15}$$

of the Gell-Mann matrices to sum over the four colour indices c_1, c_2, c_3, c_4, and we find

$$\begin{aligned}|\mathcal{M}_{4\,\mathrm{quarks}}|^2 = \frac{1}{4N_{\mathrm{av}}N_{\mathrm{perm}}} \sum_{\sigma_1,\ldots,\sigma_6} \Big[& 9\left|\mathcal{M}^{\mathrm{weak}}_{+}\right|^2 + 9\left|\mathcal{M}^{\mathrm{weak}}_{-}\right|^2 \\ & + 2\left|\mathcal{M}^{\mathrm{gluon}}_{+}\right|^2 + 2\left|\mathcal{M}^{\mathrm{gluon}}_{-}\right|^2 + 6\mathrm{Re}\left(\mathcal{M}^{\mathrm{weak}}_{+}(\mathcal{M}^{\mathrm{weak}}_{-})^*\right) \\ & + 8\mathrm{Re}\left(\mathcal{M}^{\mathrm{weak}}_{+}(\mathcal{M}^{\mathrm{gluon}}_{-})^*\right) + 8\mathrm{Re}\left(\mathcal{M}^{\mathrm{weak}}_{-}(\mathcal{M}^{\mathrm{gluon}}_{+})^*\right) \\ & - \frac{4}{3}\mathrm{Re}\left(\mathcal{M}^{\mathrm{gluon}}_{+}(\mathcal{M}^{\mathrm{gluon}}_{-})^*\right) \Big]\end{aligned} \tag{2.16}$$

for the squared matrix element with four quarks. The case of a matrix element with six quarks is not considered because it is dominated by pure QCD. For the consideration of this process the equivalent of formula (2.3) including a three gluon vertex is needed.

2.1.2 Four-fermion plus photon production

The matrix elements for four-fermion plus photon production have been constructed in the same way. For the two fundamental topologies the functions from Ref. [26] defined as

$$\mathcal{M}^{\sigma'_{f_1},\sigma'_{f_2},\sigma'_{f_3},\sigma'_{f_4},\sigma'_{f_5},\sigma'_{f_6},\lambda}_{V_1V_2}(p'_{f_1},p'_{f_2},p'_{f_3},p'_{f_4},p'_{f_5},p'_{f_6},p_\gamma) =$$

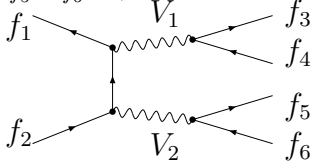

$+\,\gamma,$ (2.17)

$$\mathcal{M}^{\sigma'_{f_1},\sigma'_{f_2},\sigma'_{f_3},\sigma'_{f_4},\sigma'_{f_5},\sigma'_{f_6},\lambda}_{VWW}(p'_{f_1},p'_{f_2},p'_{f_3},p'_{f_4},p'_{f_5},p'_{f_6},p_\gamma) =$$

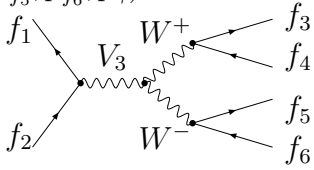

$+\,\gamma,$ (2.18)

were used. The expression $+\,\gamma$ to the graph in this formulae has to be understood as a photon line attached to all charged lines in the graph. The

photon momentum p_γ and the polarization λ are always defined for an outgoing photon. Again we use the particle number as an abbreviation for the momentum and the helicity of the particle and define

$$\mathcal{M}_\gamma^{\mathrm{a},V_1,V_2}(i_1,i_2,i_3,i_4,i_5,i_6) = \sum_{f'}$$

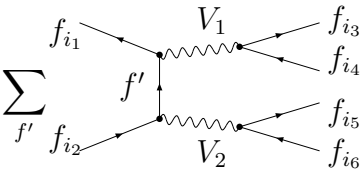

$$+\gamma, \tag{2.19}$$

$$\mathcal{M}_\gamma^{\mathrm{b},V_3}(i_1,i_2,i_3,i_4,i_5,i_6) =$$

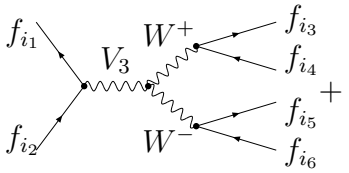

$$+\gamma. \tag{2.20}$$

The gluonic matrix element in this case is

$$\mathcal{M}_\gamma^{\mathrm{gluon},V}(i_1,i_2,i_3,i_4,i_5,i_6) = \frac{\alpha_s}{\alpha Q(f_{i_1})Q(f_{i_3})}$$

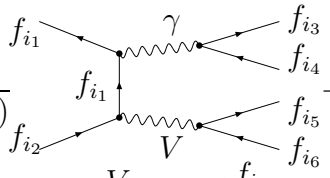

$$+\gamma$$

$$+\frac{\alpha_s}{\alpha Q(f_{i_2})Q(f_{i_6})}$$

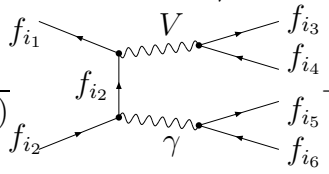

$$+\gamma. \tag{2.21}$$

For a given polarization $\sigma_1,\sigma_2,\sigma_3,\sigma_4,\sigma_5,\sigma_6,\lambda$ we can define

$$\mathcal{M}_{\gamma,\pm}^{\mathrm{weak}} = \sum_{\{i_1,i_3,i_5\}} \sum_{\{i_2,i_4,i_6\}} \frac{\mathrm{sign}(\{i_1,i_3,i_5\})\mathrm{sign}(\{i_2,i_4,i_6\}) \pm 1}{2}$$
$$\times \left[\sum_{V_1=W^\pm,Z,\gamma} \sum_{V_2=W^\pm,Z,\gamma} \mathcal{M}_\gamma^{\mathrm{a},V_1,V_2}(i_1,i_2,i_3,i_4,i_5,i_6) \right.$$
$$\left. + \sum_{V_3=Z,\gamma} \mathcal{M}_\gamma^{\mathrm{b},V_3}(i_1,i_2,i_3,i_4,i_5,i_6) \right], \tag{2.22}$$

and

$$\mathcal{M}_{\gamma,\pm}^{\mathrm{gluon}} = \sum_{\{i_1,i_3,i_5\}} \sum_{\{i_2,i_4,i_6\}} \frac{\mathrm{sign}(\{i_1,i_3,i_5\})\mathrm{sign}(\{i_2,i_4,i_6\}) \pm 1}{2}$$
$$\times \left[\sum_{V=W^\pm,Z,\gamma} \mathcal{M}_\gamma^{\mathrm{gluon},V}(i_1,i_2,i_3,i_4,i_5,i_6) \right]. \tag{2.23}$$

Here the colour structure is the same as for the matrix elements without photon emission. Thus, we can use the same formulae derived for the squared matrix elements for $2f \to 4f$:

$$|\mathcal{M}_{\gamma,2\,\mathrm{quarks}}|^2 = \frac{1}{4}\frac{N_{\mathrm{colour}}}{N_{\mathrm{av}}N_{\mathrm{perm}}}\sum_{\sigma_1,\ldots,\sigma_6}\sum_{\lambda=\pm}|\mathcal{M}^{\mathrm{weak}}_{\gamma,+}+\mathcal{M}^{\mathrm{weak}}_{\gamma,-}|^2, \tag{2.24}$$

$$\begin{aligned}|\mathcal{M}_{\gamma,4\,\mathrm{quarks}}|^2 = \frac{1}{4N_{\mathrm{av}}N_{\mathrm{perm}}}\sum_{\sigma_1,\ldots,\sigma_6}\sum_{\lambda=\pm}\Bigg[&9\left|\mathcal{M}^{\mathrm{weak}}_{\gamma,+}\right|^2+9\left|\mathcal{M}^{\mathrm{weak}}_{\gamma,-}\right|^2\\ &+2\left|\mathcal{M}^{\mathrm{gluon}}_{\gamma,+}\right|^2+2\left|\mathcal{M}^{\mathrm{gluon}}_{\gamma,-}\right|^2+6\mathrm{Re}\left(\mathcal{M}^{\mathrm{weak}}_{\gamma,+}(\mathcal{M}^{\mathrm{weak}}_{\gamma,-})^*\right)\\ &+8\mathrm{Re}\left(\mathcal{M}^{\mathrm{weak}}_{\gamma,+}(\mathcal{M}^{\mathrm{gluon}}_{\gamma,-})^*\right)+8\mathrm{Re}\left(\mathcal{M}^{\mathrm{weak}}_{\gamma,-}(\mathcal{M}^{\mathrm{gluon}}_{\gamma,+})^*\right)\\ &-\frac{4}{3}\mathrm{Re}\left(\mathcal{M}^{\mathrm{gluon}}_{\gamma,+}(\mathcal{M}^{\mathrm{gluon}}_{\gamma,-})^*\right)\Bigg].\end{aligned} \tag{2.25}$$

2.2 The matrix elements in double-pole approximation

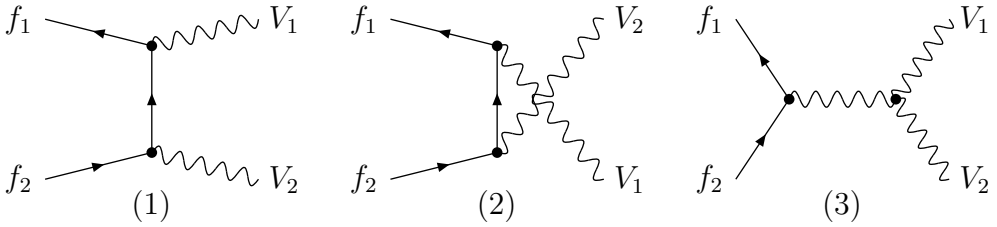

Figure 2.3: Diagrams for gauge-boson pair production

The electroweak corrections to the production of gauge bosons have been implemented in DPA. There are two on-shell gauge bosons produced that decay into two pairs of fermions. The process is divided into the production of on-shell gauge bosons and the decay of these bosons (see figure 1.2),

$$f_1(p_1,\sigma_1)\quad f_2(p_2,\sigma_2) \;\to\; V_1(k_1,\lambda_1)V_2(k_2,\lambda_2), \tag{2.26}$$

$$V_1(k_1,\lambda_1) \;\to\; f_3(p_3,\sigma_3)f_4(p_4,\sigma_4), \tag{2.27}$$

$$V_2(k_2,\lambda_2) \;\to\; f_5(p_5,\sigma_5)f_6(p_6,\sigma_6), \tag{2.28}$$

where p, k denote the momenta of the particles and σ, λ are the helicities of the fermions and the polarizations of the gauge bosons, respectively. The charges of the particles are denoted by Q_i for the fermions and by Q_{V_1} and Q_{V_2} for the outgoing gauge bosons. For DPA we take all pairs of massive gauge bosons (i.e. W^+W^-, $W^\pm Z$, ZZ) into account. For the electroweak-radiative corrections we have to consider the mixing of the Z boson with the γ which leads to matrix elements for $W^\pm\gamma$ and $Z\gamma$ production.

2.2.1 Formulae for the DPA matrix elements

In the Weyl–van der Waerden formalism the polarization vectors can be defined via

$$\begin{aligned}
\varepsilon_{+,\dot{A}B}(k) &= \sqrt{2} n_{2,\dot{A}} n_{1,B}, \\
\varepsilon_{-,\dot{A}B}(k) &= \sqrt{2} n_{1,\dot{A}} n_{2,B}, \\
\varepsilon_{0,\dot{A}B}(k) &= \frac{1}{M_V}(\lambda_1 n_{1,\dot{A}} n_{1,B} - \lambda_2 n_{2,\dot{A}} n_{2,B}),
\end{aligned} \tag{2.29}$$

where $n_1(k)$ and $n_2(k)$ are normalized Weyl spinors defined in Ref. [27]. If we denote the polar angle of the momentum k with θ and the azimuthal angle with ϕ these normalized spinors are given by

$$\begin{aligned}
n_{1,A} &= \begin{pmatrix} e^{-\mathrm{i}\phi}\cos\frac{\theta}{2} \\ \sin\frac{\theta}{2} \end{pmatrix}, \quad \lambda_1 = k^0 + |\vec{k}|, \\
n_{2,A} &= \begin{pmatrix} \sin\frac{\theta}{2} \\ -e^{\mathrm{i}\phi}\cos\frac{\theta}{2} \end{pmatrix}, \quad \lambda_2 = k^0 - |\vec{k}|.
\end{aligned} \tag{2.30}$$

A similar spinor is defined for a fermion with light-like momentum p^μ by $p_A = \sqrt{2p^0} n_{1,A}$. A general four momentum k^μ can be represented as a matrix $K_{\dot{A}B} = \sum_{i=1,2} \lambda_i n_{i,\dot{A}} n_{i,B}$. For Weyl spinors u, v a spinor product is defined in this formalism by

$$\begin{aligned}
\langle uv \rangle &= u_A v^A = u_1 v_2 - u_2 v_1, \\
\langle uv \rangle^* &= u_{\dot{A}} v^{\dot{A}} = (u_1 v_2 - u_2 v_1)^*.
\end{aligned} \tag{2.31}$$

To get a general result for all polarization states instead of this polarization vectors we used

$$\begin{aligned}
\varepsilon'_{\sigma,\dot{A}B}(k_1) &= \phi_{\dot{A}} \psi_B, \\
\varepsilon'_{\sigma,\dot{A}B}(k_2) &= \eta_{\dot{A}} \xi_B
\end{aligned} \tag{2.32}$$

as a generic form for the two polarization vectors in the calculation of the matrix elements. In this way we get for the three diagrams in Figure 2.3 the matrix elements

$$\begin{aligned}
\mathcal{M}'_{V_1V_2,1} &= -\frac{\mathrm{i}e^2}{t}\left(\delta_{\sigma 2}\delta_{\tau 2}C^-_{f_1V_1}C^-_{f_2V_2}\left\langle p_1\psi\right\rangle\left\langle p_2\eta\right\rangle^*\left(\left\langle\phi P_2\xi\right\rangle - \left\langle\phi K_2\xi\right\rangle\right)\right.\\
&\quad \left. + \delta_{\sigma 1}\delta_{\tau 1}C^+_{f_1V_1}C^+_{f_2V_2}\left\langle p_2\xi\right\rangle\left\langle p_1\phi\right\rangle^*\left(\left\langle\psi P_2\eta\right\rangle^* - \left\langle\psi K_2\eta\right\rangle^*\right)\right)\\
\mathcal{M}'_{V_1V_2,2} &= -\frac{\mathrm{i}e^2}{u}\left(\delta_{\sigma 2}\delta_{\tau 2}C^-_{f_1V_2}C^-_{f_2V_1}\left\langle p_1\xi\right\rangle\left\langle p_2\phi\right\rangle^*\left(\left\langle\psi P_2\eta\right\rangle^* - \left\langle\psi K_1\eta\right\rangle^*\right)\right.\\
&\quad \left. + \delta_{\sigma 1}\delta_{\tau 1}C^+_{f_1V_2}C^+_{f_2V_1}\left\langle p_2\psi\right\rangle\left\langle p_1\eta\right\rangle^*\left(\left\langle\phi P_2\xi\right\rangle - \left\langle\phi K_1\xi\right\rangle\right)\right)\\
\mathcal{M}'_{V_1V_2,3} &= \frac{\mathrm{i}e^2}{s-M^2_{V_3}}C_{V_3V_1V_2}\\
&\quad \times\left[\delta_{\sigma 1}\delta_{\tau 1}C^+_{f_1V_3}\left[\left\langle\phi\eta\right\rangle^*\left\langle\psi\xi\right\rangle\left\langle p_1K_1p_2\right\rangle\right.\right.\\
&\quad + \left\langle p_1\eta\right\rangle^*\left\langle p_2\xi\right\rangle\left(\left\langle p_1\phi\right\rangle^*\left\langle p_1\psi\right\rangle + \left\langle p_2\phi\right\rangle^*\left\langle p_2\psi\right\rangle\right)\\
&\quad \left.\left. - \left\langle p_1\phi\right\rangle^*\left\langle p_2\psi\right\rangle\left(\left\langle p_1\eta\right\rangle^*\left\langle p_1\xi\right\rangle + \left\langle p_2\eta\right\rangle^*\left\langle p_2\xi\right\rangle\right)\right]\right.\\
&\quad + \delta_{\sigma 2}\delta_{\tau 2}C^-_{f_1V_3}\left[\left\langle\phi\eta\right\rangle^*\left\langle\psi\xi\right\rangle\left\langle p_1K_1p_2\right\rangle^*\right.\\
&\quad + \left\langle p_2\eta\right\rangle^*\left\langle p_1\xi\right\rangle\left(\left\langle p_2\phi\right\rangle^*\left\langle p_2\psi\right\rangle + \left\langle p_1\phi\right\rangle^*\left\langle p_1\psi\right\rangle\right)\\
&\quad \left.\left.\left. - \left\langle p_2\phi\right\rangle^*\left\langle p_1\psi\right\rangle\left(\left\langle p_2\eta\right\rangle^*\left\langle p_2\xi\right\rangle + \left\langle p_1\eta\right\rangle^*\left\langle p_1\xi\right\rangle\right)\right]\right]
\end{aligned} \tag{2.33}$$

with

$$\left\langle\phi Q\psi\right\rangle := \phi_{\dot{A}}Q^{\dot{A}B}\psi_B, \tag{2.34}$$

and the usual definitions for the Mandelstam variables $s = (p_1+p_2)^2$, $t=(p_1-k_1)^2$, $u=(p_1-k_2)^2$. The numerical values of the coupling constants $C^{\pm}_{fV}$ can be found in Ref. [28]. The physical matrix element is then obtained by forming the linear combination given in (2.29). This means that ϕ,ψ or η,ξ are replaced by the spinors $n_1(k), n_2(k)$ and a factor $\sqrt{2}$ or λ_i/M_V must be applied if the polarization is $\sigma=\pm$ or $\sigma=0$ respectively. For example inserting the polarization vector for V_1 leads to

$$\begin{aligned}
\mathcal{M}_{V_1^+V_2,i} &= \sqrt{2}\mathcal{M}'_{V_1V_2,i}(\phi\to n_1(k_1),\psi\to n_2(k_1))\\
\mathcal{M}_{V_1^-V_2,i} &= \sqrt{2}\mathcal{M}'_{V_1V_2,i}(\phi\to n_2(k_1),\psi\to n_1(k_1))\\
\mathcal{M}_{V_1^0V_2,i} &= \frac{1}{M_{V_1}}\Big(\lambda_1(k_1)\mathcal{M}'_{V_1V_2,i}(\phi\to n_1(k_1),\psi\to n_1(k_1))\\
&\quad -\lambda_2(k_1)\mathcal{M}'_{V_1V_2,i}(\phi\to n_2(k_1),\psi\to n_2(k_1))\Big).
\end{aligned} \tag{2.35}$$

With (2.35) the matrix element for the gauge-boson production process is defined as

$$\mathcal{M}_{f_1 f_2 \to V_1^{\tau_1} V_2^{\tau_2}}(f_{i_3}, \bar{f}_{i_4}) = \sum_{i=1}^{3} \mathcal{M}_{V_1^{\tau_1} V_2^{\tau_2}, i}. \tag{2.36}$$

This matrix element depends on the helicities of the incoming fermions σ_1 and σ_2 and the polarizations of the produced gauge bosons τ_1 and τ_2. The on-shell projection which has to be used in this matrix element is indicated by the fermion pair $(f_{i_3}, \bar{f}_{i_4})$.

In the calculation of radiative corrections matrix elements for the production of scalar particle pairs are needed. These matrix elements arise from the use of the gauge-boson equivalence theorem in the calculation. The gauge-boson equivalence theorem tells us that a matrix element including n longitudinal gauge bosons $V_1^{\mathrm{L}} \dots V_n^{\mathrm{L}}$ and m other particles $\varphi_1 \dots \varphi_m$ can be written as

$$\mathcal{M}^{\varphi_1 \dots \varphi_m V_1^{\mathrm{L}} \dots V_n^{\mathrm{L}}} = \left(\prod_{k=1}^{n} \mathrm{i}^{(1-Q'_{V_k})} \right) \mathcal{M}^{\varphi_1 \dots \varphi_m \Phi_1 \dots \Phi_n}, \tag{2.37}$$

in the high-energy limit. Here Φ_k is the Goldstone boson corresponding to the gauge boson V_k. The charges Q'_{V_k} of the gauge bosons are considered to be incoming. However, the longitudinal gauge bosons represent the physical states which are measured in a detector. Especially in the case of the Born cross section in DPA it is more convenient to use the matrix elements including longitudinal gauge bosons. For this reason we decided to consequently only use the physical matrix elements. We can now use this to express the matrix elements involving scalars in the leading-logarithmic electroweak corrections by matrix elements with longitudinal gauge bosons. In this work all matrix elements with external would-be Goldstone-bosons are used as shorthands for matrix elements with external longitudinal gauge bosons:

$$\mathcal{M}_{f_1 f_2 \to \Phi_1 \Phi_2} = \mathrm{i}^{(Q'_{V_1}-1)} \mathrm{i}^{(Q'_{V_2}-1)} \mathcal{M}_{f_1 f_2 \to V_1^{\mathrm{L}} V_2^{\mathrm{L}}}, \tag{2.38}$$

$$\mathcal{M}_{f_1 f_2 \to H \Phi} = \mathrm{i}^{(Q'_{V}-1)} \mathcal{M}_{f_1 f_2 \to H V^{\mathrm{L}}}. \tag{2.39}$$

Due to the coupling of the Z boson to the Higgs boson H and the would-be Goldstone boson χ, matrix elements describing the production of Higgs bosons also become relevant and must be included. Again we use the physical longitudinal state of the gauge boson to calculate the matrix element for

Higgs-boson production

$$\begin{aligned}\mathcal{M}_{f_1f_2\to \mathrm{HV}^\mathrm{L}} = {} & \frac{\mathrm{i}e^2}{s-M_V^2} C_{V\mathrm{H}V} \\ & \times \Big[\delta_{\sigma 1}\delta_{\tau 1} C^+_{f_1V}\Big(\lambda_1 \langle p_1 n_1\rangle^* \langle p_2 n_1\rangle - \lambda_2 \langle p_1 n_2\rangle^* \langle p_2 n_2\rangle\Big) \\ & + \delta_{\sigma 2}\delta_{\tau 2} C^-_{f_1V}\Big(\lambda_1 \langle p_2 n_1\rangle^* \langle p_1 n_1\rangle - \lambda_2 \langle p_2 n_2\rangle^* \langle p_1 n_2\rangle\Big)\Big] \end{aligned} \tag{2.40}$$

with $V = \mathrm{W}^\pm, \mathrm{Z}$ and λ_i, n_i calculated from the momentum of the involved gauge boson.

The decay of a gauge boson was treated in the same way as the contributions given in (2.33). Here the generic matrix element is given by

$$\mathcal{M}'_{V\to f_1f_2} = \mathrm{i}e\left(\delta_{\sigma 1}\delta_{\tau 1} C^+_{Vf_1f_2} \langle p_1\phi\rangle^* \langle p_2\psi\rangle + \delta_{\sigma 2}\delta_{\tau 2} C^-_{Vf_1f_2} \langle p_2\phi\rangle^* \langle p_1\psi\rangle\right). \tag{2.41}$$

Again the physical matrix element is obtained by inserting the proper polarization vector given in (2.29).

2.2.2 Construction of $|\mathcal{M}^{\mathrm{DPA}}_{\mathrm{Born}}|^2$

In general two possibilities exist to group the final-state particles into fermion–antifermion pairs. For both possibilities different momenta k_1 and k_2 for the on-shell projected gauge bosons must be constructed (see chapter 1.4.2). We denote these fermion pairs by $(f_{i_3}, \bar{f}_{i_4})$ and $(f_{i_5}, \bar{f}_{i_6})$ and the sum over these possibilities as $\sum_{(f_{i_3},\bar{f}_{i_4})}$. For the DPA matrix elements depending on the on-shell projection we introduce

$$\begin{aligned}\mathcal{M}^{\mathrm{DPA}}_{\mathrm{Born}}(f_{i_3}, \bar{f}_{i_4}) = {} & \sum_{\tau_1,\tau_2} \mathcal{M}_{f_1f_2\to V_1^{\tau_1}V_2^{\tau_2}}(f_{i_3}, \bar{f}_{i_4}) P_{V_1,(f_{i_3}\bar{f}_{i_4})} P_{V_2,(f_{i_5}\bar{f}_{i_6})} \\ & \times \mathcal{M}_{V_1^{\tau_1}\to f_{i_3}\bar{f}_{i_4}} \mathcal{M}_{V_2^{\tau_2}\to f_{i_5}\bar{f}_{i_6}} \end{aligned} \tag{2.42}$$

with the gauge-boson propagators defined as

$$P_{V,(f_i,\bar{f}_j)} = \frac{\mathrm{i}}{k^2 - M_V^2 + \mathrm{i}M_V\Gamma_V}. \tag{2.43}$$

The momentum k is given by the sum of the fermion momenta p_{i_3} and p_{i_4}. For the width Γ_{V_j} of the gauge boson we use a fixed quantity.

In the squared Born matrix element in DPA we have to take the sum over all possible particle pairs $(f_{i_3}, \bar{f}_{i_4})$ for the on-shell projection

$$|\mathcal{M}^{\mathrm{DPA}}_{\mathrm{Born}}|^2 = \frac{N_{\mathrm{colour}}}{4N_{\mathrm{av}}N_{\mathrm{perm}}} \sum_{\sigma_1,\ldots,\sigma_6} \left| \sum_{(f_{i_3},\bar{f}_{i_4})} \mathcal{M}^{\mathrm{DPA}}_{\mathrm{Born}}(f_{i_3}, \bar{f}_{i_4}) \right|^2 , \tag{2.44}$$

where the sum over $\sigma_1, \ldots, \sigma_6$ is the sum over the fermion helicities.

Chapter 3

Virtual corrections

3.1 Definition of the contributions

The virtual corrections are completely given in DPA. We distinguish between corrections from the gauge-boson production and the gauge-boson decay and the non-factorizable corrections. In DPA the next-to-leading-order matrix element is

$$\begin{aligned}\delta\mathcal{M}^{\rm NLO}_{\rm virt}(f_{i_3},\bar{f}_{i_4}) &= \delta\mathcal{M}^{\rm DPA}_{\rm production}(f_{i_3},\bar{f}_{i_4})+\delta\mathcal{M}^{\rm DPA}_{\rm decay}(f_{i_3},\bar{f}_{i_4}) \\ &\quad +\delta\mathcal{M}^{\rm DPA}_{\rm non-fac}(f_{i_3},\bar{f}_{i_4}) \qquad (3.1)\end{aligned}$$

with the subcontributions given by

$$\begin{aligned}\delta\mathcal{M}^{\rm DPA}_{\rm production}(f_{i_3},\bar{f}_{i_4}) &= \sum_{\tau_1,\tau_2}\delta\mathcal{M}_{f_1f_2\to V_1^{\tau_1}V_2^{\tau_2}}(f_{i_3},\bar{f}_{i_4})P_{V_1,(f_{i_3}\bar{f}_{i_4})}P_{V_2,(f_{i_5}\bar{f}_{i_6})} \\ &\quad \times\mathcal{M}_{V_1^{\tau_1}\to f_{i_3}\bar{f}_{i_4}}\mathcal{M}_{V_2^{\tau_2}\to f_{i_5}\bar{f}_{i_6}}, \qquad (3.2)\\ \delta\mathcal{M}^{\rm DPA}_{\rm decay}(f_{i_3},\bar{f}_{i_4}) &= \sum_{\tau_1,\tau_2}\mathcal{M}_{f_1f_2\to V_1^{\tau_1}V_2^{\tau_2}}(f_{i_3},\bar{f}_{i_4})P_{V_1,(f_{i_3}\bar{f}_{i_4})}P_{V_2,(f_{i_5}\bar{f}_{i_6})} \\ &\quad \times\Big(\delta\mathcal{M}_{V_1^{\tau_1}\to f_{i_3}\bar{f}_{i_4}}\mathcal{M}_{V_2^{\tau_2}\to f_{i_5}\bar{f}_{i_6}} \\ &\quad +\mathcal{M}_{V_1^{\tau_1}\to f_{i_3}\bar{f}_{i_4}}\delta\mathcal{M}_{V_2^{\tau_2}\to f_{i_5}\bar{f}_{i_6}}\Big), \qquad (3.3)\\ \delta\mathcal{M}^{\rm DPA}_{\rm non-fac}(f_{i_3},\bar{f}_{i_4}) &= \frac{1}{2}\delta^{\rm non-fac}_{(f_{i_3},\bar{f}_{i_4})}\mathcal{M}^{\rm DPA}_{\rm Born}(f_{i_3},\bar{f}_{i_4}). \qquad (3.4)\end{aligned}$$

The one-loop matrix element $\delta\mathcal{M}_{f_1f_2\to V_1^{\tau_1}V_2^{\tau_2}}$ for the gauge-boson production process is evaluated in chapter 3.2 and the matrix elements $\delta\mathcal{M}_{V_i^{\tau_i}\to f_{j_1}f_{j_2}}$ for the decay of gauge-bosons in next-to-leading order are given in chapter

3.3. The factor $\delta^{\mathrm{non-fac}}_{(f_{i_3},\bar{f}_{i_4})}$ from the non-factorizable corrections is given in chapter 3.4. All corrections were calculated in leading-logarithmic approximation.

The contribution to the total cross section coming from the virtual corrections reads

$$\begin{aligned} \mathrm{d}\sigma_{\mathrm{virt}} &= \frac{1}{2\hat{s}}\frac{N_{\mathrm{colour}}}{4N_{\mathrm{av}}N_{\mathrm{perm}}}\sum_{\sigma_1,\ldots,\sigma_6} 2\mathrm{Re}\Bigg\{\Bigg(\sum_{(f_{i_3},\bar{f}_{i_4})}\mathcal{M}^{\mathrm{NLO}}_{\mathrm{virt}}(f_{i_3},\bar{f}_{i_4})\Bigg) \\ &\quad\times\Bigg(\sum_{(f_{i_3},\bar{f}_{i_4})}\mathcal{M}^{\mathrm{DPA}}_{\mathrm{Born}}(f_{i_3},\bar{f}_{i_4})\Bigg)^*\Bigg\}, \end{aligned} \tag{3.5}$$

The combinatorial factors N_{colour}, N_{av}, and N_{perm} have been explained in (2.8).

3.2 Corrections to gauge-boson production

At energies large compared to the electroweak scale ($\sqrt{s} \gg M_{\mathrm{W}}$) the leading contributions to the electroweak radiative corrections emerge from terms proportional to $\alpha\log^2(s/M^2_{\mathrm{W}})$, known as Sudakov logarithms [29], and terms proportional to $\alpha\log(s/M^2_{\mathrm{W}})$. We call the quadratic logarithms leading and the single logarithms next-to-leading. All these terms only depend on tree-level amplitudes and on the particles on the external legs. In this sense they are universal for all processes. The leading-logarithmic electroweak corrections to the production of two gauge bosons have been evaluated by Stefano Pozzorini and Ansgar Denner [30]. They can be written in the form

$$\delta\mathcal{M} = \delta^{\mathrm{LSC}}\mathcal{M} + \delta^{\mathrm{SSC}}\mathcal{M} + \delta^{\mathrm{C}}\mathcal{M} + \delta^{\mathrm{PR}}\mathcal{M}. \tag{3.6}$$

Here δ^{LSC} denotes the contribution of leading soft-collinear corrections and $\delta^{\mathrm{SSC}}\mathcal{M}$ denotes the contribution of the next-to-leading soft-collinear corrections that are angular-dependent. The term $\delta^{\mathrm{C}}\mathcal{M}$ contains the collinear logarithms and the logarithms related to the renormalization of the incoming and outgoing fields. Finally $\delta^{\mathrm{PR}}\mathcal{M}$ are the logarithmic corrections that arise due to parameter renormalization.

The different contributions to the corrections include UV-divergent terms. These divergent terms can be regularized by dimensional regularization. Using D instead of 4 dimensions brings in a regularization mass μ which cancels if all contributions to the virtual corrections are summed. In order to avoid large logarithms related to μ we set $\mu^2 = s$ in all following correction terms. The IR-divergences are regularized by introducing a mass $M_\gamma = \lambda$ for the photon.

3.2.1 Leading soft-collinear corrections

If we denote a matrix element with n external particles $\varphi_1 \dots \varphi_n$ with $\mathcal{M}^{\varphi_1 \cdots \varphi_n}$ and the Born matrix element to this process by $\mathcal{M}_0^{\varphi_1 \cdots \varphi_n}$ the leading soft-collinear terms factorize in the following form

$$\delta^{\mathrm{LSC}} \mathcal{M}^{\varphi_1 \cdots \varphi_n} = \sum_{k=1}^{n} \sum_{\varphi_k'} \delta^{\mathrm{LSC}}_{\varphi_k' \varphi_k} \mathcal{M}_0^{\varphi_1 \cdots \varphi_k' \cdots \varphi_n} \tag{3.7}$$

with

$$\delta^{\mathrm{LSC}}_{\varphi_k' \varphi_k} = -\frac{\alpha}{8\pi} C^{\mathrm{ew}}_{\varphi_k' \varphi_k} \log^2\left(\frac{s}{M_{\mathrm{W}}^2}\right) + \delta_{\varphi_k' \varphi_k} \left\{ \frac{\alpha}{4\pi} (I^Z)^2_{\varphi_k} \log\left(\frac{s}{M_{\mathrm{W}}^2}\right) \log\left(\frac{M_{\mathrm{Z}}^2}{M_{\mathrm{W}}^2}\right) - \frac{1}{2} Q^2_{\varphi_k} L^{\mathrm{em}}(s, \lambda^2, M^2_{\varphi_k}) + \delta^{\mathrm{LSC,h}}_{\varphi_k} \right\}. \tag{3.8}$$

The explicit values of the constants $C^{\mathrm{ew}}_{\varphi_k' \varphi_k}$ and $(I^Z)^2_{\varphi_k}$ can be found in appendix A.2. The term L^{em} contains all logarithms of pure electromagnetic origin. It is defined by

$$L^{\mathrm{em}}(s, \lambda^2, M_\varphi^2) := \frac{\alpha}{4\pi} \left\{ 2 \log\left(\frac{s}{M_{\mathrm{W}}^2}\right) \log\left(\frac{M_{\mathrm{W}}^2}{\lambda^2}\right) + \log^2\left(\frac{M_{\mathrm{W}}^2}{\lambda^2}\right) - \log^2\left(\frac{M_\varphi^2}{\lambda^2}\right) \right\}. \tag{3.9}$$

There are additional logarithms, denoted by $\delta^{\mathrm{LSC,h}}_{\varphi_k}$, that only occur if one of the external particles φ_k is a heavy quark like t, b or a Higgs boson H or a longitudinal gauge boson. Since we consider all external fermions as massless these terms are only taken into account for longitudinal gauge bosons. Since longitudinal gauge bosons are replaced by their corresponding Goldstone-bosons, these terms read

$$\delta^{\mathrm{LSC,h}}_{\chi} = \frac{\alpha}{4\pi} \frac{1}{4 s_{\mathrm{w}}^2 c_{\mathrm{w}}^2} \log^2\left(\frac{M_{\mathrm{H}}^2}{M_{\mathrm{Z}}^2}\right), \tag{3.10}$$

$$\delta^{\mathrm{LSC,h}}_{\mathrm{H}} = \frac{\alpha}{4\pi} \left[\frac{1}{4 s_{\mathrm{w}}^2 c_{\mathrm{w}}^2} \log^2\left(\frac{M_{\mathrm{H}}^2}{M_{\mathrm{Z}}^2}\right) + \frac{1}{2 s_{\mathrm{w}}^2} \log^2\left(\frac{M_{\mathrm{H}}^2}{M_{\mathrm{W}}^2}\right) \right], \tag{3.11}$$

$$\delta^{\mathrm{LSC,h}}_{\phi^\pm} = \frac{\alpha}{4\pi} \frac{1}{4 s_{\mathrm{w}}^2} \log^2\left(\frac{M_{\mathrm{H}}^2}{M_{\mathrm{W}}^2}\right). \tag{3.12}$$

In terms of the gauge-boson production process this gives for transverse gauge bosons

$$\begin{aligned}\delta^{\mathrm{LSC}}\mathcal{M}_{f_1f_2\to V_1^{\mathrm{T}}V_2^{\mathrm{T}}}(f_{i_3},\bar{f}_{i_4}) &= \left(\delta^{\mathrm{LSC}}_{f_1f_1}+\delta^{\mathrm{LSC}}_{f_2f_2}+\delta^{\mathrm{LSC}}_{V_1V_1}+\delta^{\mathrm{LSC}}_{V_2V_2}\right)\\ &\quad\times\mathcal{M}_{f_1f_2\to V_1^{\mathrm{T}}V_2^{\mathrm{T}}}(f_{i_3},\bar{f}_{i_4})\\ &\quad+\delta_{V_1Z}\delta^{\mathrm{LSC}}_{AV_1}\mathcal{M}_{f_1f_2\to AV_2^{\mathrm{T}}}(f_{i_3},\bar{f}_{i_4})\\ &\quad+\delta_{V_2Z}\delta^{\mathrm{LSC}}_{AV_2}\mathcal{M}_{f_1f_2\to V_1^{\mathrm{T}}A}(f_{i_3},\bar{f}_{i_4}),\end{aligned}\tag{3.13}$$

and for longitudinal gauge bosons

$$\begin{aligned}\delta^{\mathrm{LSC}}\mathcal{M}_{f_1f_2\to V_1^{\mathrm{L}}V_2^{\mathrm{L}}}(f_{i_3},\bar{f}_{i_4}) &= \left(\delta^{\mathrm{LSC}}_{f_1f_1}+\delta^{\mathrm{LSC}}_{f_2f_2}+\delta^{\mathrm{LSC}}_{\Phi_1\Phi_1}+\delta^{\mathrm{LSC}}_{\Phi_2\Phi_2}\right)\\ &\quad\times\mathcal{M}_{f_1f_2\to\Phi_1\Phi_2}(f_{i_3},\bar{f}_{i_4}),\end{aligned}\tag{3.14}$$

where Φ_1 and Φ_2 denote the Goldstone bosons corresponding to V_1^{L} and V_2^{L}, respectively.

3.2.2 Subleading soft-collinear corrections

The subleading soft–collinear corrections contain angular-dependent terms. Their general form therefore must be written as a sum over pairs of external legs

$$\delta^{\mathrm{SSC}}\mathcal{M}^{\varphi_1\dots\varphi_n}=\sum_{k=1}^{n}\sum_{l<k}\sum_{V^a=A,\mathrm{Z},\mathrm{W}^\pm}\sum_{\varphi'_k,\varphi'_l}\delta^{V^a,\mathrm{SSC}}_{\varphi'_k\varphi_k\varphi'_l\varphi_l}\mathcal{M}_0^{\varphi_1\dots\varphi'_l\dots\varphi'_k\dots\varphi_n}.\tag{3.15}$$

In the case of two incoming fermions f_1, f_2 and two outgoing gauge bosons V_1, V_2 this correction can be written as

$$\begin{aligned}\delta^{\mathrm{SSC}}\mathcal{M}_{f_1f_2\to V_1V_2} &= \frac{\alpha}{2\pi}\sum_{V=A,\mathrm{Z},\mathrm{W}^\pm}\sum_{f',V'}\left[\log\left(\frac{s}{M_{\mathrm{W}}^2}\right)+\log\left(\frac{M_{\mathrm{W}}^2}{M_V^2}\right)\right]\\ &\quad\times\left\{\log\left(\frac{|t|}{s}\right)\left[C_{\bar{V}\bar{f}'f_1}C_{VV'\bar{V}_1}\mathcal{M}_{f'f_2\to V'V_2}+C_{\bar{V}\bar{f}'f_2}C_{VV'\bar{V}_2}\mathcal{M}_{f_1f'\to V_1V'}\right]\right.\\ &\quad\left.+\log\left(\frac{|u|}{s}\right)\left[C_{\bar{V}\bar{f}'f_1}C_{VV'\bar{V}_2}\mathcal{M}_{f'f_2\to V_1V'}+C_{\bar{V}\bar{f}'f_2}C_{VV'\bar{V}_1}\mathcal{M}_{f_1f'\to V'V_2}\right]\right\},\end{aligned}\tag{3.16}$$

with $s=(p_1+p_2)^2$, $t=(p_1-k_1)^2$, and $u=(p_1-k_2)^2$. The symbol $\bar{V}$ denotes the anti-particle of the gauge boson V. The Couplings $C_{\bar{V}\bar{f}'f_i}$ and $C_{V_1V_2\bar{V}_3}$ are given in appendix A.1. Note that in order to use these couplings in the form they are given here or in Ref. [28] the particle f_i must be a fermion. If

f_i is an anti-fermion the coupling must be complex conjugated and gets an additional factor of -1. The same holds for the coupling $C_{V_1V_2\bar{V}_3}$ which is antisymmetric in the three indices V_1, V_2 and $\bar{V}_3$. Here V_1 must be a neutral particle and V_2, V_3 a particle–anti-particle pair in order to use the formula in Ref. [28].

In case of the exchange of a neutral gauge boson in the loop the quantum numbers of the emitting fermion f_i in the initial state and the quantum numbers of the corresponding gauge boson V_j in the final state are not changed and $f' = f_i$ and $V' = V_j$. In the case of $V = \mathrm{W}^\pm$ there is only a contribution if f' has the opposite isospin as f_i and V' is the gauge boson with the matching charge for the process. When we have a diagonal CKM matrix and f_i' denotes the isospin partner of f_i and V_i' substitutes V_i the sum over f' and V' can be carried out and we get for neutral gauge bosons V in the loop and transverse gauge bosons in the final state

$$\begin{aligned}\delta^{\mathrm{SSC}}_{\mathrm{neutral}}\mathcal{M}_{f_1f_2\to V_1^{\mathrm{T}}V_2^{\mathrm{T}}} = \frac{\alpha}{2\pi}\sum_{V=A,Z}\left[\log\left(\frac{s}{M_{\mathrm{W}}^2}\right)+\log\left(\frac{M_{\mathrm{W}}^2}{M_V^2}\right)\right]\\ \times\Bigg\{\log\left(\frac{|t|}{s}\right)\left[C_{\bar{V}\bar{f}_1f_1}C_{VV_1\bar{V}_1}+C_{\bar{V}\bar{f}_2f_2}C_{VV_2\bar{V}_2}\right]\\ +\log\left(\frac{|u|}{s}\right)\left[C_{\bar{V}\bar{f}_1f_1}C_{VV_2\bar{V}_2}+C_{\bar{V}\bar{f}_2f_2}C_{VV_1\bar{V}_1}\right]\Bigg\}\mathcal{M}_{f_1f_2\to V_1^{\mathrm{T}}V_2^{\mathrm{T}}}\end{aligned} \tag{3.17}$$

and for charged gauge bosons V in the loop and transverse gauge bosons in the final state

$$\begin{aligned}\delta^{\mathrm{SSC}}_{\mathrm{charged}}\mathcal{M}_{f_1f_2\to V_1^{\mathrm{T}}V_2^{\mathrm{T}}} &= \frac{\alpha}{2\pi}\sum_{V=\mathrm{W}^\pm}\log\left(\frac{s}{M_{\mathrm{W}}^2}\right)\\ &\quad\times\Bigg\{\log\left(\frac{|t|}{s}\right)\sum_{f_1'}C_{\bar{V}\bar{f}_1'f_1}C_{VV_1'\bar{V}_1}\mathcal{M}_{f_1'f_2\to V_1^{\mathrm{T}\prime}V_2^{\mathrm{T}}}\\ &\quad+\log\left(\frac{|t|}{s}\right)\sum_{f_2'}C_{\bar{V}\bar{f}_2'f_2}C_{VV_2'\bar{V}_2}\mathcal{M}_{f_1f_2'\to V_1^{\mathrm{T}}V_2^{\mathrm{T}\prime}}\\ &\quad+\log\left(\frac{|u|}{s}\right)\sum_{f_1'}C_{\bar{V}\bar{f}_1'f_1}C_{VV_2'\bar{V}_2}\mathcal{M}_{f_1'f_2\to V_1^{\mathrm{T}}V_2^{\mathrm{T}\prime}}\\ &\quad+\log\left(\frac{|u|}{s}\right)\sum_{f_2'}C_{\bar{V}\bar{f}_2'f_2}C_{VV_1'\bar{V}_1}\mathcal{M}_{f_1f_2'\to V_1^{\mathrm{T}\prime}V_2^{\mathrm{T}}}\Bigg\}.\end{aligned} \tag{3.18}$$

The sums over the particles f_1' and f_2' only include particles which couple via a W boson to f_1 or f_2, respectively. The corrections to longitudinal

gauge bosons are treated using the Goldstone-boson equivalence theorem, i.e. all longitudinal gauge bosons are replaced by the corresponding Goldstone bosons ($\mathrm{Z} \to \chi, \mathrm{W}^\pm \to \phi^\pm$). Due to the $\mathrm{ZH}\chi$ coupling matrix elements including a Higgs boson in the final state also contribute. In this case the two contributions to δ^{SSC} read

$$\begin{aligned}
\delta^{\mathrm{SSC}}_{\mathrm{neutral}}\mathcal{M}_{f_1f_2\to V_1^{\mathrm{L}}V_2^{\mathrm{L}}} &= \mathrm{i}^{((1-Q_{V_1})+(1-Q_{V_2}))}\delta^{\mathrm{SSC}}_{\mathrm{neutral}}\mathcal{M}_{f_1f_2\to S_1S_2} \\
&= \mathrm{i}^{((1-Q_{V_1})+(1-Q_{V_2}))}\frac{\alpha}{2\pi}\sum_{V=A,Z}\sum_{S'=\chi,\mathrm{H},\phi^\pm}\left[\log\left(\frac{s}{M_{\mathrm{W}}^2}\right)+\log\left(\frac{M_{\mathrm{W}}^2}{M_V^2}\right)\right] \\
&\times\left\{\log\left(\frac{|t|}{s}\right)\left[-C_{\bar{V}\bar{f}_1f_1}C_{VS'\bar{S}_1}\mathcal{M}_{f_1f_2\to S'S_2}-C_{\bar{V}\bar{f}_2f_2}C_{VS'\bar{S}_2}\mathcal{M}_{f_1f_2\to S_1S'}\right]\right. \\
&\left.+\log\left(\frac{|u|}{s}\right)\left[-C_{\bar{V}\bar{f}_1f_1}C_{VS'\bar{S}_2}\mathcal{M}_{f_1f_2\to S_1S'}-C_{\bar{V}\bar{f}_2f_2}C_{VS'\bar{S}_1}\mathcal{M}_{f_1f_2\to S'S_2}\right]\right\},
\end{aligned} \tag{3.19}$$

$$\begin{aligned}
\delta^{\mathrm{SSC}}_{\mathrm{charged}}\mathcal{M}_{f_1f_2\to V_1^{\mathrm{L}}V_2^{\mathrm{L}}} &= \mathrm{i}^{((1-Q_{V_1})+(1-Q_{V_2}))}\delta^{\mathrm{SSC}}_{\mathrm{charged}}\mathcal{M}_{f_1f_2\to S_1S_2} \\
&= \mathrm{i}^{((1-Q_{V_1})+(1-Q_{V_2}))}\frac{\alpha}{2\pi}\sum_{V=\mathrm{W}^\pm}\sum_{S'=\chi,\mathrm{H},\phi^\pm}\log\left(\frac{s}{M_{\mathrm{W}}^2}\right) \\
&\times\left\{-\log\left(\frac{|t|}{s}\right)\sum_{f_1'}C_{\bar{V}\bar{f}_1'f_1}C_{VS'\bar{S}_1}\mathcal{M}_{f_1'f_2\to S'S_2}\right. \\
&-\log\left(\frac{|t|}{s}\right)\sum_{f_2'}C_{\bar{V}\bar{f}_2'f_2}C_{VS'\bar{S}_2}\mathcal{M}_{f_1f_2'\to S_1S'} \\
&-\log\left(\frac{|u|}{s}\right)\sum_{f_1'}C_{\bar{V}\bar{f}_1'f_1}C_{VS'\bar{S}_2}\mathcal{M}_{f_1'f_2\to S_1S'} \\
&\left.-\log\left(\frac{|u|}{s}\right)\sum_{f_2'}C_{\bar{V}\bar{f}_2'f_2}C_{VS'\bar{S}_1}\mathcal{M}_{f_1f_2'\to S'S_2}\right\}
\end{aligned} \tag{3.20}$$

Again in the sums over f_1' and f_2' just particles are taken into account which couple to f_1 or f_2 via a $\mathrm{W}^\pm$ boson.

3.2.3 Collinear Logarithms

In this contribution two different kinds of corrections are summed up. The first are mass-singular logarithms which occur if a virtual gauge boson is emitted collinear to one of the external legs and the second arises from the

renormalization of the asymptotic fields which gives corrections to the particle wave functions and the Goldstone-boson equivalence theorem.

Since the collinear corrections and the corrections due to the renormalization of the wave-functions factorize to the same Born matrix elements we can put these contributions together in one correction factor

$$\delta^{\mathrm{C}}\mathcal{M}^{\varphi_1\dots\varphi_n} = \sum_{k=1}^{n}\sum_{\varphi'}\mathcal{M}_0^{\varphi_1\dots\varphi'_k\dots\varphi_n}\delta^{\mathrm{C}}_{\varphi'_k\varphi_k} \tag{3.21}$$

with

$$\delta^{\mathrm{C}}_{\varphi'_k\varphi_k} = \left(\delta^{\mathrm{WF}}_{\varphi'_k\varphi_k} + \delta^{\mathrm{coll}}_{\varphi'_k\varphi_k}\right)\Big|_{\mu^2=s}. \tag{3.22}$$

In the case of massless fermions on the external legs this contribution is diagonal in f'_k, f_k:

$$\delta^{\mathrm{C}}_{f_\sigma f_\sigma} = \frac{\alpha}{4\pi}\left[\frac{3}{2}C^{\mathrm{ew}}_{f_\sigma}\log\left(\frac{s}{M_{\mathrm{W}}^2}\right) + Q_f^2\left(\frac{1}{2}\log\left(\frac{M_{\mathrm{W}}^2}{m_f^2}\right) + \log\left(\frac{M_{\mathrm{W}}^2}{\lambda^2}\right)\right)\right]. \tag{3.23}$$

For the collinear correction factors to gauge bosons we have to distinguish between transverse and longitudinal gauge bosons. For transverse gauge bosons a mixing between the Z and the photon A exists. Together with the diagonal contribution this gives the five different factors

$$\delta^{\mathrm{C}}_{\mathrm{W^T W^T}} = \frac{\alpha}{4\pi}\left[\frac{19}{12s_{\mathrm{w}}^2}\log\left(\frac{s}{M_{\mathrm{W}}^2}\right) + \log\left(\frac{M_{\mathrm{W}}^2}{\lambda^2}\right) + \frac{M_{\mathrm{W}}^2}{24s_{\mathrm{w}}^2M_{\mathrm{W}}^2}\log\left(\frac{M_{\mathrm{H}}^2}{M_{\mathrm{W}}^2}\right) + \frac{1}{2s_{\mathrm{w}}^2}\log\left(\frac{m_t^2}{M_{\mathrm{W}}^2}\right)\right], \tag{3.24}$$

$$\delta^{\mathrm{C}}_{Z^{\mathrm{T}}Z^{\mathrm{T}}} = \frac{\alpha}{4\pi}\left[\frac{19-38s_{\mathrm{w}}^2-22s_{\mathrm{w}}^4}{12s_{\mathrm{w}}^2c_{\mathrm{w}}^2}\log\left(\frac{s}{M_{\mathrm{W}}^2}\right) + \frac{M_{\mathrm{Z}}^2}{24s_{\mathrm{w}}^2M_{\mathrm{W}}^2}\log\left(\frac{M_{\mathrm{H}}^2}{M_{\mathrm{W}}^2}\right) + \frac{9-24s_{\mathrm{w}}^2+32s_{\mathrm{w}}^4}{36s_{\mathrm{w}}^2c_{\mathrm{w}}^2}\log\left(\frac{m_t^2}{M_{\mathrm{W}}^2}\right)\right], \tag{3.25}$$

$$\delta^{\mathrm{C}}_{AA} = \frac{\alpha}{4\pi}\left[\frac{-11}{6}\log\left(\frac{s}{M_{\mathrm{W}}^2}\right) + \frac{8}{9}\log\left(\frac{m_t^2}{M_{\mathrm{W}}^2}\right) - \frac{1}{2}\Delta\alpha(M_{\mathrm{W}}^2)\right], \tag{3.26}$$

$$\delta^{\mathrm{C}}_{AZ^{\mathrm{T}}} = \frac{\alpha}{4\pi}\left[-\frac{19+22s_{\mathrm{w}}^2}{6s_{\mathrm{w}}c_{\mathrm{w}}}\log\left(\frac{s}{M_{\mathrm{W}}^2}\right) + \frac{16s_{\mathrm{w}}^2-6}{9s_{\mathrm{w}}c_{\mathrm{w}}}\log\left(\frac{m_t^2}{M_{\mathrm{W}}^2}\right)\right], \tag{3.27}$$

$$\delta^{\mathrm{C}}_{Z^{\mathrm{T}}A} \;=\; 0. \tag{3.28}$$

Here

$$\Delta\alpha(M_{\mathrm{W}}^2) = \frac{\alpha}{3\pi}\sum_{f\neq t} N^f_{\mathrm{colour}} Q_f^2 \log\left(\frac{M_{\mathrm{W}}^2}{m_f^2}\right) \tag{3.29}$$

is used to describe the running of α from zero to the electroweak scale. In the case of longitudinal gauge bosons the correction factor is diagonal and the explicit terms for $\mathrm{W}^{\pm}$ and Z read

$$\delta^{\mathrm{C}}_{\mathrm{W^L W^L}} = \frac{\alpha}{4\pi}\left[\frac{1+2c_{\mathrm{w}}^2}{2s_{\mathrm{w}}^2 c_{\mathrm{w}}^2}\log\left(\frac{s}{M_{\mathrm{W}}^2}\right) - \frac{3}{4s_{\mathrm{w}}^2}\frac{m_t^2}{M_{\mathrm{W}}^2}\log\left(\frac{s}{m_t^2}\right) + \log\left(\frac{M_{\mathrm{W}}^2}{\lambda^2}\right) + \frac{M_{\mathrm{W}}^2}{8s_{\mathrm{w}}^2 M_{\mathrm{W}}^2}\log\left(\frac{M_{\mathrm{H}}^2}{M_{\mathrm{W}}^2}\right)\right], \tag{3.30}$$

$$\delta^{\mathrm{C}}_{Z^{\mathrm{L}} Z^{\mathrm{L}}} = \frac{\alpha}{4\pi}\left[\frac{1+2c_{\mathrm{w}}^2}{2s_{\mathrm{w}}^2 c_{\mathrm{w}}^2}\log\left(\frac{s}{M_{\mathrm{W}}^2}\right) - \frac{3}{4s_{\mathrm{w}}^2}\frac{m_t^2}{M_{\mathrm{W}}^2}\log\left(\frac{s}{m_t^2}\right) + \frac{M_{\mathrm{Z}}^2}{8s_{\mathrm{w}}^2 M_{\mathrm{W}}^2}\log\left(\frac{M_{\mathrm{H}}^2}{M_{\mathrm{W}}^2}\right)\right]. \tag{3.31}$$

The contribution to the gauge-boson-production matrix element is in the case of transverse gauge bosons

$$\begin{aligned}\delta^{\mathrm{C}}\mathcal{M}_{f_1f_2\to V_1^{\mathrm{T}}V_2^{\mathrm{T}}} \;=\;& \left(\delta^{\mathrm{C}}_{f_1f_1} + \delta^{\mathrm{C}}_{f_2f_2} + \delta^{\mathrm{C}}_{V_1^{\mathrm{T}}V_1^{\mathrm{T}}} + \delta^{\mathrm{C}}_{V_2^{\mathrm{T}}V_2^{\mathrm{T}}}\right)\mathcal{M}_{f_1f_2\to V_1^{\mathrm{T}}V_2^{\mathrm{T}}} \\ &+\delta_{V_1Z}\delta^{\mathrm{C}}_{AV_1^{\mathrm{T}}}\mathcal{M}_{f_1f_2\to AV_2^{\mathrm{T}}} \\ &+\delta_{V_2Z}\delta^{\mathrm{C}}_{AV_2^{\mathrm{T}}}\mathcal{M}_{f_1f_2\to V_1^{\mathrm{T}}A},\end{aligned} \tag{3.32}$$

and in the case of longitudinal gauge bosons

$$\delta^{\mathrm{C}}\mathcal{M}_{f_1f_2\to V_1^{\mathrm{L}}V_2^{\mathrm{L}}} \;=\; \left(\delta^{\mathrm{C}}_{f_1f_1} + \delta^{\mathrm{C}}_{f_2f_2} + \delta^{\mathrm{C}}_{V_1^{\mathrm{L}}V_1^{\mathrm{L}}} + \delta^{\mathrm{C}}_{V_2^{\mathrm{L}}V_2^{\mathrm{L}}}\right)\mathcal{M}_{f_1f_2\to V_1^{\mathrm{L}}V_2^{\mathrm{L}}} \tag{3.33}$$

3.2.4 Logarithms from Parameter Renormalization

The parameter renormalization gives rise to so-called counterterm diagrams. In dimensional regularization they depend on the parameter μ which has the dimension of a mass. This dependence on μ cancels the contributions from the loop diagrams, because this dependence is directly related to the ultraviolet divergences which have to cancel at every loop order. As before we choose $\mu^2 = s$ to avoid large logarithms.

The general form of this contributions to the matrix element $\mathcal{M}$ is given by

$$\delta^{\mathrm{PR}}\mathcal{M}^{\varphi_1\ldots\varphi_n} = \sum_{\lambda_i} \frac{\partial \mathcal{M}_0^{\varphi_1\ldots\varphi_n}}{\partial\lambda_i}\delta\lambda_i\bigg|_{\mu^2=s} \tag{3.34}$$

where the different parameters are denoted by λ_i and their counterterms by $\delta\lambda_i = \lambda_{i,0} - \lambda_i$. The counterterms depend on the explicit renormalization conditions which determines a set of independent parameters. We here choose the set

$$\lambda_i = e, c_{\mathrm{w}}, h_{\mathrm{H}}, h_t, \tag{3.35}$$

which are the electrical charge e, the cosine of the Weinberg angle $c_{\mathrm{w}} = M_{\mathrm{W}}/M_{\mathrm{Z}}$ and the two mass ratios $h_{\mathrm{H}} = M_{\mathrm{H}}^2/M_{\mathrm{W}}^2$ and $h_t = m_t/M_{\mathrm{W}}$. We want to apply this to the production of two gauge bosons where the Born amplitude can be written as

$\mathcal{M}_{f_1f_2\to V_1^TV_2^T} =$ 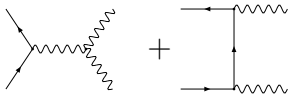 (3.36)

for the transverse gauge bosons and

$\mathcal{M}_{f_1f_2\to V_1^LV_2^L} = \mathrm{i}^{(1-Q_{V_1})+(1-Q_{V_2})}$ 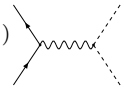 (3.37)

for longitudinal gauge bosons. The counterterm diagrams therefore can be expressed via

$\mathcal{M}^{\mathrm{counterterm}}_{f_1f_2\to V_1^TV_2^T} =$ 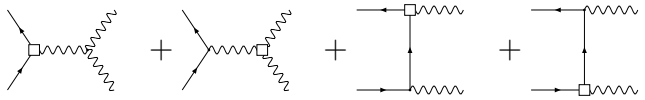 (3.38)

and

$\mathcal{M}^{\mathrm{counterterm}}_{f_1f_2\to V_1^LV_2^L} = \mathrm{i}^{(1-Q_{V_1})+(1-Q_{V_2})}$ 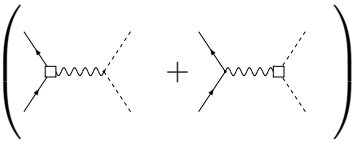 . (3.39)

The small box $\square$ denotes the counterterm coupling to the coupling $ieC_{\varphi_1\varphi_2\varphi_3}$ which is defined as

$$\begin{aligned}\square &= \sum_{\lambda_i}\left(\frac{\partial}{\partial\lambda_i} ieC_{\varphi_1\varphi_2\varphi_3}\right)\delta\lambda_i \\ &= \left(\mathrm{i}eC_{\varphi_1\varphi_2\varphi_3}\right)\frac{\delta e}{e} + \left(\mathrm{i}e\frac{\partial C_{\varphi_1\varphi_2\varphi_3}}{\partial c_{\mathrm{w}}}\right)\delta c_{\mathrm{w}}.\end{aligned} \tag{3.40}$$

Here only derivatives with respect to e and c_w are taken, because none of the couplings which occur in the considered processes depends on the mass ratios h_H or h_t. For the renormalized electric charge the counterterm is given by

$$\frac{\delta e}{e} = \frac{1}{2}\left[-\frac{\alpha}{4\pi}\left(-\frac{11}{3}\right)\log\left(\frac{s}{M_\mathrm{W}^2}\right)+\Delta\alpha(M_\mathrm{W}^2)\right]. \tag{3.41}$$

and for the cosine of the Weinberg angle we get the counterterm

$$\frac{\delta c_\mathrm{w}^2}{c_\mathrm{w}^2} = \frac{\alpha}{4\pi}\left[\frac{s_\mathrm{w}}{c_\mathrm{w}}\left(-\frac{19+22s_\mathrm{w}^2}{6s_\mathrm{w}c_\mathrm{w}}\right)\log\left(\frac{s}{M_\mathrm{W}^2}\right)+\frac{5}{6c_\mathrm{w}^2}\log\left(\frac{M_\mathrm{H}^2}{M_\mathrm{W}^2}\right)\right.$$
$$\left.-\frac{9+6s_\mathrm{w}^2-32s_\mathrm{w}^4}{18s_\mathrm{w}^2c_\mathrm{w}^2}\log\left(\frac{m_t^2}{M_\mathrm{W}^2}\right)\right]. \tag{3.42}$$

Finally δc_w is given by

$$\delta c_\mathrm{w} = \frac{1}{2}\frac{\delta c_\mathrm{w}^2}{c_\mathrm{w}}. \tag{3.43}$$

3.3 Corrections to gauge-boson decay

The radiative corrections to the gauge-boson decay yield no large logarithms from Z or $\mathrm{W}^\pm$ exchange in loop diagrams. Hence it is sufficient to take only the photonic part of the one-loop corrections into account. For massless fermions this correction turns out to be proportional to the Born matrix element. The correction is therefore given as a factor $\delta_{\mathrm{Z}f\bar{f}}$, $\delta_{\mathrm{W}f_1f_2}$ for the decay of a Z boson or a W boson, respectively. The matrix element for the decay in leading-logarithmic approximation is

$$\delta\mathcal{M}_{V^\tau\to f\bar{f}} = \delta_{Vf\bar{f}}\mathcal{M}_{V^\tau\to f\bar{f}} \tag{3.44}$$

with the correction factors given in the leading logarithmic approximation for $V=\mathrm{Z}$ and $V=\mathrm{W}^\pm$ by

$$\delta_{\mathrm{Z}f\bar{f}} = \frac{\alpha}{4\pi}Q_f^2\left[-2\log\frac{\lambda^2}{m_f^2}+\log^2\frac{m_f^2}{\lambda^2}-\log^2\frac{M_\mathrm{Z}^2}{\lambda^2}+3\log\frac{M_\mathrm{Z}^2}{m_f^2}\right]$$
$$+\frac{1}{2}\Delta\alpha(M_\mathrm{Z}^2), \tag{3.45}$$

$$\delta_{\mathrm{W}f_1\bar{f}_2} = \frac{\alpha}{4\pi}\left[-\frac{1}{2}(Q_{f_1}^2+Q_{f_2}^2)\log^2\frac{M_\mathrm{W}^2}{\lambda^2}+\frac{1}{2}Q_{f_1}^2\log^2\frac{m_{f_1}^2}{\lambda^2}+\frac{1}{2}Q_{f_2}^2\log^2\frac{m_{f_2}^2}{\lambda^2}\right.$$
$$+(Q_{f_2}-Q_{f_1})^2\log\frac{M_\mathrm{W}^2}{\lambda^2}+Q_{f_1}^2\log\frac{m_{f_1}^2}{\lambda^2}+Q_{f_2}^2\log\frac{m_{f_2}^2}{\lambda^2}$$
$$\left.+\frac{3}{2}Q_{f_1}^2\log\frac{M_\mathrm{W}^2}{m_{f_1}^2}+\frac{3}{2}Q_{f_2}^2\log\frac{M_\mathrm{W}^2}{m_{f_2}^2}\right]+\frac{1}{2}\Delta\alpha(M_\mathrm{W}^2). \tag{3.46}$$

3.4 Non-factorizable corrections

The non-factorizable corrections arise from the Feynman diagrams shown in figure 3.1. The explicit form of these corrections is given in Refs. [19, 31, 32]. The non-factorizable corrections are calculated in the leading-logarithmic ap-

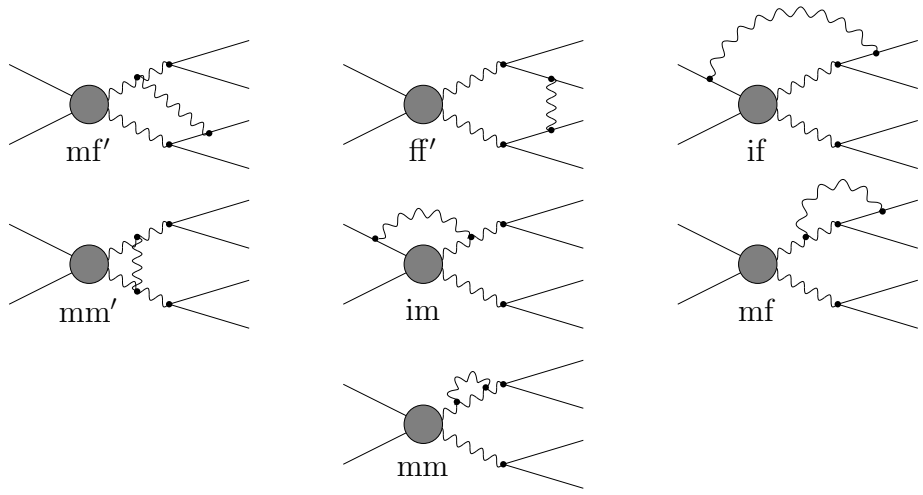

Figure 3.1: Diagrams contributing to the non-factorizable corrections

proximation. They only include photonic contributions. The non-factorizable photonic corrections are proportional to the lowest-order cross-section in DPA. Therefore the factor $\delta^{\rm virt}_{\rm nfact}$ given in formula (3.5) is

$$\delta^{\rm non-fac}_{\rm virt} = \frac{\alpha}{\pi}{\rm Re}\left[\Delta^{\rm virt}_{\rm mf'}+\Delta^{\rm virt}_{\rm ff'}+\Delta^{\rm virt}_{\rm if}+\Delta^{\rm virt}_{\rm mm'}+\Delta^{\rm virt}_{\rm im}+\Delta^{\rm virt}_{\rm mf}+\Delta^{\rm virt}_{\rm mm}\right] \tag{3.47}$$

where the corrections contained in $\Delta^{\rm virt}_{\rm mf'}$, $\Delta^{\rm virt}_{\rm ff'}$, $\Delta^{\rm virt}_{\rm if}$, $\Delta^{\rm virt}_{\rm mm'}$, $\Delta^{\rm virt}_{\rm im}$, $\Delta^{\rm virt}_{\rm mf}$ and $\Delta^{\rm virt}_{\rm mm}$ arise from diagrams of the seven different types shown in figure 3.1. The actual expressions for these terms can be found in Appendix B.2. Using the abbreviations Δ_1 and Δ_2 and conservation of charge we can put the non-factorizable corrections in the form

$$\begin{aligned}\delta^{\rm non-fac}_{\rm virt} = \frac{\alpha}{\pi}\Bigg(&-\sum_{i=3}^{4}\sum_{j=5}^{6}Q_iQ_j\theta_d(i)\theta_d(j){\rm Re}\{\Delta_1(k_1,p_i,k_2,p_j)\}\\ &+\sum_{n=1}^{2}\sum_{i=3}^{4}Q_nQ_i\theta_d(n)\theta_d(i){\rm Re}\{\Delta_2(p_n,k_1,p_i)\}\\ &+\sum_{n=1}^{2}\sum_{j=5}^{6}Q_nQ_j\theta_d(n)\theta_d(j){\rm Re}\{\Delta_2(p_n,k_2,p_j)\}\Bigg).\end{aligned} \tag{3.48}$$

Here we used the functions θ_d to determine the correct sign. The function $\theta_d(i)$ is defined to be 1 if the line of the fermion i points towards the diagram and -1 otherwise. We denote the momenta of fermions with $p_1 \dots p_6$ and the momenta of the two gauge bosons with k_1, k_2. In the high-energy limit we assume $M_{\mathrm{W}}^2/s \to 0$, for any kinematical invariant s, which is not fixed to a certain mass value like $s_{34} = (p_3+p_4)^2 = M_V^2$ after on-shell projection. If we apply these simplifications to the non-factorizable corrections we find rather simple expressions for the quantities Δ_1 and Δ_2. Only one loop integral remains which still contains dilogarithms:

$$\begin{aligned}
\Delta_1(k_1,p_i;k_2,p_j) &= \frac{1}{2}(s_{ij}\bar{s} - \hat{s}_{1j}\hat{s}_{2i}) \\
&\quad \times D_0^{\mathrm{he}}(-k_2+p_j, k_1+p_j, p_i+p_j, m_j, M_2, M_1, m_i) \\
&\quad + \log\left(\frac{(k_2^2-\overline{M}_2^2)M_1}{(k_1^2-\overline{M}_1^2)M_2}\right)\log\frac{\hat{s}_{2i}}{\hat{s}_{1j}} \\
&\quad + \left[2+\log\frac{s_{ij}}{\bar{s}}\right]\left[\log\frac{\lambda M_2}{\overline{M}_2^2-k_2^2} + \log\frac{\lambda M_1}{\overline{M}_1^2-k_1^2}\right] \qquad (3.49) \\
\Delta_2(p_n,k_l,p_j) &= 2\log\frac{\lambda M_l}{\overline{M}_l^2-k_l^2}\left[\log\frac{\hat{t}_{nl}}{t_{nj}} - 1\right]. \qquad (3.50)
\end{aligned}$$

The invariants are defined as $\hat{s}_{nj} = (k_n+p_j)^2$, $\hat{t}_{ij} = (k_i-p_j)^2$, $s_{ij} = (p_i+p_j)^2$, $t_{ij} = (p_i-p_j)^2$ and $\bar{s} = s_{12} = (p_1+p_2)^2$ and have to be calculated using the appropriate on-shell projected momenta. For the calculation of the D_0^{he} function also the on-shell projected momenta have to be used. The masses $\overline{M_l} = \sqrt{M_l^2 - \mathrm{i}M_l\Gamma_l}$ are the complex masses of the gauge bosons and the corresponding squared momenta k_l^2 are calculated from the original set of momenta without performing an on-shell projection. The function D_0^{he} is the loop integral occurring in the $\Delta_{ff'}^{\mathrm{virt}}$ part of the non-factorizable corrections taken in the high-energy limit. It is given by

$$\begin{aligned}
D_0^{\mathrm{he}} &= D_0^{\mathrm{he}}(-k_2+p_j, k_1+p_j, p_i+p_j, m_j, M_2, M_1, m_i) \\
&= -\frac{1}{\hat{s}_{1j}\hat{s}_{2i} - \bar{s}s_{ij}} \\
&\quad \times \left[\mathcal{L}i_2\left(-\frac{M_1M_2}{\hat{s}_{2i}} + \mathrm{i}\varepsilon, -x_1\right) + \mathcal{L}i_2\left(-\frac{M_1M_2}{\hat{s}_{1j}} + \mathrm{i}\varepsilon, -\frac{1}{x_2}\right)\right. \\
&\quad - \mathcal{L}i_2\left(-\frac{M_1M_2}{\bar{s}} + \mathrm{i}\varepsilon, -x_1\right) - \mathcal{L}i_2\left(-\frac{M_1M_2}{\bar{s}} + \mathrm{i}\varepsilon, -\frac{1}{x_2}\right) \\
&\quad \left. - \left[\log\frac{\hat{s}_{2i}+\mathrm{i}\varepsilon}{s_{ij}+\mathrm{i}\varepsilon} + \log\frac{\hat{s}_{1j}+\mathrm{i}\varepsilon}{\bar{s}+\mathrm{i}\varepsilon}\right]\left[\log(-x_1) - \log(-x_2)\right]\right], \qquad (3.51)
\end{aligned}$$

with

$$\begin{aligned}
\mathcal{L}i_2(x,y) &= \mathrm{Li}_2(1-xy) + [\log(xy) - \log(x) - \log(y)]\log(1-xy), \\
x_1 &= \frac{(\hat{s}_{2i} - s_{ij})z}{M_1 M_2}\left(1 - \mathrm{i}\varepsilon s_{ij}(\hat{s}_{1j} - s_{ij})\right), \\
x_2 &= \frac{M_1 M_2}{(\hat{s}_{1j} - s_{ij})z}\left(1 + \mathrm{i}\varepsilon s_{ij}(\hat{s}_{2i} - s_{ij})\right), \\
z &= \frac{\hat{s}_{1j}\hat{s}_{2i} - \bar{s}s_{ij}}{(\hat{s}_{1j} - s_{ij})(\hat{s}_{2i} - s_{ij})}.
\end{aligned} \tag{3.52}$$

Chapter 4

Real corrections

The real corrections arise from the emission of additional photons in the $2f \to 4f$ process. If the energy of these photons is small or the angle to the nearest fermion is small these photons cannot be measured in a detector. Hence the contributions of such photons must be added to the total cross section for the four-fermion production process. Furthermore the contributions of such additional photons become singular at the borders of the phase space. This leads to infrared singularities for photon energies $E_\gamma \to 0$ and collinear singularities for small angles $\theta_{\gamma f}$ between the photon and the fermions. According to the Bloch–Nordsieck theorem [18] the infrared singularities have to cancel between real and virtual corrections. To regularize the infrared singularities we use a small photon mass λ and for the regularization of the collinear divergences we introduce masses m_f for the fermions. If our observables are inclusive enough the dependence of the real corrections on this fermion masses cancels for fermions in the final state with the corresponding contribution from the virtual corrections [33]. One way to perform these cancellations numerically is the phase space-slicing method described in the following section.

4.1 Phase-space slicing

In the phase-space-slicing method the regions of the phase space, where the amplitude for $2f \to 4f + \gamma$ gets singular are treated separately. In these parts we can integrate out the contribution of the photon using regulators for the divergences.

In order to separate the divergent parts from the regular part we define an energy cut ΔE parameterized by δ_s and an angular cut parameterized by δ_c for the photon. The energy cut is defined in the centre-of-mass frame of

the partonic subprocess as

$$E_\gamma \;>\; \Delta E = \delta_s \frac{\sqrt{\hat{s}}}{2} = \delta_s \frac{\sqrt{(p_1+p_2)^2}}{2}. \tag{4.1}$$

The separation of the collinear part is done using the smallest angle $\theta_{\gamma f}$ of the photon with a charged fermion f again defined in the centre-of-mass frame of the partonic subprocess. With these cuts the phase space Φ_5 for $2f \to 4f\gamma$ can be separated in three different regions

$$\Phi_{\text{finite}} = \Phi_5(E_\gamma > \Delta E, \cos\theta_{\gamma f} < 1-\delta_c \mid \forall f \text{ with } Q_f \neq 0), \tag{4.2}$$

$$\Phi_{\text{soft}} = \Phi_5(E_\gamma < \Delta E), \tag{4.3}$$

$$\Phi_{\text{coll}} = \Phi_5(E_\gamma > \Delta E, \cos\theta_{\gamma f} > 1-\delta_c \mid f \text{ with } Q_f \neq 0). \tag{4.4}$$

The disadvantage of this method is that one still has to integrate over $\mathrm{d}\sigma_{2f\to 4f\gamma}$ in phase-space regions close to the singularities in order to avoid the errors introduced by using an approximation for small photon energies and collinear photons. The errors $\mathcal{O}(\delta_s)$ and $\mathcal{O}(\delta_c)$ caused by the use of an approximation for the singular parts must be adjusted to be below the integration error of the integration over the finite part $\mathrm{d}\sigma_{\text{real}}$. The smaller we choose δ_s and δ_c the more accurate our calculation becomes in terms of using an approximation. But on the other hand we get larger integration errors in the integration over the finite part $\int_{\Phi_{\text{finite}}} \mathrm{d}\sigma_{\text{real}}$ and therefore need much more computer time to reduce this numerical error.

4.1.1 Phase-space slicing with collinear cuts

For sufficiently small values of δ_s and δ_c the singular part of the squared amplitude for $2f \to 4f\gamma$ can be written as a factor to or a convolution over the squared Born amplitude for $2f \to 4f$. For small values of δ_s and δ_c the sum of the cross section $\mathrm{d}\sigma_{\text{real}}$ for the integration over Φ_{finite} and the approximated cross sections $\mathrm{d}\sigma_{\text{soft}}$ and $\mathrm{d}\sigma_{\text{coll}}$ for the integration over Φ_{soft} and Φ_{coll} is independent of the energy cut ΔE and the angular cut on $\cos\theta_{\gamma f}$, respectively. The full contribution of the real corrections is given by

$$\int_{\Phi_5} \mathrm{d}\sigma_{\text{real}} = \int_{\Phi_5} \mathrm{d}\sigma_{\text{finite}} + \int_{\Phi_4} \mathrm{d}\sigma_{\text{soft}} + \int_{\Phi_4} \mathrm{d}\sigma_{\text{coll}}. \tag{4.5}$$

To calculate the singular part for vanishing photon energy we used the soft-photon approximation (see for example Ref. [28]). In the soft-photon approximation the cross section of the partonic subprocess reads

$$\mathrm{d}\sigma_{\text{soft}} = -\mathrm{d}\sigma_{\text{Born}} \frac{\alpha}{4\pi^2} \sum_{i=1}^{6} \sum_{j=1}^{6} Q_i Q_j \theta_d(i)\theta_d(j) I_{ij}. \tag{4.6}$$

Here we used the functions θ_d to determine the correct sign. The function $\theta_d(i)$ is defined to be 1 if the line of the fermion i points towards the diagram and -1 otherwise. The soft-photon integrals I_{ij} are defined as

$$I_{ij} = \int\limits_{\substack{E_\gamma<\Delta E \\ |\vec{k}|^2=E_\gamma^2-\lambda^2}} \frac{\mathrm{d}^3\vec{k}}{E_\gamma}\frac{p_ip_j}{(kp_i)(kp_j)}. \tag{4.7}$$

We use E_γ and E_i for the energies of the photon and the fermions in the centre-of-mass frame of the partonic subprocess. The masses of the fermions are denoted by m_i. Since we only investigate high energies we can assume $E_i \gg m_i$. In this limit we only keep the fermion masses m_i as regulators so that $\mathrm{d}\sigma_{\mathrm{soft}}$ can be written as

$$\begin{aligned}\mathrm{d}\sigma_{\mathrm{soft}} = \mathrm{d}\sigma_{\mathrm{Born}}\frac{\alpha}{2\pi}\sum_{i=1}^{5}\sum_{j=i+1}^{6}Q_iQ_j\theta_d(i)\theta_d(j)\Bigg[2\log\left(\frac{2\Delta E}{\lambda}\right)\\ \times\left[2-\log\left(\frac{s_{ij}^2}{m_i^2m_j^2}\right)\right]-2\log\left(\frac{4E_iE_j}{m_im_j}\right)+\frac{1}{2}\log^2\left(\frac{4E_i^2}{m_i^2}\right)\\ +\frac{1}{2}\log^2\left(\frac{4E_j^2}{m_j^2}\right)+\frac{2\pi^2}{3}+2\,\mathrm{Li}_2\left(1-\frac{4E_iE_j}{s_{ij}}\right)\Bigg].\end{aligned} \tag{4.8}$$

The collinear cross section is divided in a part $\mathrm{d}\sigma_{\mathrm{coll}}^{\mathrm{initial}}$ originating from initial-state and a part $\mathrm{d}\sigma_{\mathrm{coll}}^{\mathrm{final}}$ originating from final-state radiation

$$\mathrm{d}\sigma_{\mathrm{coll}} = \mathrm{d}\sigma_{\mathrm{coll}}^{\mathrm{initial}} + \mathrm{d}\sigma_{\mathrm{coll}}^{\mathrm{final}}. \tag{4.9}$$

While the emission of photons from the final state does not change the kinematics of the subprocess, the initial-state radiation causes a loss of energy for the initial state. In the latter case the cross section reads

$$\mathrm{d}\sigma_{\mathrm{coll}}^{\mathrm{initial}} = \sum_{i=1,2}\frac{\alpha}{2\pi}Q_i^2\int_0^{1-\delta_s}\mathrm{d}z_i f(z_i)\mathrm{d}\sigma_{\mathrm{Born}}(z_ip_i), \tag{4.10}$$

with

$$f(z_i) = \frac{1+z_i^2}{1-z_i}\log\left(\frac{\hat{s}}{m_i^2}\frac{\delta_c}{2z_i}\right)-\frac{2z_i}{1-z_i}. \tag{4.11}$$

We can put this contribution in this form since we only consider a non-polarized process. In this case we can take the sum over the fermion helicities $\sigma_1,\ldots,\sigma_6$. Otherwise the initial-state radiation may lead to different results

because of a spin flip of the fermion due to the emission of the photon. The differential cross section for final-state radiation reads

$$\begin{aligned} \mathrm{d}\sigma_{\mathrm{coll}}^{\mathrm{final}} &= \sum_{i=3}^{6} \frac{\alpha}{2\pi} Q_i^2 \\ &\times \left(\left[\frac{3}{2} + 2 \log\left(\frac{\Delta E}{E_i} \right) \right] \left[1 - \log\left(\frac{4E_i^2}{m_i^2} \frac{\delta_c}{2} \right) \right] + 3 - \frac{2\pi^2}{3} \right) \mathrm{d}\sigma_{\mathrm{Born}}. \end{aligned} \quad (4.12)$$

4.1.2 Phase-space slicing with effective collinear factors

Another way to cancel the collinear divergences in the Bremsstrahlung cross section is to introduce effective collinear factors in the five-particle cross section. In this case only the integration over the infrared divergent part Φ_{soft} is separated from the five-particle phase space Φ_5. To get a finite result for the integration over the collinear part of the phase space we modify the five-particle partonic cross section by multiplying with an effective collinear factor f_{eff}. The factor f_{eff} is essentially $1+\mathcal{O}(m_f^2/s)$ and exactly replaces the collinear divergences in $\mathrm{d}\sigma_{\mathrm{real}}$ by the correct mass-regularized behavior. In this approach we get

$$\int_{\Phi_5} \mathrm{d}\sigma_{\mathrm{real}} = \int_{\Phi_{\mathrm{finite}} \cup \Phi_{\mathrm{coll}}} \mathrm{d}\sigma'_{\mathrm{real}} + \int_{\Phi_{\mathrm{soft}}} \mathrm{d}\sigma_{\mathrm{soft}}, \quad (4.13)$$

with the modified partonic cross section

$$\mathrm{d}\sigma'_{\mathrm{real}} = f_{\mathrm{eff}}^{\mathrm{coll}} \mathrm{d}\sigma_{\mathrm{real}}. \quad (4.14)$$

Since the behavior of the cross section for the production of four fermions and one additional photon is known in the limit of small scalar products $(p_i p_\gamma)$, it is possible to cancel the singular part by a simple multiplicative factor. We can sum over the polarizations of the fermions and find a common factor given by

$$\begin{aligned} f_{\mathrm{eff}}^{\mathrm{coll}} &= \sum_{\kappa_1,\ldots,\kappa_6=\pm} \left(\prod_{i=1}^{2} f_{\kappa_i}^{(\mathrm{ini})}(m_i, \frac{p_\gamma^0}{p_i^0}, p_i^0, \theta_{i\gamma}) \right) \left(\prod_{i=3}^{6} f_{\kappa_i}^{(\mathrm{fin})}(m_i, \frac{p_\gamma^0}{p_i^0}, p_i^0, \theta_{i\gamma}) \right) \\ &= \prod_{i=1}^{2} \left(f_+^{(\mathrm{ini})}(m_i, \frac{p_\gamma^0}{p_i^0}, p_i^0, \theta_{i\gamma}) + f_-^{(\mathrm{ini})}(m_i, \frac{p_\gamma^0}{p_i^0}, p_i^0, \theta_{i\gamma}) \right) \\ &\quad \times \prod_{i=3}^{6} \left(f_+^{(\mathrm{fin})}(m_i, \frac{p_\gamma^0}{p_i^0}, p_i^0, \theta_{i\gamma}) + f_-^{(\mathrm{fin})}(m_i, \frac{p_\gamma^0}{p_i^0}, p_i^0, \theta_{i\gamma}) \right), \end{aligned} \quad (4.15)$$

with the functions [34]

$$\begin{aligned} f_{-}^{(\mathrm{ini/fin})}(m_f, x_f, E_f, \theta_{f\gamma}) &= \frac{x_f^2}{x_f^2 \mp 2x_f + 2} \frac{4m_f^2 E_f^2 \sin^2(\theta_{f\gamma}/2)}{\left[4E_f^2 \sin^2(\theta_{f\gamma}/2) + m_f^2\right]^2}, \\ f_{+}^{(\mathrm{ini/fin})}(m_f, x_f, E_f, \theta_{f\gamma}) &= \left(\frac{4E_f^2 \sin^2(\theta_{f\gamma}/2)}{4E_f^2 \sin^2(\theta_{f\gamma}/2) + m_f^2}\right)^2. \end{aligned} \tag{4.16}$$

Here $\theta_{i\gamma}$ is the angle between particle i and the photon and x_f a shorthand for the energy ratio p_γ^0/p_f^0. We can use $\mathrm{d}\sigma'_{\mathrm{real}}$ to determine the cross section for $pp \to 4f\gamma$ without calculating the collinear contributions $\mathrm{d}\sigma_{\mathrm{coll}}^{\mathrm{initial}}$ and $\mathrm{d}\sigma_{\mathrm{coll}}^{\mathrm{final}}$ described in section 4.1.1.

The use of the collinear factors does not introduce the convolution we would have to calculate in $\mathrm{d}\sigma_{\mathrm{coll}}^{\mathrm{initial}}$. Unfortunately it turned out in the numerics that we do not gain any advantage of this because the integration error in this approach turns out to be larger than the integration error in the approach using extra integrations for the collinear part. For this reason we decided to use only the phase-space slicing with collinear cuts described in section 4.1.1 for our numerical evaluation.

4.2 Matching of infrared divergences

Since the virtual corrections were calculated in DPA and the real corrections were calculated using the full five-particle phase space we get no exact cancellation of the infrared divergences. To fix this problem we subtract the singular parts from the virtual corrections and add them to the real corrections in the following way

$$\begin{aligned} \sigma_{\mathrm{virt,finite}} &= \int_{\Phi_4^{\mathrm{DPA}}} \left(\mathrm{d}\sigma_{\mathrm{virt}} - \mathrm{d}\sigma_{\mathrm{virt,sing}}\right), \\ \sigma'_{\mathrm{real}} &= \int_{\Phi_5} \mathrm{d}\sigma_{\mathrm{real}} + \int_{\Phi_4} \mathrm{d}\sigma_{\mathrm{virt,sing}}. \end{aligned} \tag{4.17}$$

The new cross sections $\sigma_{\mathrm{virt,finite}}$ and σ'_{real} contain no infrared divergences any more. Mass divergences only remain from initial-state fermions and are completely contained in σ'_{real}. However the singular part $\sigma_{\mathrm{virt,sing}}$ is not uniquely defined because constant parts from the radiative corrections can always be shifted into the definition of the singular contribution. To perform

the matching in our case we chose the subtraction term defined in Ref. [19]:

$$\begin{aligned} \mathrm{d}\sigma_{\mathrm{virt,sing}} &= \mathrm{d}\sigma_{\mathrm{Born}} \frac{\alpha}{2\pi} \sum_{i=1}^{5} \sum_{j=i+1}^{6} Q_i Q_j \theta_d(i) \theta_d(j) \\ &\quad \times \left[\mathcal{L}(s_{ij}, m_i^2) + \mathcal{L}(s_{ij}, m_j^2) + C_{ij} + C_{ji} \right], \end{aligned} \tag{4.18}$$

with

$$\mathcal{L}(s_{ij}, m_i^2) = \log \frac{m_i^2}{s_{ij}} \log \frac{\lambda^2}{s_{ij}} + \log \frac{\lambda^2}{s_{ij}} - \frac{1}{2} \log^2 \frac{m_i^2}{s_{ij}} + \frac{1}{2} \log \frac{m_i^2}{s_{ij}} \tag{4.19}$$

and the constant terms C_{ij} and C_{ji} defined as

$$\begin{aligned} C_{ij} &= -\frac{\pi^2}{3} + 2, \quad \text{if } i \text{ and } j \text{ are incoming,} \\ C_{ij} &= \frac{\pi^2}{6} - 1, \quad \text{if } i \text{ is incoming and } j \text{ is outgoing,} \\ C_{ij} &= -\frac{\pi^2}{2} + \frac{3}{2}, \quad \text{if } i \text{ is outgoing and } j \text{ is incoming,} \\ C_{ij} &= -\frac{\pi^2}{3} + \frac{3}{2}, \quad \text{if } i \text{ and } j \text{ are outgoing.} \end{aligned} \tag{4.20}$$

In principle one can use other terms to shift the infrared divergences from the virtual DPA corrections to the real corrections. Note that only the Born cross section enters in the definition of $\mathrm{d}\sigma_{\mathrm{virt,sing}}$ and hence this term is gauge invariant by construction. A subtraction or addition of such gauge-invariant terms cannot lead to a violation of gauge invariance in the total cross section. However, by shifting singular parts from the virtual to the real corrections always some finite parts are included, depending on the definition of the singular parts. For example we could use the infrared singular parts defined in Ref. [35] instead of the singular parts we defined in formula (4.18). The ambiguity due to the choice of the definition for $\mathrm{d}\sigma_{\mathrm{virt,sing}}$ is of the order of non-doubly-resonant terms as was shown in Ref. [19]. Therefore it is of the same order as the uncertainty of the DPA and we can safely use this method within the accuracy of our approximations for the radiative corrections.

Chapter 5

Treatment of parton distributions

5.1 Definitions

The parton distribution functions $\Phi_{i,q}(Q,x)$ give the probability to find the parton q with energy fraction x in the nucleon i at the factorization scale Q. The dependence of the distribution functions (PDFs) on the energy scale originates from higher-order contributions that are naturally included because these functions have to be determined experimentally. In this way all orders of initial-state radiation of soft gluons are contained for a quark q coming from inside a proton. A correct description of this effects is given by the Dokshitzer–Gribov–Lipatov–Altarelli–Parisi (DGLAP) equations. These differential equations describe the evolution of the probability to find a parton which can be a quark q or a gluon g inside a proton with a certain momentum fraction x. For quarks these equations are given by

$$\frac{\mathrm{d}\Phi_{i,q}(Q,x)}{\mathrm{d}\log Q} = \frac{\alpha_s(Q^2)}{\pi}\int_x^1 \frac{\mathrm{d}z}{z}\left[P_{q\leftarrow q}(z)\Phi_{i,q}\left(Q,\frac{x}{z}\right)+P_{q\leftarrow g}(z)\Phi_{i,g}\left(Q,\frac{x}{z}\right)\right] \tag{5.1}$$

with the strong coupling constant α_s and the splitting functions

$$\begin{aligned} P_{q\leftarrow q}(z) &= \frac{4}{3}\left[\frac{1+z^2}{(1-z)_+}+\frac{3}{2}\delta(1-z)\right], \\ P_{q\leftarrow g}(z) &= \frac{1}{2}\left[z^2+(1-z)^2\right]. \end{aligned} \tag{5.2}$$

Due to the convolution over the splitting functions quarks are taken into account which originate from other quarks or gluons inside the proton at higher

momentum fractions x/z. This is similar to the case of initial-state radiation in which a loss of energy due to the production of additional particles must be considered.

For QCD corrections in infinite order the dependence on the factorization scale Q has to vanish for a physical cross section. A standard procedure in QCD calculations is to check the remaining scale dependence after the inclusion of radiative corrections. But since we do not consider QCD corrections we cannot reduce the scale dependence caused by the PDFs. In fact we would not only have to include QCD corrections to get rid of the scale dependence, but also would need QED corrected parton distribution functions which are not available at the present time.

5.2 Numerical evaluation of PDFs

The numerical behavior of the parton distributions functions is of special interest because we have to calculate a convolution integral including these functions. The PDFs for quarks inside the proton vary over many orders of magnitude and diverge for $x \to 0$. This makes it necessary to find a proper mapping for the integration. One simple possibility is given by

$$\int_0^1 \mathrm{d}x_1 \int_0^1 \mathrm{d}x_2 \to \int_{-\infty}^{\infty} \mathrm{d}y \int_0^{\tau_{\max}} \mathrm{d}\tau, \tag{5.3}$$

where the centre-of-mass pair rapidity y and the scaling variable τ are used. These quantities are defined as

$$\begin{aligned} y &= \frac{1}{2} \log \frac{x_1}{x_2}, \\ \tau &= x_1 x_2. \end{aligned} \tag{5.4}$$

For the mapping of parton distribution functions (PDFs) different schemes have been implemented.

5.2.1 Combined mapping

One possibility for the integration over the parton distribution functions is given by the substitution

$$\int_0^1 \mathrm{d}x_1 \int_0^1 \mathrm{d}x_2 \to \int_{\log^2 \tau_0}^0 \mathrm{d}(\log^2 \tau) \int_{\log \tau}^0 \mathrm{d}(\log x_2) \frac{\tau}{2 \log \tau}, \tag{5.5}$$

where $\tau = x_1 x_2$ and τ_0 is determined by the minimum-energy cut for the partonic center of mass frame. The factor $\tau/(2 \log \tau)$ from the Jacobian of

this substitution cancels the τ dependence in the flux factor $1/\hat{s} = 1/(\tau s)$ which occurs in the amplitudes. This mapping is very useful in the high-energy case, i.e. in the region where the radiative correction we implemented are valid. The use of the minimum-energy cut in the first integration prevents the generation of phase-space points which do not fulfil the minimum-energy conditions. In this way less phase-space points are rejected in the Monte Carlo integration.

In our numerical analysis in which we are always in a high-energy regime with partonic CMS energies $\sqrt{\hat{s}} \geq 500\text{GeV}$ we always use this combined mapping in the numerical integration.

5.2.2 Mapping of a single parton distribution

If in a calculation low values of $\sqrt{\hat{s}}$ can appear it can be an advantage to have a good mapping of the PDFs over the full range of the momentum fraction x. For example tree-level cross sections with anomalous gauge-boson couplings can be such a case. For the Monte Carlo integration in these cases it might be recommendable to have a proper mapping of the PDFs at low x or a proper mapping of the s-channel in the topologies F and G shown in figure 1.3. We implemented an s-channel mapping and the mapping of one of the parton distributions for these topologies.

To map a single PDF we can find a function which comes very close to the actual shape of the parton distribution. We can approximate a parton distribution function by the following three functions

$$\begin{aligned} f(x) = &\quad \tfrac{1}{x+\varepsilon} + c_1, && \text{if} \quad 0 < x < x_1 = 0.1, \\ f(x) = &\quad \exp(c_2 x + c_3), && \text{if} \quad x_1 \leq x < x_2 = 0.7, \\ f(x) = &\quad c_4(1-x)^4, && \text{if} \quad x_2 \leq x \leq 1, \end{aligned} \tag{5.6}$$

where the constants c_1, c_2, c_3, c_4 are fitted to the parton distribution function $\Phi_{i,q}$ in the following way

$$\begin{aligned} c_1 &= -\frac{1}{x_1+\varepsilon} + \Phi_{i,q}(Q, x_1), \\ c_2 &= \frac{\log \Phi_{i,q}(Q, x_1) - \log \Phi_{i,q}(Q, x_2)}{x_1 - x_2}, \\ c_3 &= -x_2 \frac{\log \Phi_{i,q}(Q, x_1) - \log \Phi_{i,q}(Q, x_2)}{x_1 - x_2} + \log \Phi_{i,q}(Q, x_2), \\ c_4 &= \frac{\Phi_{i,q}(Q, x_2)}{(1-x_2)^4}. \end{aligned} \tag{5.7}$$

Note that not $f(x)$ itself but the derivative of $f(x)$ will appear in the density function g. Therefore we do not find an exact cancellation of the dependence on x described by $f(x)$. But the overall shape of $f'(x)$ is similar to the shape of $f(x)$ so we can use it for a mapping by generating a Bjorken x by the inverted function $x(\xi) = f^{-1}(\xi)$.

The parameter ε is used to generate a finite value for the mapping function at $x = 0$. It was set to $\varepsilon = 10^{-2}$, but the actual value of this parameter has no numerical effect, because events with $x = 0$ result in zero center of mass energy for the partonic subprocess and do not contribute to the cross section due to the cuts on $\sqrt{\hat{s}}$ for physical processes. For the scale Q we used 5000 GeV to determine the shape of the mapping functions. To apply this mapping we have to skip the substitution given in (5.3) and directly integrate over the two momentum fractions x_1 and x_2. The convolution is then written as

$$\int_0^1 \mathrm{d}x_1 \int_0^1 \mathrm{d}x_2 \to \int_0^1 \mathrm{d}\xi \frac{\mathrm{d}x_1(\xi)}{\mathrm{d}\xi} \int_{\hat{s}_{\min}}^{\hat{s}_{\max}} \mathrm{d}\hat{s} \frac{1}{x_1 s} \tag{5.8}$$

in the case of a s-channel propagator and

$$\int_0^1 \mathrm{d}x_1 \int_0^1 \mathrm{d}x_2 \to \int_0^1 \mathrm{d}\xi \frac{\mathrm{d}x_1(\xi)}{\mathrm{d}\xi} \int_0^1 \mathrm{d}x_2 \tag{5.9}$$

otherwise.

5.3 Renormalization of PDFs

The partonic cross section in $\mathcal{O}(\alpha)$ includes mass singular terms of the form $\alpha \log m_f$ with small fermion masses m_f. These mass singularities are introduced by the collinear emission of photons in the final or initial state. The mass singularities from the initial-state radiation contain terms proportional to $\alpha \log m_1$ and $\alpha \log m_2$ where m_1 and m_2 are the masses of the interacting partons. The masses of the partons are not a physical observable since there are no free quarks in nature because of the confinement of QCD. In order to get a prediction for the cross section which does not depend on quark masses we have to absorb this singular terms depending on the quark masses into the parton distribution functions. This is done in analogy to next-to-leading order QCD calculations in the $\overline{\mathrm{MS}}$ factorization scheme by renormalizing the parton distribution functions:

$$\begin{aligned} \Phi_{i,q}^{\text{renormalized}}(Q, x_i) &= \Phi_{i,q}(Q, x_i) - \frac{\alpha}{2\pi} Q_q^2 \int_{x_i}^1 \frac{\mathrm{d}z}{z} \Phi_{i,q}\left(Q, \frac{x_i}{z}\right) \\ &\quad \times \left[P_{ff}(z) \left(\log \frac{Q^2}{m_q^2} - 2\log(1-z) - 1 \right) \right]_+ \end{aligned} \tag{5.10}$$

with the splitting function $P_{ff}(z) = (1+z^2)/(1-z)$. The soft-photon pole in equation (**??**) for $z \to 1$ is excluded from the integration by using the $[\dots]_+$ prescription which is defined as

$$\int_x^1 \mathrm{d}z \, [f(z)]_+ \, g(z) = \int_x^1 \mathrm{d}z f(z)g(z) - \int_0^1 \mathrm{d}z f(z)g(1). \tag{5.11}$$

Unfortunately at the present time there exist no PDFs in which the photonic $\mathcal{O}(\alpha)$ corrections are included if one considers the DGLAP evolution. To obtain a $\mathcal{O}(\alpha)$ corrected PDF the DGLAP evolution of the PDF has to be calculated in the corresponding loop order and experimental data must be used to determine this QED-corrected PDF.

We define the contribution from the renormalization of the PDFs as

$$\begin{aligned} \mathrm{d}\sigma_{\mathrm{re-PDF}} &= -\frac{\alpha}{2\pi} \sum_{i=1}^{2} Q_i^2 \int_{x_i}^1 \frac{\mathrm{d}z}{z} \frac{\Phi_{i,f_i}(Q, \frac{x_i}{z})}{\Phi_{i,f_i}(Q, x_i)} \\ &\quad \times \left[P_{ff}(z) \left(\log \frac{Q^2}{m_i^2} - 2\log(1-z) - 1 \right) \right]_+ \mathrm{d}\sigma_{\mathrm{Born}}(x_1, x_2). \end{aligned} \tag{5.12}$$

5.3.1 Treatment for the Splitting function P_{ff}

The integration over the splitting function

$$P_{ff}(z) = \frac{1+z^2}{1-z} \tag{5.13}$$

introduces a pole for $z = 1$ which is excluded by using the $[\dots]_+$ prescription. Anyhow a direct numerical integration leads to numerical instabilities which can only be avoided if a proper mapping is introduced. Therefore we perform the following substitution on the integral in (5.12). We set

$$z_2 = (1-z)^\alpha, \quad \text{with} \quad \alpha = -\frac{\log z_2}{z_2}. \tag{5.14}$$

Unfortunately the equation for α cannot be written in terms of z in an algebraic way but we can express z in terms of z_2:

$$z = 1 - z_2^{\frac{1}{\alpha}} = 1 - e^{-z_2}. \tag{5.15}$$

A short calculation shows that we can write

$$\int_x^1 \mathrm{d}z P_{ff}(z) = \int_{-\log(1-x)}^{\infty} \mathrm{d}z_2 \left(2 - 2e^{-z_2} + e^{-2z_2} \right). \tag{5.16}$$

Chapter 6

Numerical Results

6.1 Constants in the numerical evaluation

For the numerical evaluation the parameters of the standard model are fixed by the values in Ref. [36]. For the Fermi constant we used the value $G_\mu = 0.1166370 \cdot 10^{-4}\mathrm{GeV}^{-2}$ and the electromagnetic coupling constant is given by $\alpha = 1/137.0359895$. At the scale of the Z mass the electromagnetic coupling constant is $\alpha(M_\mathrm{Z}) = 1/128.88700$. We have implemented three schemes for the use of these couplings. In the numerical calculations we can use α, $\alpha(M_\mathrm{Z})$, or $\alpha_{G_\mu} = \sqrt{2}G_\mu M_\mathrm{W}^2 s_\mathrm{w}^2/\pi = 7.543596 \cdot 10^{-3}$. By using $\alpha(M_\mathrm{Z})$ or α_{G_μ} higher-order contributions from the running of the electromagnetic coupling are taken into account. For the strong coupling constant of QCD we use $\alpha_s = 0.117$. The electroweak mixing angle is determined by the masses of the gauge bosons $c_\mathrm{w} = M_\mathrm{W}/M_\mathrm{Z}$. The actual values of the masses used in the program are shown in table 6.1. For all numerical results shown in

leptons	up-type quarks	down-type quarks
$m_\mathrm{e} = 0.5109989 \cdot 10^{-3}$	$m_\mathrm{u} = 0.066$	$m_\mathrm{d} = 0.066$
$m_\mu = 0.105658365$	$m_\mathrm{c} = 1.20$	$m_\mathrm{s} = 0.15$
$m_\tau = 1.77699$	$m_\mathrm{t} = 178.0$	$m_\mathrm{b} = 4.9$

gauge-boson masses	gauge-boson widths	Higgs boson
$M_\mathrm{W} = 80.425$	$\Gamma_\mathrm{W} = 2.09936$	$M_\mathrm{H} = 150.00000$
$M_\mathrm{Z} = 91.1876$	$\Gamma_\mathrm{Z} = 2.50504$	

Table 6.1: Masses and widths used in the Monte Carlo program. All numbers are given in units of GeV

the following sections we used the fixed-width scheme with the mass values given in the table and the gauge-boson widths calculated from the following standard formulae

$$\begin{aligned}\Gamma_{\mathrm{Z}} &= \frac{\alpha M_{\mathrm{Z}}}{24 s_{\mathrm{w}}^2 c_{\mathrm{w}}^2}\left[21 - 40 s_{\mathrm{w}}^2 + \frac{160}{3} s_{\mathrm{w}}^4 + \frac{m_{\mathrm{b}}^4}{M_{\mathrm{Z}}^4}\left(24 s_{\mathrm{w}}^2 - 16 s_{\mathrm{w}}^4\right) - 9\frac{m_{\mathrm{b}}^2}{M_{\mathrm{Z}}^2}\right. \\ &\quad \left. + \frac{\alpha_s}{\pi}\left(15 - 28 s_{\mathrm{w}}^2 + \frac{88}{3} s_{\mathrm{w}}^4\right)\right] = 2.505044\ldots \text{ GeV} \qquad (6.1)\end{aligned}$$

and

$$\Gamma_{\mathrm{W}} = \frac{\alpha M_{\mathrm{W}}}{2 s_{\mathrm{w}}^2}\left[\frac{3}{2} + \frac{\alpha_s}{\pi}\right] = 2.099360\ldots \text{ GeV}. \qquad (6.2)$$

For calculations with only one quark generation like cross sections for $\bar{\mathrm{d}}\mathrm{u} \to 4f$ which we calculated for some numerical checks we use the identity matrix as quark-mixing matrix. In the results presented in sections 6.7.1, 6.7.2, and 6.7.3 we are considering the mixing between the quarks of different generations and we generate a matrix from $|V_{\mathrm{ud}}| = 0.974$ which is at present the matrix element with the smallest error in the following way

$$V_{\mathrm{CKM}} = \begin{pmatrix} V_{\mathrm{ud}} & V_{\mathrm{us}} & V_{\mathrm{ub}} \\ V_{\mathrm{cd}} & V_{\mathrm{cs}} & V_{\mathrm{cb}} \\ V_{\mathrm{td}} & V_{\mathrm{ts}} & V_{\mathrm{tb}} \end{pmatrix} = \begin{pmatrix} |V_{\mathrm{ud}}| & \sqrt{1-|V_{\mathrm{ud}}|^2} & 0 \\ -\sqrt{1-|V_{\mathrm{ud}}|^2} & |V_{\mathrm{ud}}| & 0 \\ 0 & 0 & 1 \end{pmatrix}. \qquad (6.3)$$

In the initial state we neglect the contributions from top and bottom quarks i.e. we set $\Phi_{\mathrm{b}}(Q,x) = \Phi_{\mathrm{t}}(Q,x) = 0$. As parton distributions we have used the CTEQ(6M) [37] with the factorization scale Q defined as

$$Q^2 = \frac{1}{2}\left(M_{V_1}^2 + M_{V_2}^2 + P_{\mathrm{T}}^2(V_1) + P_{\mathrm{T}}^2(V_2)\right). \qquad (6.4)$$

Here $P_{\mathrm{T}}(V_1)$ and $P_{\mathrm{T}}(V_2)$ denote the transverse momenta of the reconstructed intermediate gauge bosons. The full reconstruction of the transverse momenta of the gauge bosons is only possible for WZ or ZZ production if four or three charged particles are detected in the final state. Considering WW production we only find two charged leptons in the final state which makes a full reconstruction impossible so that we use

$$Q^2 = \frac{1}{2}\left(M_{V_1}^2 + M_{V_2}^2 + P_{\mathrm{T}}^2(l^-) + P_{\mathrm{T}}^2(l^+) + \left(P_{\mathrm{miss}}^{\mathrm{T}}\right)^2\right). \qquad (6.5)$$

Furthermore we take the average of the factorization scales if there are two possible reconstructions of intermediate gauge bosons. A description of the reconstruction of intermediate gauge bosons is given in chapter 6.4. The energy of the proton beams at the LHC is 7 TeV which gives a centre-of-mass energy of $\sqrt{s} = 14\,\mathrm{TeV}$.

6.2 Cuts on the phase space

To match the several different possibilities to select special events in an experiment different sets of cuts can be applied. Some of these cuts are already used within the phase-space generator to prevent the generation of events that must be rejected according to these cuts. In the Monte Carlo program angular cuts to the beam axis or other particles can be given directly for each fermion. It is also possible to give cuts for the energies or the invariant masses s_{ij} of particle pairs. In this scheme all cuts must be given explicitly for every particle. Furthermore a more general set of cuts was implemented which allows to give conditions for certain species of particles like leptons or quarks. In addition it allows to give conditions for the intermediate gauge bosons. As additional observable we define the transverse momentum of the particle i

$$p^{\mathrm{T}}(i) = \sqrt{(p_i^1)^2 + (p_i^2)^2}. \tag{6.6}$$

The pseudo rapidity η_i of leptons and quarks is given by

$$\eta_i = -\log\left(\tan\frac{\theta_i}{2}\right) \tag{6.7}$$

where θ_i is the angle between the direction of the particle i to the beam axis. For distinguishing the tracks of different particles the rapidity–azimuthal-angle separation between the particles i and j is used

$$\Delta R_{ij} = \sqrt{(\eta_i - \eta_j)^2 + (\phi_i - \phi_j)^2} \tag{6.8}$$

with the azimuthal angles ϕ_i, ϕ_j. For neutrinos which cannot be seen in the detector we introduce the missing transverse momentum

$$p^{\mathrm{T}}_{\mathrm{miss}} = \sqrt{\left(\sum_{f_i} \delta_{f_i\nu} p_i^1\right)^2 + \left(\sum_{f_i} \delta_{f_i\nu} p_i^2\right)^2}. \tag{6.9}$$

For the identification of gauge bosons, cuts are applied on the transverse momentum or the transverse mass of a fermion pair:

$$p^{\mathrm{T}}(i,j) = \sqrt{\left(p_i^1 + p_j^1\right)^2 + \left(p_i^2 + p_j^2\right)^2}, \tag{6.10}$$

$$M^{\mathrm{T}}(i,j) = \sqrt{E^{\mathrm{T}2}(i,j) - p^{\mathrm{T}2}(i,j)} \tag{6.11}$$

with the transverse energy $E^{\mathrm{T}}(i,j) = |p^{\mathrm{T}}(i)| + |p^{\mathrm{T}}(j)|$. The standard values for these cuts are given in table 6.2.

Table 6.2: Standard Cuts

Particle	Observable	Cut
charged leptons	$p^{\mathrm{T}}(i)$	> 20 GeV
	$\lvert\eta_i\rvert$	< 3
quarks	$p^{\mathrm{T}}(i)$	> 20 GeV
	$\lvert\eta_i\rvert$	< 3
one neutrino in the final state	$p^{\mathrm{T}}_{\mathrm{miss}}$	> 20 GeV
two neutrinos in the final state	$p^{\mathrm{T}}_{\mathrm{miss}}$	> 25 GeV

6.3 Recombination of photons

If the energy of a photon is not high enough or it is very close to another particle in the final state the detectors in the high-energy experiments are not able to resolve it as a separate particle. To simulate this behavior of the detector we implemented a photon-recombination procedure. If the photon is to close to the beam axis it will be hidden in the fragments of the protons. Therefore we assume that the photon is only visible for $|\eta_\gamma| < 3$. If the separation to a fermion f_i in the rapidity-azimuthal angle $\Delta R_{i\gamma} < 0.1$ the photon momentum is added to the momentum of the fermion. Photons with energies E_γ below 2 GeV are always recombined to the closest fermion.

6.4 Reconstruction of gauge bosons

The reconstruction of gauge bosons allows to select a special region of the phase space. Similar to the procedure in an experiment a generated set of momenta is examined and it is checked if certain combinations of the measured outgoing particles can form a $\mathrm{W}^\pm$, Z or γ in an intermediate state. if the charges of the fermions i and j add to zero we use the following cuts to identify Z bosons

$$M_{\mathrm{Z}} - \Delta M_{\mathrm{Z}} < \sqrt{(p_i + p_j)^2} < M_{\mathrm{Z}} + \Delta M_{\mathrm{Z}} \tag{6.12}$$

with $\Delta M_{\mathrm{Z}} = 20\,\mathrm{GeV}$. In processes with neutrino production, e.g. in the case of a $\mathrm{W}^\pm$ boson decaying into a lepton l and a neutrino ν_l, it is not possible to measure the momentum of the neutrino. But if only one neutrino is produced

in the full process we can measure the transverse momentum of this neutrino by the amount of missing transverse momentum. In this case we can use the transverse mass $M_{\mathrm{T}}(l\nu_l)$ for the reconstruction of the W boson. Here we demand

$$\sqrt{(|p_l^{\mathrm{T}}| + |p_{\mathrm{miss}}^{\mathrm{T}}|)^2 - (p_l^{\mathrm{T}} + p_{\mathrm{miss}}^{\mathrm{T}})^2} < M_{\mathrm{W}} + \Delta M_{\mathrm{W}} \tag{6.13}$$

with $\Delta M_{\mathrm{W}} = 20\,\mathrm{GeV}$ for the reconstruction of the W boson. For final states with two neutrinos the reconstruction of a possible $\mathrm{W^+W^-}$ fails and we cannot apply a reconstruction in this case. However, we can still reconstruct a ZZ pair with two neutrinos in the final state.

If there is more than one pair of gauge bosons which passes our reconstruction cuts we determine the best reconstructed pair by the difference of the poles to the gauge-boson masses. This means we calculate the reconstructed gauge-boson masses $M_{\mathrm{Z,recon}} = \sqrt{(p_i + p_j)^2}$ for Z bosons and if possible $M_{\mathrm{W,recon}} = \sqrt{(|p_l^{\mathrm{T}}| + |p_{\mathrm{miss}}^{\mathrm{T}}|)^2 - (p_l^{\mathrm{T}} + p_{\mathrm{miss}}^{\mathrm{T}})^2}$ for W bosons. These reconstructed masses we can compare for the different cases by calculating

$$\Delta(V_1, V_2) \;=\; (M_{V_1,\mathrm{recon}} - M_{V_1})^2 + (M_{V_2,\mathrm{recon}} - M_{V_2})^2 . \tag{6.14}$$

For the calculations of distributions we only take the gauge-boson pair into account which has the smallest $\Delta(V_1, V_2)$.

6.5 Consistency of the program

Several consistency checks have been performed on the program. Especially the results for the $\mathrm{W^{\pm}Z}$ production process have been compared with a program written by Elena Accomando. In these tests the discrepancy between the programs was less than 0.1% which was still within the statistical error of the test. The two programs are completely independent and the radiative corrections to gauge-boson production were implemented in a completely different way.

In the phase-space slicing approach discussed in chapter 4.1 we have introduced additional cuts parameterized by δ_c and δ_s to split off the parts in which the cross sections gets divergent. The cross section has to be independent of the values of these additional cuts. Here we use the standard cuts in table 6.2 and the process $\mathrm{PP} \to \nu_{\mathrm{e}}\mathrm{e^+}\mu^-\mu^+$ to demonstrate the effect of the variation of the parameters δ_c and δ_s which are defined in chapter 4.1. For the values $10^{-2} < \delta_c < 10^{-1}$ one can see a clear dependence of the total cross section on the angular cut in the phase space in figure 6.1. For values $\delta_c < 10^{-2}$ the cross section gets constant within the integration error with respect to variation of δ_c. In this regime the error due to the integration is

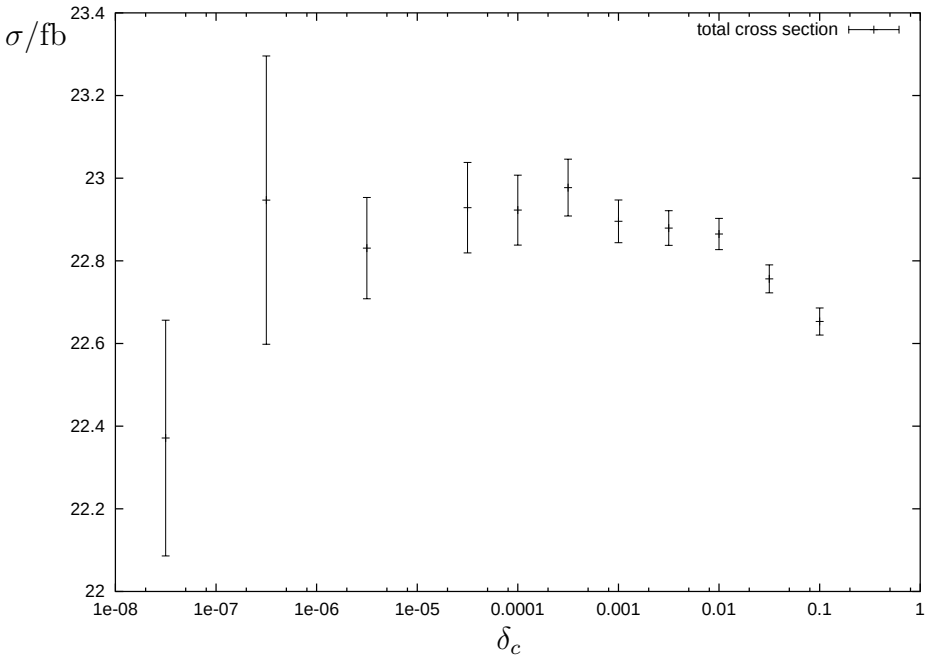

Figure 6.1: Dependence of the total cross section on the cut δ_c.

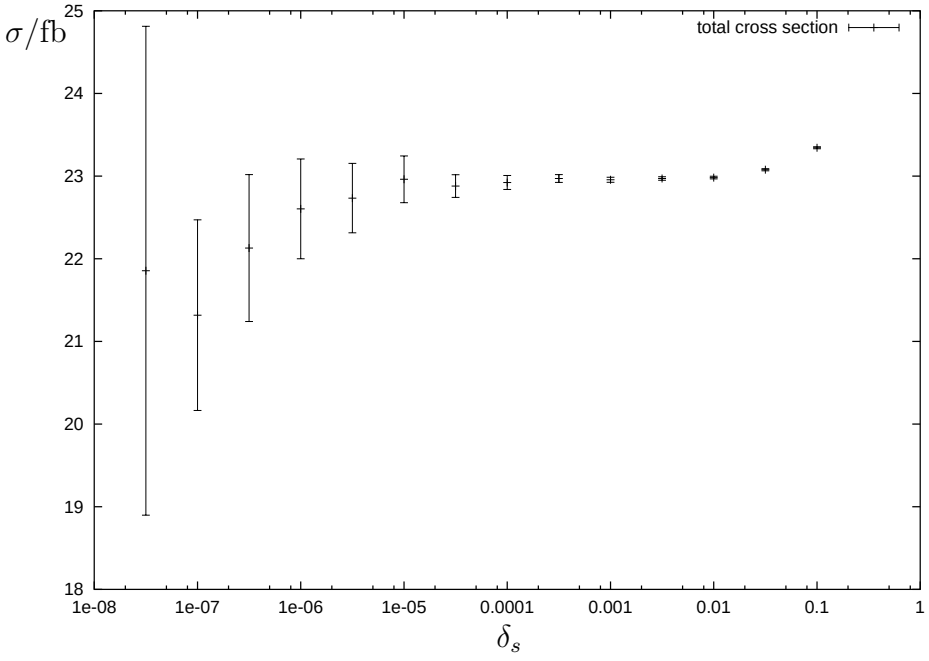

Figure 6.2: Dependence of the total cross section on the cut δ_s.

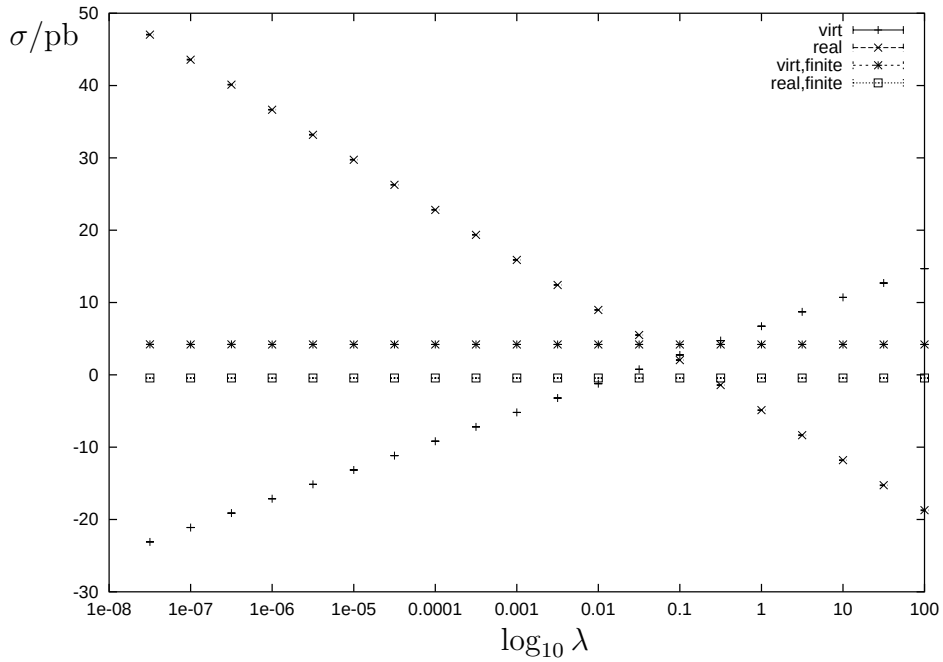

Figure 6.3: Cancellation of infrared divergences by the subtraction of the singular parts. The cross sections for $\sigma_{\text{virt,finite}}$ and $\sigma_{\text{real,finite}}$ do not depend on the photon mass λ.

bigger than the error due to the use of an approximation at the phase space boundary. For the numerical evaluations we fixed the value to $\delta_c = 10^{-3}$. The same arguments hold for the dependence on the energy cut δ_s shown in figure 6.2. For energy fractions $10^{-7} < \delta_s < 10^{-3}$ we find a region in which the cross section is flat within the error bars. It is convenient to choose $\delta_s = 10^{-4}$ for numerical evaluation because here the integration error is still small.

The cancellation of the infrared divergences is one of the crucial points in the calculations of radiative corrections. In figure 6.3 the photon-mass dependence of the virtual and real corrections is shown. After subtracting the singular parts from the virtual corrections and adding the corresponding singular parts to the real corrections as explained in formula (4.17) the cross sections become independent of the photon mass λ. This proves that the cancellation of the infrared divergences works and our cross sections do not depend on the regulators. We performed the same test also for different values for the fermion masses m_f which are used as regulators for the collinear divergences. If we choose $10^{-5}\,\text{GeV} < m_f < 10^{-1}\,\text{GeV}$ we observe that the finite virtual corrections $\sigma_{\text{virt,finite}}$ show no dependence on m_f and that the dependence in σ'_{real} also vanishes if we add the contribution from the

renormalized parton distributions given in formula (5.12).

6.6 Accuracy of the DPA

Since the DPA is used in the calculation of the virtual radiative corrections we have to ensure that we apply proper phase-space cuts to stay in a regime in which this approximation is valid. In this section we present a comparison between the Born cross section with and without DPA. This can be used to estimate the systematic error in the radiative corrections due to our approach. In figure 6.4 the difference between Born cross sections with or without DPA

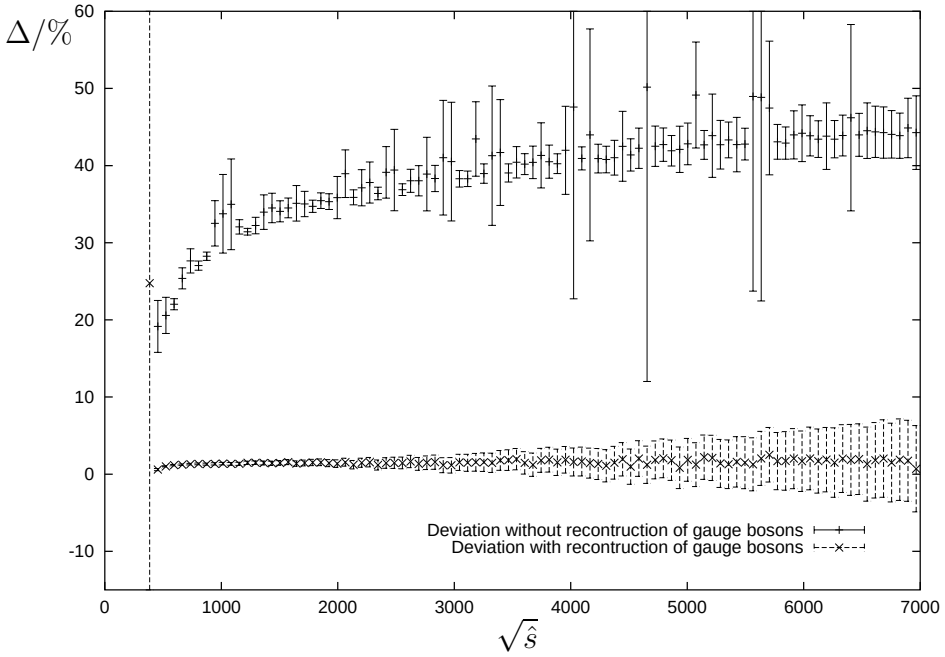

Figure 6.4: Percentage of difference between the Born cross section and the Born cross section in DPA in the case of WZ production. The upper curve shows the deviation without using reconstruction cuts for the gauge bosons. The lower curve was obtained using reconstructed gauge bosons.

is shown depending on the centre-of-mass energy of the partonic subprocess. Here the partonic subprocess is given by $\bar{\mathrm{d}}\mathrm{u} \to \mu^+\mu^-\nu_\mathrm{e}\mathrm{e}^+$. For both curves the cuts shown in table 6.2 have been applied. Without any reconstruction we observe a deviation of $\sim 25\%$ for energies below 1000 GeV which grows up to 40% if we investigate the highest kinematically allowed values for the energy $\sqrt{\hat{s}}$. If the reconstruction cuts are used the error due to the use of

the DPA goes down to 1 to 2% over the whole range for the energy $\sqrt{\hat{s}}$. For high energies the error due to the numerical integration indicated by the errorbars is even higher than the systematical error due to the DPA. For the reconstruction of the Z boson and the W boson we restrict the reconstructed mass of the Z boson $M_{\mathrm{Z,recon}} = \sqrt{(p_i + p_j)^2}$ to be within the interval $[M_{\mathrm{Z}} - 20\,\mathrm{GeV}, M_{\mathrm{Z}} + 20\,\mathrm{GeV}]$ and require the transverse reconstructed $\mathrm{W}^{\pm}$ mass $M_{\mathrm{W,recon}}$ defined in (6.13) to be below $M_{\mathrm{W}} + 20\,\mathrm{GeV}$.

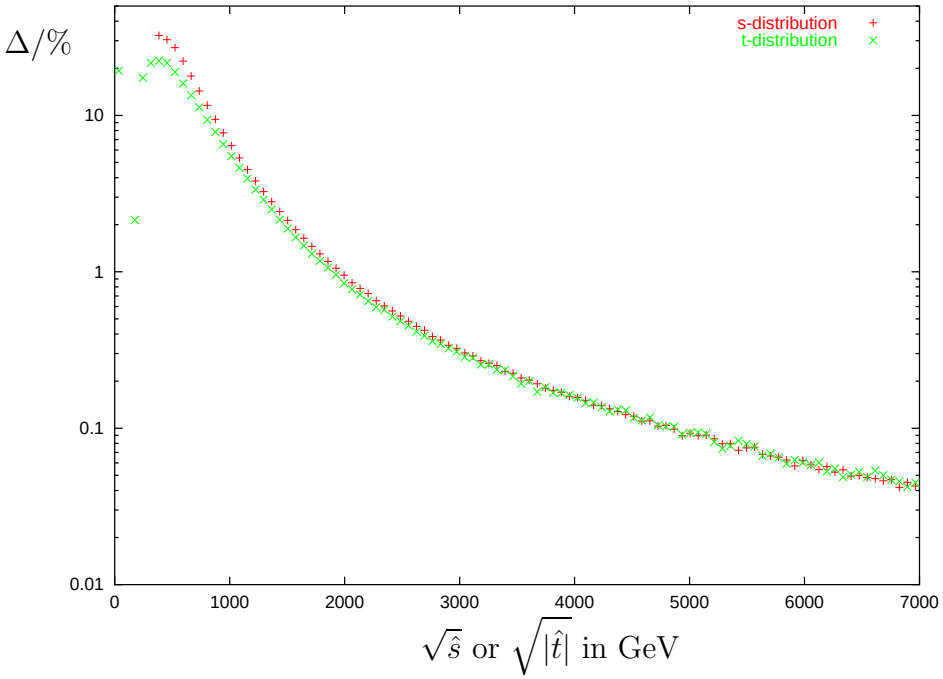

Figure 6.5: Percentage of difference due to the absence of mixed transverse longitudinal gauge-boson production. We show distributions for WZ production in the partonic process $\bar{\mathrm{d}}u \to \nu_{\mathrm{e}}\mathrm{e}^+\mu^-\mu^+$ with standard cuts.

In figure 6.5 we show the systematic error we do by neglecting matrix elements with one transverse and one longitudinal gauge boson in the DPA. Again we used the Born cross sections for the partonic subprocess $\bar{\mathrm{d}}\mathrm{u} \to \mu^+\mu^-\nu_{\mathrm{e}}\mathrm{e}^+$ and the cuts shown in table 6.2. The t-distribution was calculated from the momentum of the reconstructed Z boson $\hat{t} = (p_{\bar{\mathrm{d}}} - p_{\mathrm{Z}})^2$. We plotted the percentage of difference between the DPA cross section $\sigma_{\mathrm{Born}}^{\mathrm{DPA,TT+LL+TL}}$ including transverse longitudinal mixed states and the cross section $\sigma_{\mathrm{Born}}^{\mathrm{DPA,TT+LL}}$ in which these contributions are neglected. We find that these cross sections deviate up to 15% at energies below 1 TeV. In the high-energy regime above 1 TeV the agreement is improving very fast and for energy scales bigger

than 2.5 TeV the error already drops below 0.5%. This behaviour was expected, since the contributions of matrix elements with one transverse and one longitudinal gauge boson do not contribute in the high-energy limit.

For our corrections these results show, that the systematic error is well below 5% for using DPA and below 15% for neglecting polarization mixed states within the DPA. As a worst case scenario we could end up with a systematical error of 15% on the radiative corrections which themselves have a typical size of 15% of the Born cross section. With this assumptions we find for the radiative corrections in the scenarios discussed in section 6.7 a maximal total error of $\approx 2\%$ on the total corrected cross sections.

6.7 Corrections to gauge-boson production

For the investigation of gauge-boson production processes we always impose the standard cuts given in table 6.2 and the recombination procedure for the photons from section 6.3. In addition we reconstruct the gauge bosons as described in section 6.4 whenever this is possible. The only case described in this work in which there is no reconstruction is the case of WW production. In this case there are two neutrinos in the final state so that it is not possible to reconstruct the transverse W-boson momentum with the help of the missing momentum.

For the numerical results shown in the following sections we neglected all extra logarithms including the Higgs mass and logarithms including the top mass. To be consistent with the FORTRAN program written by Elena Accomondo we also drop logarithms of $M_{\mathrm{W}}/M_{\mathrm{Z}}$ which appear in the subleading soft-collinear corrections. This means we assume

$$\log\frac{M_{\mathrm{H}}^2}{M_{\mathrm{Z}}^2}=0,\quad \log\frac{M_{\mathrm{H}}^2}{M_{\mathrm{W}}^2}=0,\quad \log\frac{m_{\mathrm{t}}^2}{M_{\mathrm{W}}^2}=0,\ \text{and}\quad \log\frac{M_{\mathrm{W}}^2}{M_{\mathrm{Z}}^2}=0, \tag{6.15}$$

in all formulae given in chapter 3. In addition we use the G_μ scheme in which the running of the coupling α is already included so that we have to set $\Delta\alpha(M_{\mathrm{W}}^2)=0$.

6.7.1 WZ production

In this section we study the leptonic processes $\mathrm{pp}\to l\nu_l l'\bar{l}'$ with $l,l'=\mathrm{e}$ or μ. These final states can be mediated by WZ production and allow to test the trilinear WWZ couplings.

For this case we have chosen to investigate four distributions which include the final states $\mathrm{e}^-\bar{\nu}_\mathrm{e}\mu^-\mu^+$ and $\nu_\mathrm{e}\mathrm{e}^+\mu^-\mu^+$. To investigate the behaviour at different energies we show two momentum distributions:

$P_{\mathrm{T}}^{\mathrm{miss}}$**:** missing transverse momentum,

$P_{\mathrm{T}}^{\mathrm{max}}(l)$**:** maximal transverse momentum of the charged leptons,

and two angular distributions:

$\Delta y(\mathrm{Z}l) = y(\mathrm{Z}) - y(l)$**:** rapidity difference between reconstructed Z boson and charged lepton from W-boson decay,

$y(l^-)$**:** rapidity of the negatively charged lepton coming from the reconstructed Z boson.

The rapidity y is defined from the energy E and the longitudinal momentum P_{L} by $y = 0.5 \log((E + P_{\mathrm{L}})/(E - P_{\mathrm{L}}))$.

We note that under the kinematical cuts in table 6.2 and the use of the reconstruction described in section 6.4 the exact result is well approximated by the DPA. The difference, which is about 15% without gauge-boson reconstruction, goes down to per-cent level (for a detailed discussion see Ref. [16]). Thus, we can safely adopt the DPA for calculating EW radiative corrections.

As an illustration of the role played by $\mathcal{O}(\alpha)$ corrections, we study the above-mentioned distributions in two different kinematical regions both characterized by large energies and scattering angles in the di-boson rest frame.

As a first scenario, we restrict the transverse momentum of the reconstructed Z boson, $P_{\mathrm{T}}(\mathrm{Z})$, by

$$P_{\mathrm{T}}(\mathrm{Z}) > 300\,\mathrm{GeV}. \tag{6.16}$$

As a second scenario, we impose cuts on the invariant mass of the three charged leptons, $M_{\mathrm{inv}}(ll'\bar{l}')$, and the difference $\Delta y(\mathrm{Z}l) = y(\mathrm{Z}) - y(l)$ between the rapidity of the reconstructed Z boson and of the charged lepton coming from the W-boson decay:

$$M_{\mathrm{inv}}(ll'\bar{l}') > 500\,\mathrm{GeV}, \qquad |\Delta y(\mathrm{Z}l)| < 3. \tag{6.17}$$

Under these cuts, all invariants $\hat{s}, \hat{t}, \hat{u}$ are large compared to the W-boson mass. In particular, $\sqrt{\hat{s}} \gtrsim 600\,\mathrm{GeV}$ and $\sqrt{\hat{t}}, \sqrt{\hat{u}} \gtrsim 200\,\mathrm{GeV}$ for most events and $\sqrt{\hat{s}} > 500\,\mathrm{GeV}$ and $\sqrt{\hat{t}}, \sqrt{\hat{u}} > 100\,\mathrm{GeV}$ for all.[1] Thus, the conditions equation, under which the logarithmic high-energy approximation is valid, are well fulfilled in these two kinematical regions.

[1]Note that the high-energy approximation can be applied as long as $\sqrt{\hat{s}}, \sqrt{\hat{t}}, \sqrt{\hat{u}} \gtrsim M_{\mathrm{W}}$. If the invariants are of the order of M_{W} but larger, the logarithms become small and the large corrections are switched off. The high-energy approximation yields wrong results, once the invariants are smaller than M_{W}.

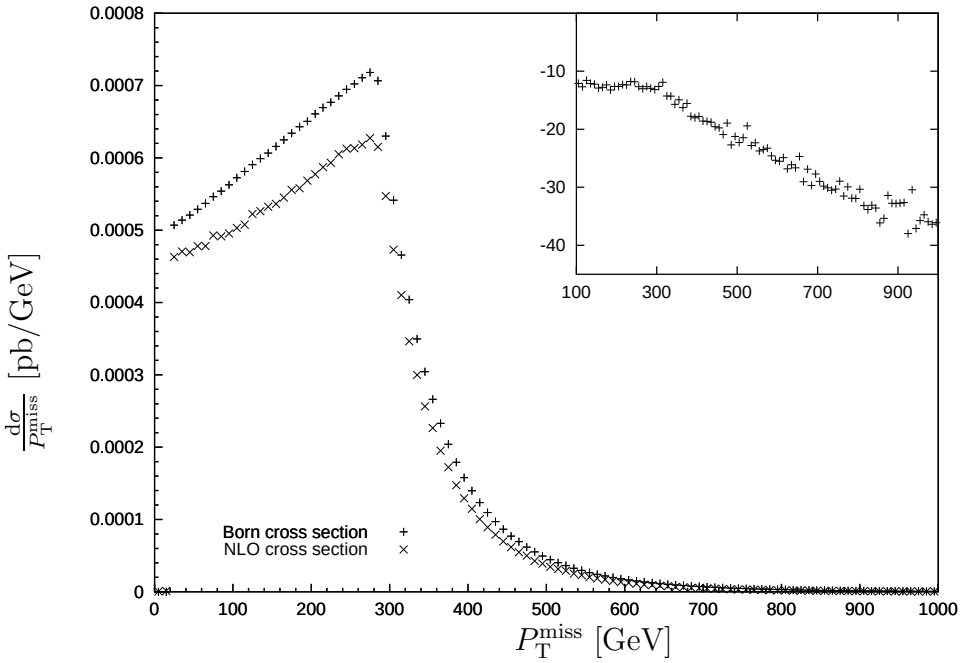

Figure 6.6: Missing-transverse-momentum distribution for WZ production. The plot shows the sum over the final states $e^-\bar{\nu}_e\mu^-\mu^+$ and $\nu_e e^+\mu^-\mu^+$ with standard cuts and $P_T(Z) > 300\,\text{GeV}$.

We start discussing the scenario equation (6.16). In the figures 6.6, 6.7, 6.8, and 6.9 we have plotted the four differential distributions for the complete process $PP \to e^-\bar{\nu}_e\mu^-\mu^+, \nu_e e^+\mu^-\mu^+$, i.e. we sum over the two charge-conjugate final states. The inset plots show the percentage of difference between the Born and our NLO cross section. As a general feature the EW corrections are negative and lower the Born cross section by more than 10%. For the individual distributions we observe the following. EW corrections reduce the distribution in $P_T^{max}(l^-)$ by the order of 10% at low to modest $P_T^{max}(l^-)$ values. This effect grows with increasing $P_T^{max}(l^-)$ as shown by the long tail where the contribution of EW corrections can amount to more than 30%. This is of course the result of enhanced EW logarithms at large energies, which are enforced by the large $P_T^{max}(l^-)$. The missing-transverse-momentum distribution shows the same qualitative behaviour. At low values the correction amounts to about -15%, while at high P_T^{miss} it increases by a factor of more than two. As stated in the literature, the large P_T region is an ideal place to look for new physics. As an example, the $P_T(Z)$ distribution has been found to be much more sensitive to new-physics effects than the WZ invariant-mass distribution, which in principle should give a more direct access to the energy scale [8, 13]. This feature is shared by $P_T^{max}(l^-)$ and P_T^{miss} we just discussed.

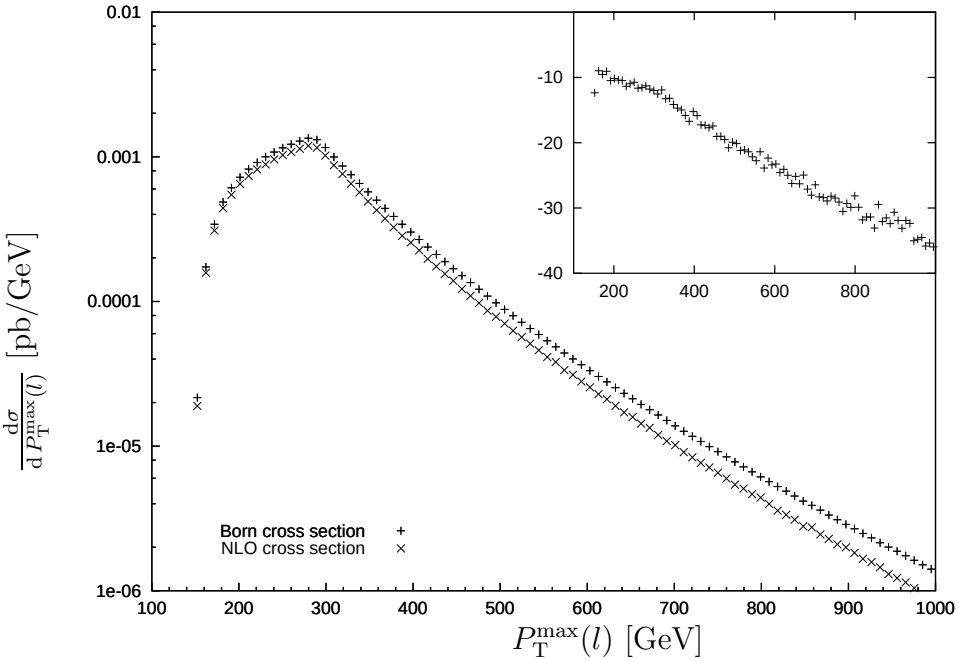

Figure 6.7: Distribution of the maximal transverse momentum of the detected leptons. The plot shows the sum over the final states $\mathrm{e}^-\bar{\nu}_\mathrm{e}\mu^-\mu^+$ and $\nu_\mathrm{e}\mathrm{e}^+\mu^-\mu^+$ with standard cuts and $P_\mathrm{T}(\mathrm{Z}) > 300\,\mathrm{GeV}$.

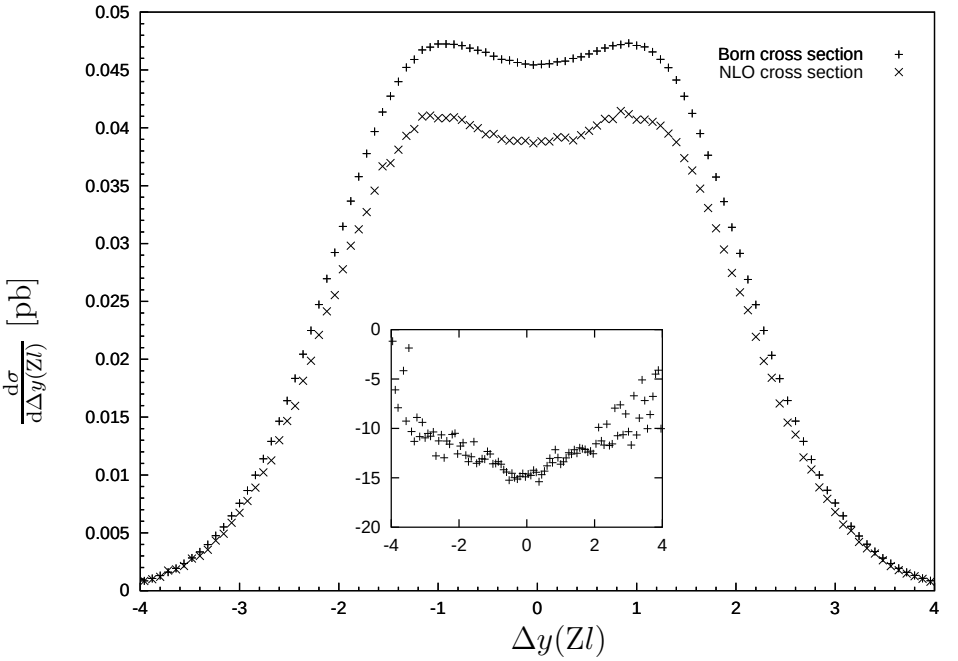

Figure 6.8: Distribution in the rapidity difference between the reconstructed Z and the $l^\pm$ from the reconstructed W. The plot shows the sum over the final states $\mathrm{e}^-\bar{\nu}_\mathrm{e}\mu^-\mu^+$ and $\nu_\mathrm{e}\mathrm{e}^+\mu^-\mu^+$ with standard cuts and $P_\mathrm{T}(\mathrm{Z}) > 300\,\mathrm{GeV}$.

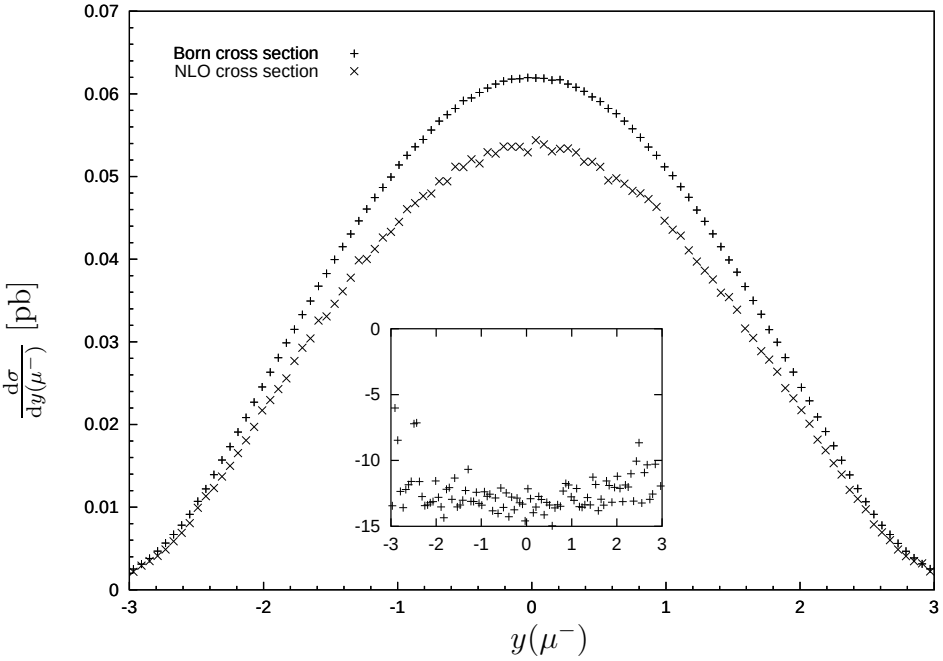

Figure 6.9: Rapidity distribution of the negatively charged muon in a WZ-production process. The final states $e^-\bar{\nu}_e\mu^-\mu^+$ and $\nu_e e^+\mu^-\mu^+$ are summed and standard cuts and $P_T(Z) > 300\,\text{GeV}$ are applied.

As to angular distributions, EW corrections are maximal at low rapidity values in both cases, where once again effects due to new physics could be more enhanced. A low rapidity corresponds in fact to large scattering angles of the produced vector bosons in their rest frame. As shown in the figure 6.8, the distribution in the rapidity difference $\Delta y(Zl)$ exhibits a characteristic dip, relic of an approximate radiation zero at high energy [38]. Of course, new physics could have observable consequences on the shape of this variable [8, 13]. The general tendency is to fill in the dip, but in certain models the approximate zero may even become more pronounced. It is thus important to consider the impact of radiative corrections to this relevant signal. In the last decade, the effect of NLO QCD corrections has been extensively analysed [8, 13]. It can completely spoil the significance of the dip, if one measures the inclusive $WZ + X$ production. By imposing a jet veto, the QCD corrections get drastically reduced to about 20% of the Born result, at the same time diminishing the dependence of the NLO cross section on the factorization scale. As shown in figure 6.8, EW corrections can be of the same order as QCD effects but with opposite sign. So, they slightly increase the dip.

Of course, radiative corrections do not only depend on the considered distribution but also on the selected cuts. In the figures 6.10, 6.11, 6.12, and 6.13 we show a second set of plots for the same set of distributions as

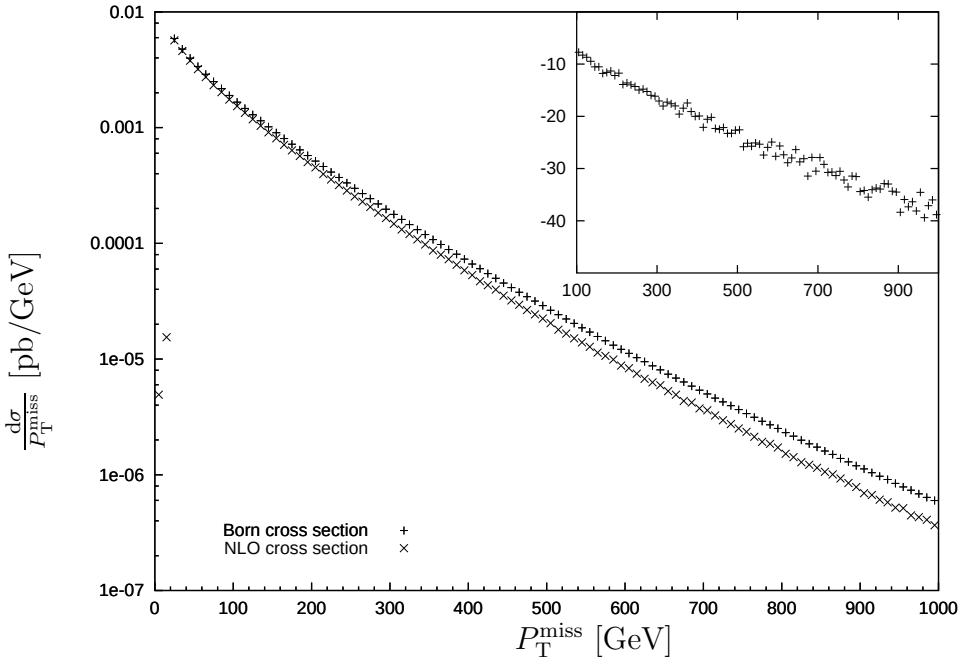

Figure 6.10: Missing-transverse-momentum distribution for WZ production. The plot shows the sum over the final states $\mathrm{e}^-\bar{\nu}_\mathrm{e}\mu^-\mu^+$ and $\nu_\mathrm{e}\mathrm{e}^+\mu^-\mu^+$ with standard cuts, $M_\mathrm{inv}(ll'\bar{l}') > 500\,\mathrm{GeV}$, and $|\Delta y(\mathrm{Z}l)| < 3$ applied.

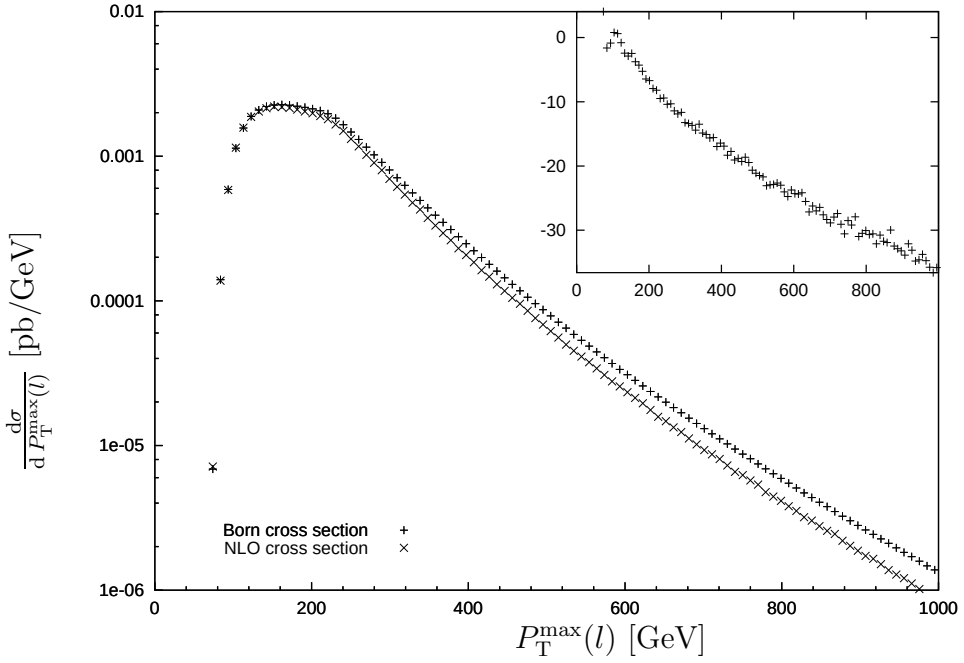

Figure 6.11: Distribution of the maximal transverse momentum of the detected leptons. The plot shows the sum over the final states $\mathrm{e}^-\bar{\nu}_\mathrm{e}\mu^-\mu^+$ and $\nu_\mathrm{e}\mathrm{e}^+\mu^-\mu^+$ with standard cuts, $M_\mathrm{inv}(ll'\bar{l}') > 500\,\mathrm{GeV}$, and $|\Delta y(\mathrm{Z}l)| < 3$ applied.

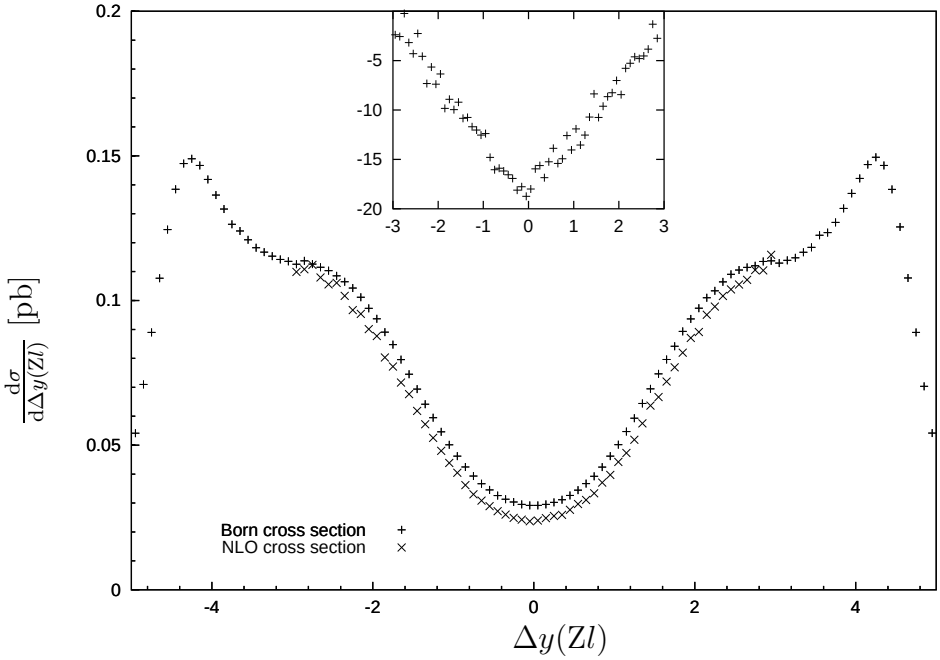

Figure 6.12: Distribution in the rapidity difference between the reconstructed Z and the $l^{\pm}$ from the reconstructed W. The plot shows the sum over the final states $e^-\bar{\nu}_e\mu^-\mu^+$ and $\nu_e e^+\mu^-\mu^+$ with standard cuts and $M_{\rm inv}(ll'\bar{l}') > 500\,\text{GeV}$. The radiative corrections are only included for $|\Delta y(Zl)| < 3$.

above but in the scenario given in equation (6.17). The influence of the radiative corrections on the two momentum-like variables is analogous to the one observed in the previous case. The main difference between the two selected kinematical regions is in the shape of the $\Delta y(Zl)$ distribution. Here, the radiation-zero dip strongly increases. This is due to the fact that the requirement $M_{\rm inv}(ll'\bar{l}') > 500\,\text{GeV}$ forces the reconstructed Z boson and the charged lepton from the W-boson decay to be produced at large separation angle. This effect translates into a depletion of events in the central region of low rapidity difference. Radiative corrections are more pronounced in this suppressed region, which corresponds to large scattering angles in the di-boson rest frame.

To measure the significance of the EW corrections, a naive but direct way is to compare their magnitude with the expected statistical error. In table 6.3 we have listed the relative deviation Δ and the statistical accuracy, estimated by taking as a luminosity $L = 100\,\text{fb}^{-1}$ for two experiments, in the scenario (6.16) for some values of the cut on the transverse momentum of the reconstructed Z boson. To this purpose, we sum over all eight final states $e^-\bar{\nu}_e\mu^-\mu^+$, $\nu_e e^+\mu^-\mu^+$, $\mu^-\bar{\nu}_\mu e^-e^+$, $\nu_\mu\mu^+e^-e^+$, $\mu^-\bar{\nu}_\mu\mu^-\mu^+$, $\nu_\mu\mu^+\mu^-\mu^+$, $e^-\bar{\nu}_e e^-e^+$, and $\nu_e e^+e^-e^+$. In table 6.4, we give the same entries but for the sce-

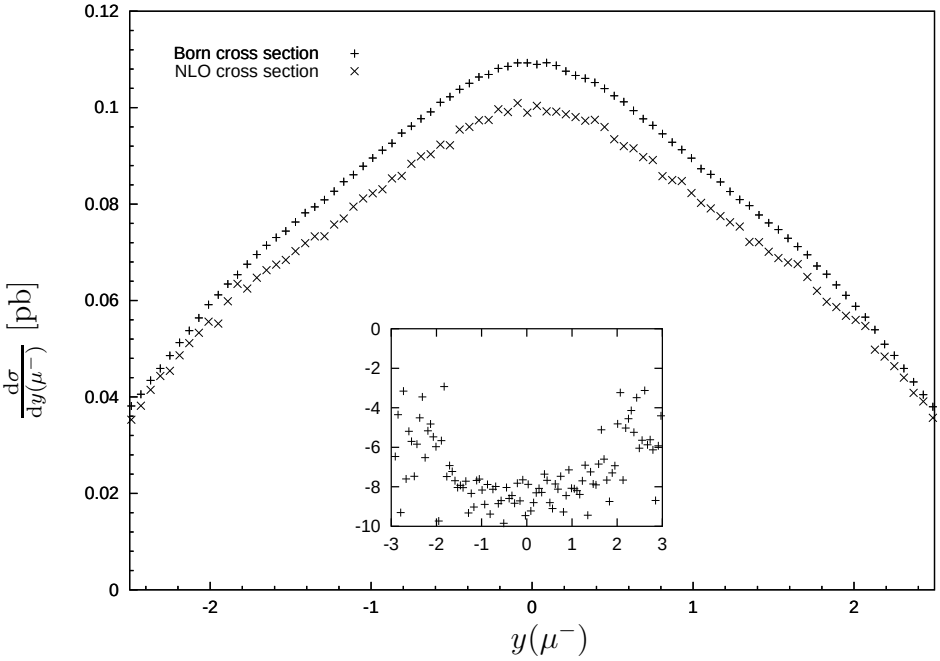

Figure 6.13: Rapidity distribution of the negatively charged muon in a WZ production process. The plot shows the sum over the final states $e^-\bar{\nu}_e\mu^-\mu^+$ and $\nu_e e^+\mu^-\mu^+$ with standard cuts, $M_{\rm inv}(ll'\bar{l}') > 500\,\text{GeV}$, and $|\Delta y(Zl)| < 3$ applied.

nario (6.17) and for different values of the charged-lepton invariant-mass cut. This comparison indicates that EW corrections are non-negligible and can be comparable with the experimental precision up to about $P_{\rm T}^{\rm cut}(Z) = 500\,\text{GeV}$ or $M_{\rm inv}^{\rm cut}(ll'\bar{l}') = 1\text{TeV}$. In these regions the corrections range between -7 and -22%, being slightly more enhanced in the first scenario. Of course, their significance depends on the available luminosity. This kind of accuracy is needed only in a high-luminosity run.

Besides the lowest-order cross section $\sigma_{\rm Born}$ and the cross section $\sigma_{\rm EW}$ including the complete leading-logarithmic EW corrections, we have also inserted two entries representing partial results in tables 6.3 and 6.4 in order to give an idea of the individual contributions. The cross section including only the leading EW logarithms originating from above the EW scale, $M_{\rm W}$, is denoted by $\sigma_{\rm AEWS}$. This term neglects all IR and mass-singular terms coming from the mass gap between the photon and the weak gauge bosons and is exactly the part computed in Ref. [16] for the same process. The column $\sigma_{\rm virt}^{\rm finite}$ contains instead the full finite virtual correction, i.e. the full leading-logarithmic EW corrections with the IR- and mass-singular contribution subtracted as defined in equation (4.17). The difference between $\sigma_{\rm AEWS}$ and $\sigma_{\rm virt}^{\rm finite}$ is numerically small, despite of the fact that it contains leading

$pp \to l\nu_l l'\bar{l}'$						
$P_T(Z)$ [GeV]	σ_{Born} [fb]	σ_{AEWS} [fb]	σ_{virt}^{finite} [fb]	σ_{EW} [fb]	Δ [%]	$1/\sqrt{2L\sigma_{Born}}$ [%]
250	1.672	1.563	1.553	1.489	-10.9	5.5
300	0.876	0.794	0.789	0.761	-13.1	7.6
350	0.489	0.431	0.428	0.413	-15.5	10.1
400	0.287	0.246	0.244	0.236	-17.8	13.2
450	0.175	0.146	0.145	0.141	-19.7	16.9
500	0.111	0.090	0.089	0.087	-21.2	21.2

Table 6.3: Cross section for PP $\to l\nu_l l'\bar{l}'$ for various values of $P_T^{cut}(Z)$. Here we have summed over all eight final states with $l, l' =$ e or μ.

$pp \to l\nu_l l'\bar{l}'$						
$M(ll'\bar{l}')$ [GeV]	σ_{Born} [fb]	σ_{AEWS} [fb]	σ_{virt}^{finite} [fb]	σ_{EW} [fb]	Δ [%]	$1/\sqrt{2L\sigma_{Born}}$ [%]
500	1.729	1.689	1.692	1.601	-7.4	5.4
600	0.899	0.858	0.860	0.814	-9.5	7.5
700	0.508	0.474	0.476	0.452	-10.9	9.9
800	0.304	0.278	0.279	0.264	-13.3	12.8
900	0.190	0.170	0.171	0.161	-15.1	16.2
1000	0.123	0.108	0.109	0.102	-16.7	20.2

Table 6.4: Cross section for PP $\to l\nu_l l'\bar{l}'$ for various values of $M_{inv}^{cut}(ll'\bar{l}')$. Here we have summed over all eight final states with $l, l' =$ e or μ.

logarithmic contributions. The dominant contribution to this difference is in fact proportional to $\alpha/(2\pi)\log(s/M^2)(\log(s/M^2)-3)$ which is numerically small for energies between 500 GeV and 1TeV owing to cancellations.

6.7.2 ZZ production

In this section we extend our analysis to the processes PP $\to l\bar{l}l'\bar{l}'$ ($l, l' =$ e or μ). This channel is proper for studying the impact of trilinear neutral gauge-boson vertices, ZZZ and ZZγ, on physical observables. While these couplings are absent in the SM Lagrangian, one-loop corrections induce small but not-vanishing values for these couplings. Significantly larger couplings are predicted by non-standard models, where new physics appearing at energy scales much larger than those which can be directly probed at forthcoming experiments can be parameterized in terms of anomalous neutral self-interactions.

At LEP2 and Tevatron, the ZZγ vertex has been measured through Zγ production. LEP2 has been able to produce also ZZ pairs but with poor statistics. At the LHC several thousands of such ZZ pairs will be produced, allowing for more stringent bounds on ZZZ and ZZγ vertices. The envisioned increase in statistics, and the possibility to observe significant deviations due to new physics interactions have gathered a renewed interest in the literature [39].

ZZZ and ZZγ couplings affect the production of longitudinal or transverse Z bosons in a different way. Therefore, the helicity of the decay products coming from ZZ production constitutes a valuable information. Up to now, on one side the aforementioned studies have been performed in the *production*$\times$*decay* approach, neglecting all spin correlations and irreducible background contributions. On the other side, accurate calculations of QCD corrections have been carried out in Ref. [8]. In this section, we illustrate the results of a complete calculation of four-fermion production mediated by ZZ production including leading-logarithmic EW corrections. We focus, in particular, on the effect of the EW corrections on the distributions mostly discussed in the literature [40].

We consider the same kind of observables as in the previous section, with the only difference that we replace the distribution in the missing transverse momentum by the distribution in the maximal transverse momentum of the reconstructed Z bosons. To be precise we plot distributions in:

$P_{\mathrm{T}}(\mathrm{Z})$**:** maximal transverse momentum of the reconstructed Z bosons,

$P_{\mathrm{T}}^{\mathrm{max}}(l)$**:** maximal transverse momentum of the charged leptons,

$\Delta y(\mathrm{ZZ})$**:** rapidity difference between the two reconstructed Z bosons,

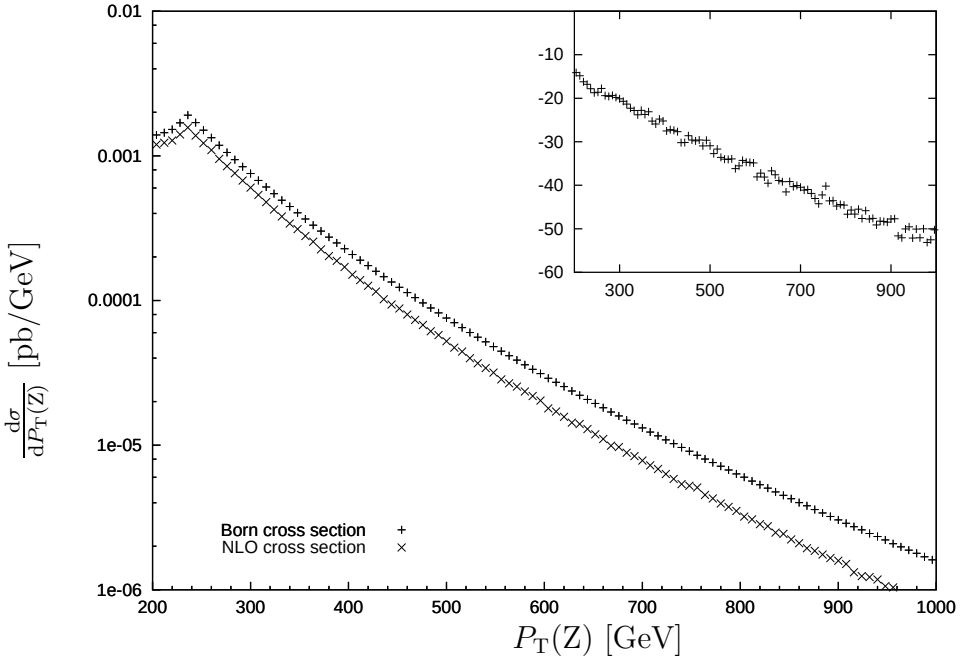

Figure 6.14: Distribution of the maximal transverse momentum of the reconstructed Z bosons. We show the $e^-e^+\mu^-\mu^+$ final state with standard cuts and $M_{\rm inv}(l\bar{l}l'\bar{l}') > 500\,\text{GeV}$ and $|\Delta y(\text{ZZ})| < 3$.

$y(\mu^-)$**:** rapidity of the μ^-.

We show results for the specific process $\text{PP} \to e^-e^+\mu^-\mu^+$ and only for the scenario characterized by the requirement

$$M_{\rm inv}(l\bar{l}l'\bar{l}') > 500\,\text{GeV}, \qquad |\Delta y(\text{ZZ})| < 3. \tag{6.18}$$

We have checked that the accuracy of the DPA is at the level of a few per cent for this case if the reconstruction procedure described in section 6.4 is used. An analogous behaviour holds for the scenario with $P_T(Z) > 300\,\text{GeV}$ for both reconstructed Z bosons. We have verified that also for these scenarios the conditions for the validity of the logarithmic high-energy approximation are well fulfilled.

As one can see in the figures 6.14, 6.15, 6.16, and 6.17, EW corrections modify the Born result in the same way as for WZ production, but the effect is typically a factor of 1.5 larger. We note that WZ production at tree level does not present any true or approximate radiation zero. The dip in the distribution of the rapidity difference of the two reconstructed Z bosons results from the fact that the partonic process $q\bar{q} \to \text{ZZ}$, dominated by the transversely polarized Z bosons, is peaked forward and backward and is enhanced by the invariant-mass cut in equation (6.18).

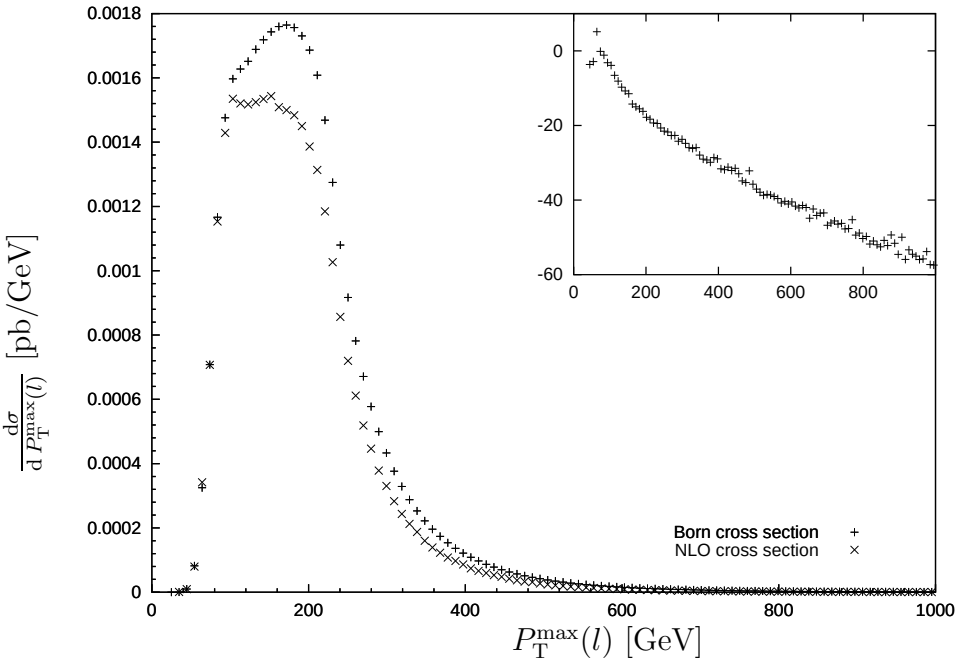

Figure 6.15: Distribution of the maximal transverse momentum of the detected leptons for the $\mathrm{e^-e^+}\mu^-\mu^+$ final state. Standard cuts, $M_{\mathrm{inv}}(l\bar{l}l'\bar{l}') > 500\,\mathrm{GeV}$, and $|\Delta y(\mathrm{ZZ})| < 3$ are imposed.

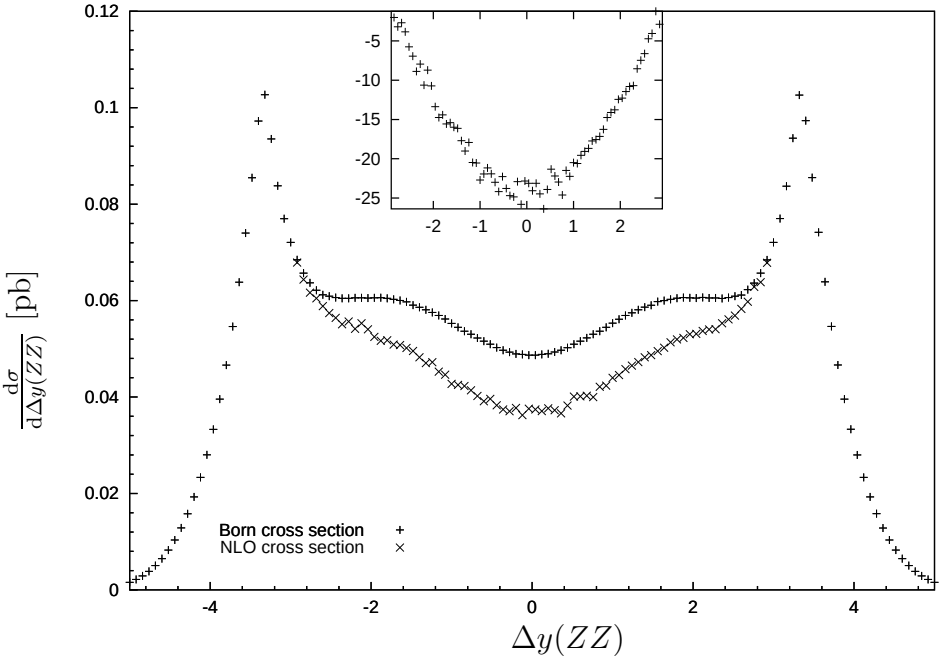

Figure 6.16: Distribution in the rapidity difference between the two reconstructed Z bosons for the $\mathrm{e^-e^+}\mu^-\mu^+$ final state with standard cuts and $M_{\mathrm{inv}}(l\bar{l}l'\bar{l}') > 500\,\mathrm{GeV}$. Radiative corrections are only included for $|\Delta y(\mathrm{ZZ})| < 3$.

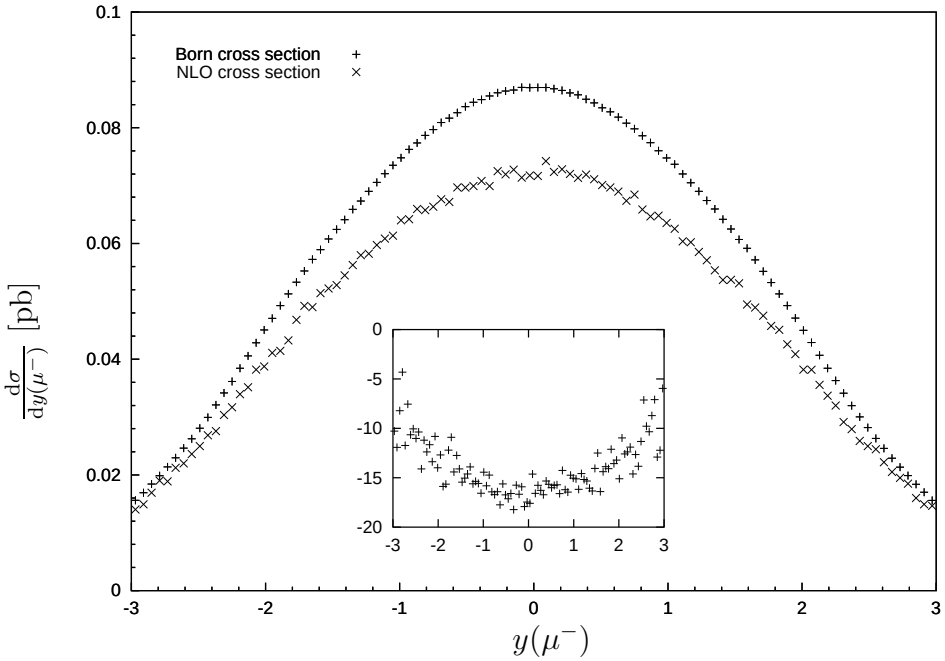

Figure 6.17: Rapidity distribution of the negatively charged muon in a ZZ production process. We show the $e^-e^+\mu^-\mu^+$ final state with standard cuts, $M_{\rm inv}(l\bar{l}l'\bar{l}') > 500\,\text{GeV}$, and $|\Delta y(\text{ZZ})| < 3$.

$pp \to l\nu_l l'\bar{l}'$						
$M_{\rm inv}^{\rm cut}(l\bar{l}l'\bar{l}')$ [GeV]	$\sigma_{\rm Born}$ [fb]	$\sigma_{\rm AEWS}$ [fb]	$\sigma_{\rm virt}^{\rm finite}$ [fb]	$\sigma_{\rm EW}$ [fb]	Δ [%]	$1/\sqrt{2L\sigma_{\rm Born}}$ [%]
500	0.692	0.637	0.633	0.588	-15.0	8.5
600	0.356	0.314	0.312	0.291	-18.3	11.9
700	0.203	0.173	0.172	0.160	-21.0	15.7
800	0.123	0.102	0.101	0.094	-23.8	20.1
900	0.078	0.063	0.062	0.058	-26.1	25.3
1000	0.051	0.040	0.040	0.037	-28.1	31.2

Table 6.5: Cross section for $PP \to e^-e^+\mu^-\mu^+$, $e^-e^+e^-e^+$, and $\mu^-\mu^+\mu^-\mu^+$ for various values of $M_{\rm inv}^{\rm cut}(l\bar{l}l'\bar{l}')$

In table 6.5 we compare the relative correction Δ to the Born cross section with the estimated experimental accuracy for some values of the cut on the partonic CM energy $M_{\rm inv}(l\bar{l}l'\bar{l}')$. To this purpose, we sum over all three final states $e^-e^+\mu^-\mu^+$, $e^-e^+e^-e^+$, and $\mu^-\mu^+\mu^-\mu^+$. The entries in table 6.5 are defined as in the previous section. One can see that, compared to WZ production, $\mathcal{O}(\alpha)$ corrections manifest the same behaviour on the shown observables, but they are globally by a factor of about 1.5 larger. At modest ZZ invariant masses, the effect of the EW corrections can amount to two standard deviations, while it becomes comparable to the experimental precision with increasing CM energy. Of course, purely leptonic final states coming from ZZ production will not be copiously generated at the LHC. A detailed study of their properties would be possible only during a high-luminosity run.

6.7.3 WW production

In this section, we discuss the processes $PP \to l\bar{\nu}_l\nu_{l'}\bar{l}'$ ($l, l' = e$ or μ). This channel contains information on the charged gauge-boson vertices WWZ and WWγ. While LEP2 could establish the non-abelian nature of the SM by measuring these couplings, high precision measurements are still missing. At the LHC, the precision will be sensitively improved, if the large background from $t\bar{t}$ production can be properly controlled. The WW channel has in fact the largest cross section among all vector-boson pair-production processes. However, owing to the presence of two neutrinos, it does not allow a clean and unambiguous reconstruction of the two W bosons.

Once again for this channel, following the study of Ref. [8] on the sensitivity to new physics effects, we choose to discuss distributions for the $\nu_e e^+\mu^-\nu_\mu$ final state in the following variables:

$P_{\rm T}^{\rm max}(l)$**:** maximal transverse momentum of the two charged leptons,

$P_{\rm T}^{\rm miss}$**:** missing transverse momentum,

$\Delta y(l\bar{l}')$**:** rapidity difference between the charged leptons,

$y(l^-)$**:** rapidity of the negatively charged lepton.

Despite of the fact that we do not perform a reconstruction of the W bosons for these processes, the quality of the DPA is better than 10%. Since we apply the DPA only to the corrections and these are below 25%, at least where the cross section is appreciable, this introduces an error of only a few per cent. We consider the scenario

$$M_{\rm inv}(l\bar{l}') > 500\,{\rm GeV}, \qquad |\Delta y(l\bar{l}')| < 3, \tag{6.19}$$

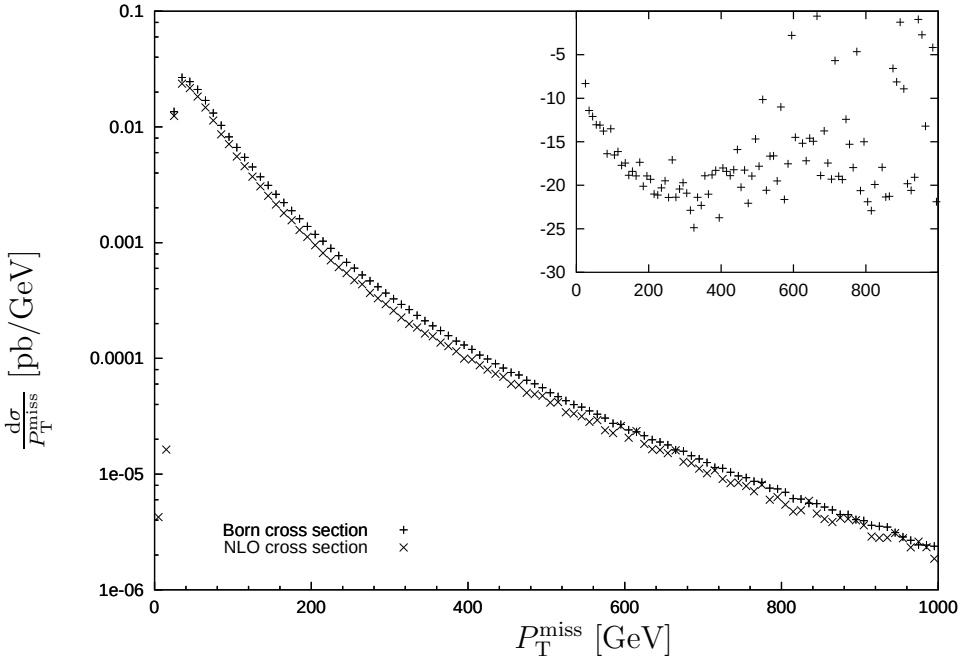

Figure 6.18: Missing-transverse-momentum distribution for WW production. We show the plot for the $\nu_e e^+ \mu^- \bar{\nu}_\mu$ final state with standard cuts, $M_{inv}(l\bar{l}') > 500\,\text{GeV}$, and $|\Delta y(l\bar{l}')| < 3$.

which fulfils the conditions for the validity of the logarithmic high-energy approximation, as we have verified. Possible ZZ intermediate states are heavily suppressed by the invariant-mass cut in equation (6.19). Therefore, we can safely neglect contributions of $l\bar{l}\nu_{l'}\bar{\nu}_{l'}$ final states with $l \neq l'$.

In the figures 6.18, 6.19, 6.20, and 6.21 we show the distributions for the final state $\nu_e e^+ \mu^- \bar{\nu}_\mu$ with our standard cuts applied. As in the previous two cases, $\mathcal{O}(\alpha)$ corrections are enhanced at high energy and large scattering angles. This translates into larger radiative corrections in the tails of transverse momentum distributions and in the central region of rapidity distributions. Let us note that also in this case the partonic process at Born level does not vanish for any scattering angle, independently on the W-boson polarization. The dip appearing in the distribution of the rapidity difference between the two charged leptons is this time due to the chosen set of cuts. In absence of any kinematical cuts, the $PP \to W^+W^-$ process is dominated by the u-quark contribution, and the rapidity-difference $\Delta y(l\bar{l}')$ for the partonic process $\bar{u}u \to 4f$ is maximal and symmetric around zero. The requirement of having a large invariant mass of the two charged leptons, forces the two leptons to be produced at large separation angles. This fact depletes the number of events in the central region of $\Delta y(l\bar{l}')$ and leaves events with larger rapidity difference, coming preferably from initial d quarks. This gives rise to the

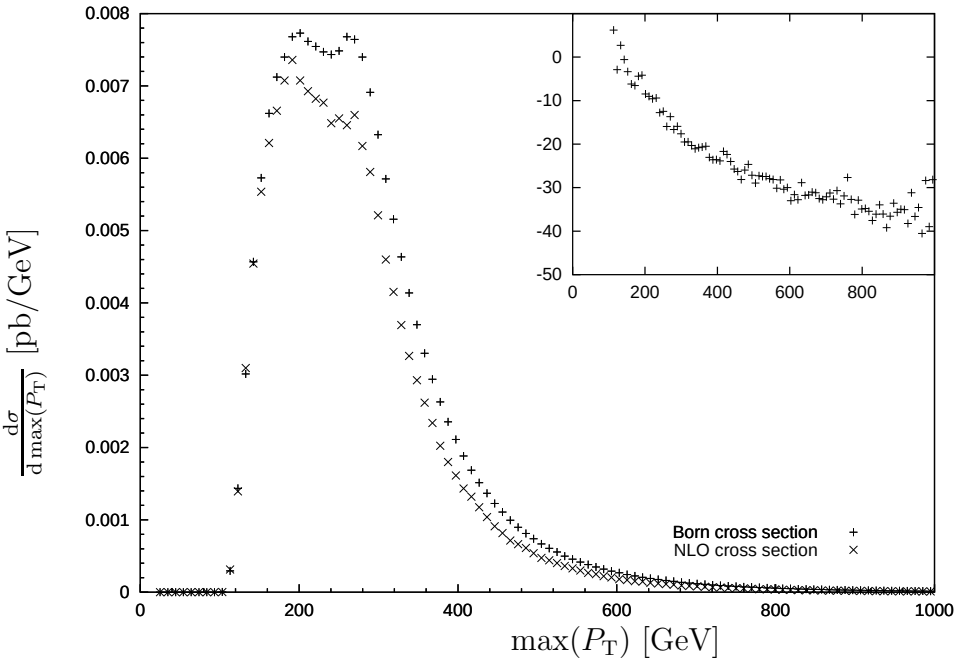

Figure 6.19: Distribution of the maximal transverse momentum of the detected leptons for the $\nu_e e^+ \mu^- \bar{\nu}_\mu$ final state. Standard cuts, $M_{\rm inv}(l\bar{l}') > 500\,\text{GeV}$, and $|\Delta y(l\bar{l}')| < 3$ are applied.

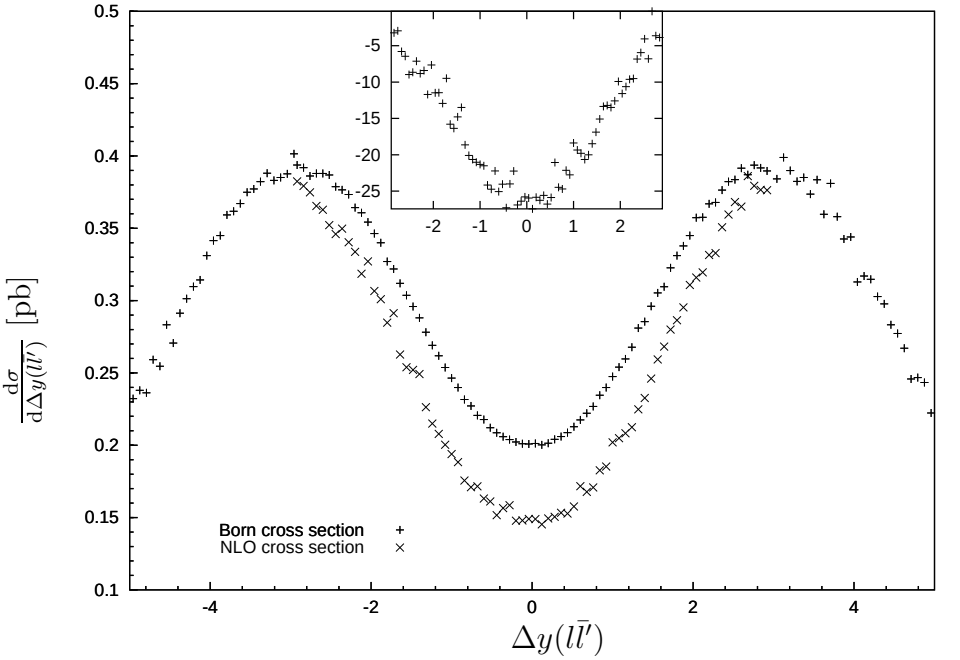

Figure 6.20: Distribution in the rapidity difference between the e^+ and the μ^- from the reconstructed W bosons for $\nu_e e^+ \mu^- \bar{\nu}_\mu$ production with standard cuts and $M_{\rm inv}(l\bar{l}') > 500\,\text{GeV}$. Radiative corrections are only included for $|\Delta y(l\bar{l}')| < 3$.

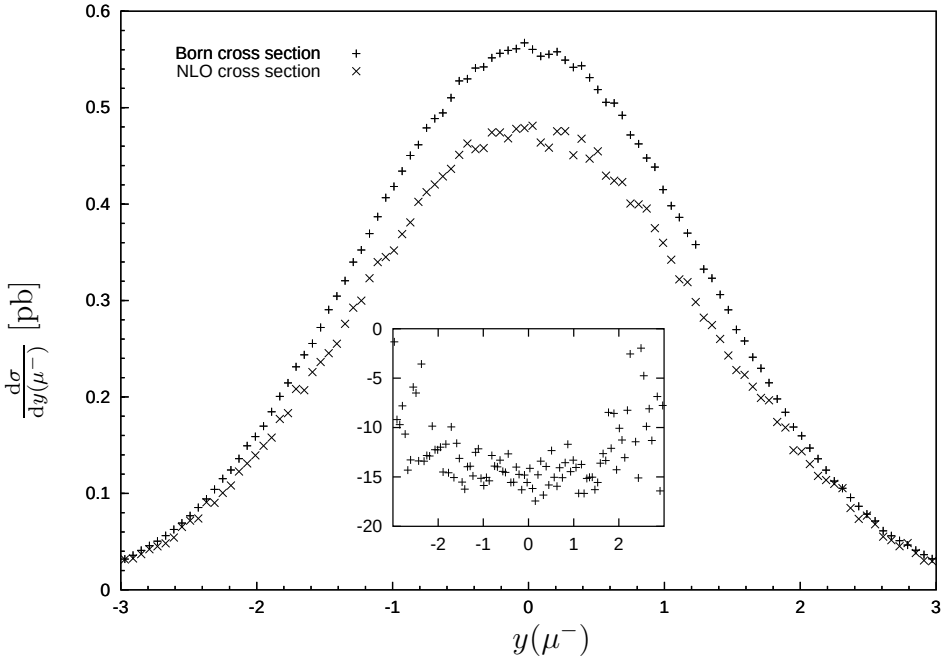

Figure 6.21: Rapidity distribution of the negatively charged muon in a WW production process with $\nu_e e^+ \mu^- \bar{\nu}_\mu$ in the final state. Standard cuts, $M_{\rm inv}(l\bar{l}') > 500\,\text{GeV}$, and $|\Delta y(l\bar{l}')| < 3$ are applied.

shape of figure 6.20.

The general behaviour of EW corrections does not present novelties compared to the previous cases. The interesting feature of WW processes is the remarkable statistics of purely leptonic final states. As shown in table 6.6, where we sum over the four final states $e^- \bar{\nu}_e \nu_\mu \mu^+$, $\nu_e e^+ \mu^- \bar{\nu}_\mu$, $\mu^- \bar{\nu}_\mu \nu_\mu \mu^+$, and $e^- \bar{\nu}_e \nu_e e^+$, the estimated experimental precision is around a few per cent at CM energies below 700 GeV. On the other hand, the deviation from the Born result given by the $\mathcal{O}(\alpha)$ contributions ranges between -14 and -24% in the same energy domain. At larger invariant masses, the overall cross section decreases but radiative corrections are still of order 2–3 standard deviations. Thus, a reliable analysis of these final states requires the inclusion of EW corrections. Note also that, in contrast to previous processes, $\mathcal{O}(\alpha)$ corrections can be relevant even in the low-luminosity run ($L = 30\,\text{fb}^{-1}$). They are about twice the standard deviation for $M_{\rm inv}^{\rm cut}(l\bar{l}') \leq 700\,\text{GeV}$, and become comparable with the experimental accuracy above that threshold.

PP $\to l\bar{\nu}_l\bar{l}'\nu_{l'}$						
$M_{\rm inv}^{\rm cut}(l\bar{l}')$ [GeV]	$\sigma_{\rm Born}$ [fb]	$\sigma_{\rm AEWS}$ [fb]	$\sigma_{\rm virt}^{\rm finite}$ [fb]	$\sigma_{\rm EW}$ [fb]	Δ [%]	$1/\sqrt{2L\sigma_{\rm Born}}$ [%]
500	7.235	6.561	6.682	6.235	-13.8	2.6
600	3.723	3.280	3.350	3.131	-15.9	3.7
700	2.059	1.765	1.808	1.688	-18.1	4.9
800	1.201	1.003	1.031	0.959	-20.2	6.5
900	0.731	0.596	0.613	0.570	-22.0	8.3
1000	0.460	0.366	0.378	0.352	-23.4	10.4

Table 6.6: Cross section for PP $\to \mathrm{e}^-\bar{\nu}_\mathrm{e}\nu_\mu\mu^+, \nu_\mathrm{e}\mathrm{e}^+\mu^-\bar{\nu}_\mu, \mu^-\bar{\nu}_\mu\nu_\mu\mu^+, \mathrm{e}^-\bar{\nu}_\mathrm{e}\nu_\mathrm{e}\mathrm{e}^+$ for various values of $M_{\rm inv}^{\rm cut}(l\bar{l}')$

Chapter 7

Conclusion

At the LHC, gauge-boson production processes will be used to measure the triple gauge-boson couplings. The relevant processes to investigate are WZ, ZZ, and WW production, and the physically interesting region is the one of high di-boson invariant mass.

We have examined these processes by means of a complete four-fermion calculation, i.e. by taking into account the decays of the gauge bosons, in the purely leptonic channels. The primary aim of our analysis was to investigate the influence of electroweak radiative corrections on the di-boson production processes at the LHC. The one-loop leading-logarithmic corrections to the full four-fermion processes have been calculated in double-pole approximation. This includes corrections to the gauge-boson pair-production processes, corrections to the gauge-boson decays, as well as the non-factorizable corrections. In this study, we have included the full QED radiative corrections in the logarithmic approximation, which involve also the emission of real photons and therefore depend on the detector resolution. We have verified that the double-pole approximation and the high-energy approximation are applicable for the considered phase-space regions of large transverse momentum or large invariant mass of the gauge-boson pair. Thus, our approach is reliable in this region.

The corrections have been implemented in a Monte Carlo program, so that arbitrary cuts and distributions can be studied. The program has been tested using various methods to check it's consistency and comparisons with other independent programs have been accomplished. Further all corrections have been included in a generic way, so that the implemented formulae do not depend on the particular process which is calculated. The program also allows to investigate the numerical effects of anomalous triple and quartic gauge-boson couplings directly for tree-level amplitudes. Together with the generic structure we used for the calculation of the matrix elements this

enables us to investigate every possible $2f \to 4f$ process with less than six quarks involved.

In order to illustrate the behaviour and the size of $\mathcal{O}(\alpha)$ contributions, we have presented different cross sections and distributions. For WZ-, ZZ-, and WW-production processes, electroweak corrections turn out to be sizeable in the high-energy region of the hard process, in particular for large transverse momentum and small rapidity separation of the reconstructed vector bosons, which is the kinematical range of maximal sensitivity to new-physics phenomena. EW radiative corrections lower the Born results for WZ, ZZ, and WW production by 7–20%, 15–25%, and 14–24%, in the region of experimental sensitivity. Their size depends sensibly not only on the CM energy but also on the applied cuts and varies according to the selected observables and kinematical regions. Despite of the strong decrease of the cross section with increasing di-boson invariant mass, radiative effects are appreciable if compared with the expected experimental precision. This depends of course on the available luminosity. For WZ and ZZ production, these effects are only relevant for a high-luminosity run of the LHC. Owing to their larger overall cross section, WW-production processes can instead show a sensitivity to radiative effects even at a low-luminosity run.

Appendix A

Feynman Rules

A.1 Coupling constants

The couplings of gauge bosons to scalars are given by

$$\begin{aligned} A\chi H &: C_{A\chi H} = 0 \\ \mathrm{Z}\chi H &: C_{\mathrm{Z}\chi H} = \frac{-\mathrm{i}}{2c_\mathrm{w}s_\mathrm{w}} \\ A\phi^+\phi^- &: C_{A\phi^+\phi^-} = -1 \\ \mathrm{Z}\phi^+\phi^- &: C_{\mathrm{Z}\phi^+\phi^-} = -\frac{s_\mathrm{w}^2 - c_\mathrm{w}^2}{2c_\mathrm{w}s_\mathrm{w}} \\ \mathrm{W}^\pm\phi^\mp H &: C_{\mathrm{W}^\pm\phi^\mp H} = \mp\frac{1}{2s_\mathrm{w}} \\ \mathrm{W}^\pm\phi^\mp\chi &: C_{\mathrm{W}^\pm\phi^\mp\chi} = -\frac{\mathrm{i}}{2s_\mathrm{w}}. \end{aligned} \tag{A.1}$$

The couplings of gauge bosons to the Higgs boson are

$$\begin{aligned} H\mathrm{ZZ} &: C_{H\mathrm{ZZ}} = \frac{M_\mathrm{W}}{s_\mathrm{w}c_\mathrm{w}^2} \\ H\mathrm{W}^+\mathrm{W}^- &: C_{H\mathrm{W}^+\mathrm{W}^-} = \frac{M_\mathrm{W}}{s_\mathrm{w}} \end{aligned} \tag{A.2}$$

The renormalization of this coupling constants lead to the counterterm couplings

$$\begin{aligned}
\delta C_{\mathrm{Z}\chi H} &= \left(\frac{\delta e}{e} - \frac{s_\mathrm{w}^2 - c_\mathrm{w}^2}{c_\mathrm{w} s_\mathrm{w}^2}\delta c_\mathrm{w}\right) C_{\mathrm{Z}\chi H} \\
\delta C_{\mathrm{Z}\phi^+\phi^-} &= \left(\frac{\delta e}{e} - \frac{1}{c_\mathrm{w} s_\mathrm{w}^2 (s_\mathrm{w}^2 - c_\mathrm{w}^2)}\delta c_\mathrm{w}\right) C_{\mathrm{Z}\phi^+\phi^-} \\
\delta C_{\mathrm{W}^\pm\phi^\mp} &= \left(\frac{\delta e}{e} + \frac{c_\mathrm{w}}{s_\mathrm{w}^2}\delta c_\mathrm{w}\right) C_{\mathrm{W}^\pm\phi^\mp}
\end{aligned} \tag{A.3}$$

The totally antisymmetric triple gauge-boson coupling are given by

$$\begin{aligned}
A\mathrm{W}^+\mathrm{W}^- &: C_{A\mathrm{W}^+\mathrm{W}^-} = 1 \\
\mathrm{Z}\mathrm{W}^+\mathrm{W}^- &: C_{\mathrm{Z}\mathrm{W}^+\mathrm{W}^-} = -\frac{c_\mathrm{w}}{s_\mathrm{w}}
\end{aligned} \tag{A.4}$$

and counterterm couplings for the triple gauge-boson vertex are

$$\begin{aligned}
\delta C_{A\mathrm{W}^+\mathrm{W}^-} &= \frac{\delta e}{e} C_{A\mathrm{W}^+\mathrm{W}^-} \\
\delta C_{\mathrm{Z}\mathrm{W}^+\mathrm{W}^-} &= \left(\frac{\delta e}{e} + \frac{1}{c_\mathrm{w} s_\mathrm{w}^2}\delta c_\mathrm{w}\right) C_{\mathrm{Z}\mathrm{W}^+\mathrm{W}^-}.
\end{aligned} \tag{A.5}$$

The couplings of gauge bosons to fermions are given by

$$\begin{aligned}
A\bar{f}f &: C_{A\bar{f}_\sigma f_\sigma} = -Q_{f_\sigma} \\
\mathrm{Z}\bar{f}f &: C_{\mathrm{Z}\bar{f}_\sigma f_\sigma} = \begin{cases} \frac{I^3_{f_\sigma} - 2 s_\mathrm{w} Q_{f_\sigma}}{s_\mathrm{w} c_\mathrm{w}} & \text{if} \quad \sigma = - \\ -\frac{s_\mathrm{w}}{c_\mathrm{w}} Q_{f_\sigma} & \text{if} \quad \sigma = + \end{cases} \\
\mathrm{W}^+\bar{f}'f &: C_{\mathrm{W}^+\bar{f}'_\sigma f_\sigma} = \begin{cases} \frac{1}{\sqrt{2} s_\mathrm{w}} V_{f'f} & \text{if} \quad \sigma = - \\ 0 & \text{if} \quad \sigma = + \end{cases} \\
\mathrm{W}^-\bar{f}'f &: C_{\mathrm{W}^-\bar{f}'_\sigma f_\sigma} = \begin{cases} \frac{1}{\sqrt{2} s_\mathrm{w}} V^\dagger_{f'f} & \text{if} \quad \sigma = - \\ 0 & \text{if} \quad \sigma = + \end{cases}
\end{aligned} \tag{A.6}$$

where $I^3_{f_\sigma} \in \{\frac{1}{2}, -\frac{1}{2}\}$ is the third component of the isospin of the fermion f_σ. Note that the CKM matrix $V_{f'f}$ is diagonal in the generations for leptons. The corresponding counterterm couplings are

$$\begin{aligned}
\delta C_{A\bar{f}_\sigma f_\sigma} &= \frac{\delta e}{e} C_{A\bar{f}_\sigma f_\sigma} \\
\delta C_{\mathrm{Z}\bar{f}_\sigma f_\sigma} &= \begin{cases} \frac{\delta e}{e} C_{\bar{f}_\sigma f_\sigma \mathrm{Z}} + \frac{e}{s_\mathrm{w} c_\mathrm{w}^2}\left(Q_{f_\sigma} + (2 I^3_{f_\sigma}) \frac{c_\mathrm{w}^2 - s_\mathrm{w}^2}{2 s_\mathrm{w}^2}\right)\delta c_\mathrm{w} & \text{if} \quad \sigma = - \\ \frac{\delta e}{e} C_{\bar{f}_\sigma f_\sigma \mathrm{Z}} + \frac{e}{s_\mathrm{w} c_\mathrm{w}^2} Q_{f_\sigma}\delta c_\mathrm{w} & \text{if} \quad \sigma = + \end{cases} \\
\delta C_{\mathrm{W}^\pm\bar{f}'_\sigma f_\sigma} &= \left(\frac{\delta e}{e} + \frac{c_\mathrm{w}}{s_\mathrm{w}^2}\delta c_\mathrm{w}\right) C_{\mathrm{W}^\pm\bar{f}'_\sigma f_\sigma}
\end{aligned} \tag{A.7}$$

A.2 Constants in LSC corrections

In the leading soft-collinear contributions the constants $C^{\rm ew}_{\varphi'\varphi}$ and $(I^{\rm Z})^2_\varphi$ must be defined for fermions, would-be Goldstone-bosons, and gauge bosons separately. For fermions f^σ one has to constants according to the helicity σ of the fermion

$$C^{\rm ew}_{f'^\sigma f^\sigma} = (I^A)^2_f + (I^{\rm Z})^2_f + (I^{\rm W})^2_f \tag{A.8}$$

with

$$(I^A)^2_f = e^2 C^2_{A\bar{f}f}, \quad (I^{\rm Z})^2_f = e^2 C^2_{{\rm Z}\bar{f}f}, \quad (I^{\rm W})^2_f = e^2 C^2_{{\rm W}\bar{f}f}. \tag{A.9}$$

For gauge bosons we have to use

$$C^{\rm ew}_{\rm AA} = 2, \quad C^{\rm ew}_{\rm ZZ} = 2\frac{c_{\rm w}^2}{s_{\rm w}^2}, \quad C^{\rm ew}_{\rm WW} = \frac{2}{s_{\rm w}^2}, \quad C^{\rm ew}_{\rm AZ} = C^{\rm ew}_{\rm ZA} = -2\frac{c_{\rm w}}{s_{\rm w}} \tag{A.10}$$

and

$$(I^{\rm Z})^2_{\rm A} = 0, \quad (I^{\rm Z})^2_{\rm Z} = 0, \quad (I^{\rm Z})^2_{\rm W} = \frac{c_{\rm w}^2}{s_{\rm w}^2}. \tag{A.11}$$

For would-be Goldstone-bosons these constants are

$$C^{\rm ew}_{\chi} = \frac{1+2c_{\rm w}^2}{4s_{\rm w}^2 c_{\rm w}^2}, \quad C^{\rm ew}_{\phi^\pm} = \frac{1+2c_{\rm w}^2}{4s_{\rm w}^2 c_{\rm w}^2}, \tag{A.12}$$

and

$$(I^{\rm Z})^2_{\chi} = \frac{1}{4s_{\rm w}^2 c_{\rm w}^2}, \quad (I^{\rm Z})^2_{\phi^\pm} = \frac{(c_{\rm w}^2 - s_{\rm w}^2)^2}{4s_{\rm w}^2 c_{\rm w}^2}. \tag{A.13}$$

Appendix B

Intermediate results for virtual corrections

B.1 Formulae for gauge-boson decay

For the decay of a gauge boson we have to calculate the radiative corrections to the $\mathrm{Z}f\bar{f}$ and the $\mathrm{W}^{\pm}f\bar{f}'$ vertex. For the exchange of a photon between two of the three external lines of such a vertex we find the three contributions

$$\delta M_1 = \frac{\alpha}{4\pi} Q_1 Q_2 \Big(-4p_1p_2(C_0+C_1+C_2)+(2-D)^2 C_{00}+(4-2D)p_1p_2C_{12} \Big), \tag{B.1}$$

where the argument of the C functions is given by

$$C_{\dots} = C_{\dots}(-p_1, p_2, \lambda, m_1, m_2), \tag{B.2}$$

and D denotes the dimension of the space time which is used in dimensional regularization,

$$\delta M_2 \;=\; \frac{\alpha}{4\pi} Q_1 Q_V \Big(4p_1p_2(C_1 \,+\, C_2 \,+\, C_{12}) \,+\, (4 \,-\, 4D)C_{00} \Big), \tag{B.3}$$

where the argument of the C functions is

$$C_{\dots} = C_{\dots}(-p_1, p_2, m_1, \lambda, M_{\mathrm{W}}), \tag{B.4}$$

$$\delta M_3 \;=\; \frac{\alpha}{4\pi} Q_2 Q_V \Big(\,-\, 4p_1p_2(C_1 \,+\, C_2 \,+\, C_{12}) \,-\, (4 \,-\, 4D)C_{00} \Big) \tag{B.5}$$

with the argument of the C function

$$C_{...} = C_{...}(p_1, -p_2, m_2, M_{\mathrm{W}}, \lambda). \tag{B.6}$$

In the limit of massless fermions we find

$$\begin{aligned}
\delta M_1 + \delta M_2 + \delta M_3 &= \frac{\alpha}{4\pi}\Bigg[(Q_1^2 + Q_2^2) + 2Q_1^2 B_0(0,0,m_1) + 2Q_2^2 B_0(0,0,m_2) \\
&\quad + Q_V^2 B_0(0,0,M_V) - 3Q_1 Q_2 B_0(M_V^2, m_1, m_2) \\
&\quad - 2M_V^2 \Big(Q_1 Q_2 C_0(-p_1, p_2, \lambda, m_1, m_2) \\
&\quad - Q_1 Q_V C_0(-p_1, p_2, m_1, \lambda, M_V) \\
&\quad + Q_2 Q_V C_0(p_1, -p_2, m_2, M_V, \lambda)\Big)\Bigg]
\end{aligned} \tag{B.7}$$

with the C_0 functions for massless fermions given by

$$\begin{aligned}
C_0(-p_1, p_2, \lambda, m_1, m_2) &= \frac{1}{M_V^2}\Bigg[-\frac{2}{3}\pi^2 + 2\log^2\frac{M_V}{\lambda} \\
&\quad - \log^2\frac{m_1}{\lambda} - \log^2\frac{m_2}{\lambda} - 2\pi\mathrm{i}\log\frac{M_V}{\lambda}\Bigg],
\end{aligned} \tag{B.8}$$

$$C_0(-p_1, p_2, m_1, \lambda, M_V) = \frac{1}{M_V^2}\left[\log^2\frac{m_1}{\lambda} - \log^2\frac{M_V}{\lambda}\right], \tag{B.9}$$

$$C_0(p_1, -p_2, m_2, M_V, \lambda) = \frac{1}{M_V^2}\left[\log^2\frac{m_2}{\lambda} - \log^2\frac{M_V}{\lambda}\right]. \tag{B.10}$$

The corresponding counterterms are given by the photonic part of the field renormalization constants

$$\begin{aligned}
\delta C_{\mathrm{W}f\bar{f}'} &= \frac{1}{2}\delta Z_{\mathrm{W}} + \frac{1}{2}\delta Z_f + \frac{1}{2}\delta Z_{f'}, \\
\delta C_{Zf\bar{f}} &= \frac{1}{2}\delta Z_{\mathrm{Z}} + \frac{1}{2}\delta Z_f + \frac{1}{2}\delta Z_{\bar{f}}.
\end{aligned} \tag{B.11}$$

B.2 Formulae for non-factorizable corrections

The explicit terms contributing to the non-factorizable corrections are given in this section. As a general convention the momenta are put onshell every-

where exept in the terms $(k_1^2 - \overline{M}_1^2)$ and $(k_2^2 - \overline{M}_2^2)$.

$$\begin{aligned}
\Delta^{\rm virt}_{\rm mf'} &= \sum_{i=3,4} \big[(-Q_{V_2})Q_i\theta_d(i)(s_{i5}+s_{i6})(k_1^2-\overline{M}_1^2) \\
&\quad \times D_0(-k_2,k_1,p_i,0,\overline{M}_2,\overline{M}_1,m_i)\big] \\
&\quad + \sum_{j=5,6} \big[(-Q_{V_1})Q_j\theta_d(j)(s_{3j}+s_{4j})(k_2^2-\overline{M}_2^2) \\
&\quad \times D_0(-p_j,-k_2,k_1,0,m_j,\overline{M}_2,\overline{M}_1)\big],
\end{aligned} \tag{B.12}$$

$$\begin{aligned}
\Delta^{\rm virt}_{\rm ff'} &= \sum_{i=3,4}\sum_{j=5,6} s_{ij}Q_i\theta_d(i)Q_j\theta_d(j)(k_1^2-\overline{M}_1^2)(k_2^2-\overline{M}_2^2) \\
&\quad \times E_0(-p_j,-k_2,k_1,p_i,\lambda,m_j,\overline{M}_2,\overline{M}_1,m_i),
\end{aligned} \tag{B.13}$$

$$\begin{aligned}
\Delta^{\rm virt}_{\rm if} &= -\sum_{l=1,2}\Bigg[\sum_{i=3,4} Q_lQ_i\theta_d(l)\theta_d(i)t_{li}(k_1^2-\overline{M}_1^2)D_0(p_l,k_1,p_i,\lambda,m_l,\overline{M}_1,m_i) \\
&\quad + \sum_{j=5,6} Q_lQ_j\theta_d(l)\theta_d(j)t_{lj}(k_2^2-\overline{M}_2^2)D_0(p_l,k_2,p_j,\lambda,m_l,\overline{M}_2,m_j)\Bigg],
\end{aligned} \tag{B.14}$$

$$\begin{aligned}
\Delta^{\rm virt}_{\rm mm'} &= s_{12}Q_{V_1}Q_{V_2}\Big[C_0(k_1,-k_2,0,\overline{M}_1,\overline{M}_2) \\
&\quad - [C_0(k_1,-k_2,\lambda,M_1,M_2)]_{k_1^2=M_1^2,k_2^2=M_2^2}\Big],
\end{aligned} \tag{B.15}$$

$$\begin{aligned}
\Delta^{\rm virt}_{\rm im} &= -\sum_{l=1,2}\sum_{n=1,2} \bar{t}_{ln}Q_l\theta_d(l)Q_{V_n} \\
&\quad \times\Big[C_0(p_l,k_n,0,m_l,\overline{M}_n) - [C_0(p_l,k_n,\lambda,m_l,M_n)]_{k_n^2=M_n^2}\Big],
\end{aligned} \tag{B.16}$$

$$\begin{aligned}
\Delta^{\rm virt}_{\rm mf} &= \Bigg[- M_1^2\sum_{i=3,4} Q_{V_1}Q_i\theta_d(i) \\
&\quad \times\Big[C_0(k_1,p_i,0,\overline{M}_1,m_i) - [C_0(k_1,p_i,\lambda,M_1,m_i)]_{k_1^2=M_1^2}\Big] \\
&\quad -M_2^2\sum_{j=5,6} Q_{V_2}Q_j\theta_d(j) \\
&\quad \times\Big[C_0(k_2,p_j,0,\overline{M}_2,m_j) - [C_0(k_2,p_j,\lambda,M_2,m_j)]_{k_2^2=M_2^2}\Big]\Bigg],
\end{aligned} \tag{B.17}$$

$$\Delta^{\rm virt}_{\rm mm} = 2\sum_{n=1,2} Q_{V_n}^2M_n^2\left[\frac{B_0(k_n^2,0,\overline{M}_n) - B_0(\overline{M}_n^2,0,\overline{M}_n)}{k_n^2-\overline{M}_n^2} - B_0'(M_n^2,\lambda,M_n)\right], \tag{B.18}$$

with the invariants defined as $\bar{t}_{ij} = (p_i - k_j)^2$, $t_{ij} = (p_i - p_j)^2$ and $s_{ij} = (p_i + p_j)^2$. In the high-energy limit this simplifies to

$$\begin{aligned}
\Delta^{\rm virt}_{\rm mf'} &= -\sum_{i=3,4} Q_{V_2} Q_i \theta_d(i) \Bigg[-\mathrm{Li}_2\left(1 - \frac{s}{s_i'}\right) + \frac{1}{2}\log^2\frac{\overline{M}_1^2 - k_1^2}{\overline{M}_2^2 - k_2^2} \\
&\quad -\frac{1}{2}\log^2\frac{-s}{M_1 M_2} + \log^2\frac{-s_i'}{M_1 M_2} - 2\log\frac{m_i}{M_1}\log\frac{-s_i'}{M_1 M_2} \\
&\quad + \log\frac{\overline{M}_1^2 - k_1^2}{\overline{M}_2^2 - k_2^2}\left(\log\frac{-s_i'}{M_1 M_2} + \log\frac{s_i'}{s} - 2\log\frac{m_i}{M_1}\right)\Bigg] \\
&\quad -\sum_{j=5,6} Q_{V_1} Q_j \theta_d(j) \Bigg[-\mathrm{Li}_2\left(1 - \frac{s}{s_j'}\right) + \frac{1}{2}\log^2\frac{\overline{M}_2^2 - k_2^2}{\overline{M}_1^2 - k_1^2} \\
&\quad -\frac{1}{2}\log^2\frac{-s}{M_1 M_2} + \log^2\frac{-s_j'}{M_1 M_2} - 2\log\frac{m_j}{M_2}\log\frac{-s_j'}{M_1 M_2} \\
&\quad + \log\frac{\overline{M}_2^2 - k_2^2}{\overline{M}_1^2 - k_1^2}\left(\log\frac{-s_j'}{M_1 M_2} + \log\frac{s_j'}{s} - 2\log\frac{m_j}{M_2}\right)\Bigg], \qquad \text{(B.19)} \\
\Delta^{\rm virt}_{\rm ff'} &= \frac{1}{2}\sum_{i=3,4}\sum_{j=5,6} Q_i \theta_d(i) Q_j \theta_d(j) \\
&\quad \times \Big[-D_0^{\rm s,he}(0) - D_0^{\rm s,he}(1) - D_0^{\rm s,he}(4) + D_0^{\rm s,he}(2) + D_0^{\rm s,he}(3) \Big], \qquad \text{(B.20)} \\
\Delta^{\rm virt}_{\rm if} &= -\sum_{l=1,2}\Bigg[\sum_{i=3,4} Q_l \theta_d(l) Q_i \theta_d(i) \Big[2\log\frac{m_l m_i}{-t_{li}}\log\frac{\lambda M_1}{\overline{M}_1^2 - k_1^2} \\
&\quad -\log^2\frac{m_l M_1}{-\bar{t}_{l1}} - \log^2\frac{m_i}{M_1} - \mathrm{Li}_2(1 - \frac{\bar{t}_{l1}}{t_{li}})\Big] \\
&\quad + \sum_{j=5,6} Q_l \theta_d(l) Q_j \theta_d(j) \Big[2\log\frac{m_l m_j}{-t_{lj}}\log\frac{\lambda M_2}{\overline{M}_2^2 - k_2^2} \\
&\quad -\log^2\frac{m_l M_2}{-\bar{t}_{l2}} - \log^2\frac{m_j}{M_2} - \mathrm{Li}_2(1 - \frac{\bar{t}_{l2}}{t_{lj}})\Big]\Bigg], \qquad \text{(B.21)} \\
\Delta^{\rm virt}_{\rm mm'} &= Q_{V_1} Q_{V_2}\Big[-\frac{1}{2}\log^2\frac{\overline{M}_1^2 - k_1^2}{\overline{M}_2^2 - k_2^2} + \frac{1}{2}\log^2\frac{s}{M_1 M_2} \\
&\quad + \log\frac{M_1^2}{s}\log\frac{\overline{M}_1^2 - k_1^2}{\lambda M_1} + \log\frac{M_2^2}{s}\log\frac{\overline{M}_2^2 - k_2^2}{\lambda M_2} + \frac{1}{4}\log^2\frac{s}{M_1^2} + \frac{1}{4}\log^2\frac{s}{M_2^2}\Big], \qquad \text{(B.22)} \\
\Delta^{\rm virt}_{\rm im} &= -\sum_{l=1,2}\sum_{n=1,2} Q_l \theta_d(l) Q_{V_n} \\
&\quad \log\frac{m_l M_n}{-\bar{t}_{ln}}\left[\log\frac{\overline{M}_n^2 - k_n^2}{-\bar{t}_{ln}} + \log\frac{\overline{M}_n^2 - k_n^2}{\lambda^2} + \log\frac{m_l}{M_n}\right], \qquad \text{(B.23)}
\end{aligned}$$

$$\Delta_{\rm mf}^{\rm virt} = \sum_{i=3,4} Q_{V_1} Q_i \theta_d(i) \log\frac{m_i}{M_1}\Big[\log\frac{m_i}{M_1} + 2\log\frac{\overline{M}_1^2 - k_1^2}{\lambda M_1}\Big] + \sum_{j=5,6} Q_{V_2} Q_j \theta_d(j) \log\frac{m_j}{M_2}\Big[\log\frac{m_j}{M_2} + 2\log\frac{\overline{M}_2^2 - k_2^2}{\lambda M_2}\Big], \tag{B.24}$$

$$\Delta_{\rm mm}^{\rm virt} = 2\sum_{n=1,2} Q_{V_n}^2 \log\frac{\lambda M_n}{k_n^2 - \overline{M}_n^2} \tag{B.25}$$

with the additional invariants $s = (p_1+p_2)^2 = (k_1+k_2)^2$, $s_i' = (p_i+k_2)^2$, and $s_j' = (p_j+k_1)^2$. In the $D_0^{\rm s,he}$ integrals the propagator factor has been cancelled which yields the expressions

$$\begin{aligned} D_0^{\rm s,he}(0) = {} & \mathcal{L}i_2\left(-\frac{M_1M_2}{\hat{s}_{2i}} + {\rm i}\varepsilon, -x_1\right) + \mathcal{L}i_2\left(-\frac{M_1M_2}{\hat{s}_{1j}} + {\rm i}\varepsilon, -\frac{1}{x_2}\right) \\ & - \mathcal{L}i_2\left(-\frac{M_1M_2}{\bar{s}} + {\rm i}\varepsilon, -x_1\right) - \mathcal{L}i_2\left(-\frac{M_1M_2}{\bar{s}} + {\rm i}\varepsilon, -\frac{1}{x_2}\right) \\ & - \left[\log\frac{\hat{s}_{2i} + {\rm i}\varepsilon}{s_{ij} + {\rm i}\varepsilon} + \log\frac{\hat{s}_{1j} + {\rm i}\varepsilon}{\bar{s} + {\rm i}\varepsilon}\right]\left[\log(-x_1) - \log(-x_2)\right], \end{aligned} \tag{B.26}$$

$$\begin{aligned} D_0^{\rm s,he}(1) = {} & \log^2\frac{s_i'}{M_{V_1}^2} - \frac{1}{2}\log^2\frac{s_i'}{M_{V_1}^2} - \log\frac{s_i'}{M_{V_1}^2}\log\frac{m_i^2}{M_{V_1}^2} + \frac{1}{2}\log^2\frac{k_1^2 - \overline{M}_1^2}{k_2^2 - \overline{M}_2^2} \\ & + \log\frac{k_1^2 - \overline{M}_1^2}{k_2^2 - \overline{M}_2^2}\left(\log\frac{s_i'}{m_i^2} - {\rm i}\pi^2\right) + \log\frac{k_1^2 - \overline{M}_1^2}{k_2^2 - \overline{M}_2^2}\log\frac{s_i'}{s} - \frac{1}{2}\pi^2, \end{aligned} \tag{B.27}$$

$$\begin{aligned} D_0^{\rm s,he}(4) = {} & \log^2\frac{s_j'}{M_{V_2}^2} - \frac{1}{2}\log^2\frac{s_j'}{M_{V_2}^2} - \log\frac{s_j'}{M_{V_2}^2}\log\frac{m_j^2}{M_{V_2}^2} + \frac{1}{2}\log^2\frac{k_2^2 - \overline{M}_2^2}{k_1^2 - \overline{M}_1^2} \\ & + \log\frac{k_2^2 - \overline{M}_2^2}{k_1^2 - \overline{M}_1^2}\left(\log\frac{s_j'}{m_j^2} - {\rm i}\pi^2\right) + \log\frac{k_2^2 - \overline{M}_2^2}{k_1^2 - \overline{M}_1^2}\log\frac{s_j'}{s} - \frac{1}{2}\pi^2, \end{aligned} \tag{B.28}$$

$$\begin{aligned} D_0^{\rm s,he}(2) = {} & 2\left(\log\frac{s_{ij}}{m_i m_j} - {\rm i}\pi\right)\log\frac{k_1^2 - \overline{M}_1^2}{M_{V_1}\lambda} - \frac{1}{4}\log^2\frac{m_i^2}{M_{V_1}^2} \\ & - \log^2\frac{s_j^2}{m_j M_{V_1}} + \pi^2, \end{aligned} \tag{B.29}$$

and

$$D_0^{\mathrm{s,he}}(3) \;=\; 2\left(\log\frac{s_{ij}}{m_i m_j} - \mathrm{i}\pi\right)\log\frac{k_2^2-\overline{M}_2^2}{M_{V_2}\lambda} - \frac{1}{4}\log^2\frac{m_j^2}{M_{V_2}^2} - \log^2\frac{s_i^2}{m_i M_{V_2}} + \pi^2. \tag{B.30}$$

Bibliography

[1] S. Haywood *et al.*, S. Haywood, P. R. Hobson, W. Hollik, Z. Kunszt *et al.*, arXiv:hep-ph/0003275, in *Standard Model Physics (and more) at the LHC*, eds. G. Altarelli and M. L. Mangano, (CERN-2000-004, Genève, 2000) p. 117 [arXiv:hep-ph/0003275].

[2] W. Beenakker *et al.*, Nucl. Phys. B **410** (1993) 245.

[3] P. Ciafaloni and D. Comelli, Phys. Lett. B **446** (1999) 278 [arXiv:hep-ph/9809321]; J. H. Kühn, S. Moch, A. A. Penin and V. A. Smirnov, arXiv:hep-ph/0106298; V. S. Fadin, L. N. Lipatov, A. D. Martin and M. Melles, Phys. Rev. D **61** (2000) 094002 [arXiv:hep-ph/9910338]; M. Melles, arXiv:hep-ph/0104232; W. Beenakker and A. Werthenbach, Phys. Lett. B **489** (2000) 148 [arXiv:hep-ph/0005316]; M. Beccaria *et al.*, Phys. Rev. D **61** (2000) 073005 [arXiv:hep-ph/9906319]; J. Layssac and F. M. Renard, Phys. Rev. D **64** (2001) 053018 [arXiv:hep-ph/0104205].

[4] A. Denner and S. Pozzorini, Eur. Phys. J. C **18** (2001) 461 [arXiv:hep-ph/0010201].

[5] A. Denner and S. Pozzorini, Eur. Phys. J. C **21** (2001) 63 [arXiv:hep-ph/0104127].

[6] S. Pozzorini, *Dissertation, University of Zurich*, 2001, [arXiv:hep-ph/0201077].

[7] K. L. Adamson, D. de Florian and A. Signer, Phys. Rev. D **65** (2002) 094041 [arXiv:hep-ph/0202132].

[8] L. J. Dixon, Z. Kunszt and A. Signer, Phys. Rev. D **60** (1999) 114037 [arXiv:hep-ph/9907305].

[9] D. De Florian and A. Signer, Eur. Phys. J. C **16** (2000) 105 [arXiv:hep-ph/0002138].

[10] J. M. Campbell and R. K. Ellis, Phys. Rev. D **60** (1999) 113006 [arXiv:hep-ph/9905386].

[11] J. Ohnemus, Phys. Rev. D **44** (1991) 3477.

[12] S. Frixione, P. Nason and G. Ridolfi, Nucl. Phys. B **383** (1992) 3.

[13] U. Baur, T. Han and J. Ohnemus, Phys. Rev. D **51** (1995) 3381 [arXiv:hep-ph/9410266].

[14] U. Baur, S. Keller and D. Wackeroth, Phys. Rev. D **59** (1999) 013002 [arXiv:hep-ph/9807417]; U. Baur and D. Wackeroth, arXiv:hep-ph/0011080; U. Baur, O. Brein, W. Hollik, C. Schappacher and D. Wackeroth, KA-TP-26-2001, [arXiv:hep-ph/0108274]; S. Dittmaier and M. Krämer, DESY 01-121, [arXiv:hep-ph/0109062];
U. Baur and D. Wackeroth, [arXiv:hep-ph/0405191].

[15] E. Maina, S. Moretti and D. A. Ross, arXiv:hep-ph/0403050;
E. Maina, S. Moretti, M. R. Nolten and D. A. Ross, Phys. Lett. B **570** (2003) 205 [arXiv:hep-ph/0307021].

[16] E. Accomando, A. Denner and S. Pozzorini, Phys. Rev. D **65** (2002) 073003 [arXiv:hep-ph/0110114].

[17] F. Abe *et al.* (CDF Collaboration), Phys. Rev. Lett. **75** (1995) 1017; F. Abachi *et al.* (D0 Collaboration), Phys. Rev. Lett. **77** (1996) 3301; Phys. Rev. Lett. **79** (1997) 1441.

[18] F. Bloch and A. Nordsieck, Phys. Rev. **52** (1937) 54.

[19] A. Denner, S. Dittmaier, M. Roth and D. Wackeroth, Nucl. Phys. B **587** (2000) 67 [arXiv:hep-ph/0006307].

[20] W. Beenakker, *ICHEP '96 : Proceedings*, 1996, [arXiv:hep-ph/9612295].

[21] W. Beenakker *et al.*, Nucl. Phys. B **500** (1997) 255 [arXiv:hep-ph/9612260].

[22] M. Roth, *Dissertation, ETH Zürich, Diss. ETH No.13363*, 1999, [arXiv:hep-ph/0008033].

[23] P. J. Dervan, A. Signer, W. J. Stirling and A. Werthenbach, J. Phys. G **26** (2000) 607 [arXiv:hep-ph/0002175].

[24] A. Denner, S. Dittmaier, M. Roth and D. Wackeroth, Eur. Phys. J. C **20** (2001) 201 [arXiv:hep-ph/0104057].

[25] I. B. Marfin, V. A. Mossolov and T. V. Shishkina, arXiv:hep-ph/0304250.

[26] A. Denner, S. Dittmaier, M. Roth and D. Wackeroth, Nucl. Phys. B **560** (1999) 33 [arXiv:hep-ph/9904472].

[27] S. Dittmaier, Phys. Rev. D **59** (1999) 016007 [arXiv:hep-ph/9805445].

[28] A. Denner, Fortsch. Phys. **41** (1993) 307.

[29] V. V. Sudakov, Sov. Phys. JETP **3** (1956) 65 [Zh. Eksp. Teor. Fiz. **30** (1956) 87].

[30] S. Pozzorini, arXiv:hep-ph/0201077.

[31] W. Beenakker, A. P. Chapovsky and F. A. Berends, Nucl. Phys. B **508** (1997) 17 [arXiv:hep-ph/9707326].

[32] A. Denner, S. Dittmaier and M. Roth, Nucl. Phys. B **519** (1998) 39 [arXiv:hep-ph/9710521].

[33] M. Böhm, H. Spiesberger and W. Hollik, Fortsch. Phys. **34** (1986) 687.

[34] S. Dittmaier and M. Krämer, Phys. Rev. D **65** (2002) 073007 [arXiv:hep-ph/0109062].

[35] D. R. Yennie, S. C. Frautschi and H. Suura, Annals Phys. **13** (1961) 379.

[36] K. Hagiwara *et al.* [Particle Data Group Collaboration], Phys. Rev. D **66** (2002) 010001.

[37] H. L. Lai *et al.* [CTEQ Collaboration], Eur. Phys. J. C **12** (2000) 375 [arXiv:hep-ph/9903282].

[38] U. Baur, T. Han and J. Ohnemus, Phys. Rev. Lett. **72** (1994) 3941 [arXiv:hep-ph/9403248].

[39] G. J. Gounaris, J. Layssac, F. M. Renard, Phys. Rev. D **62** (2000) 073013; G. J. Gounaris, J. Layssac, F. M. Renard, Phys. Rev. D **61** (2000) 073013; D. Choudhury, S. Dutta, S. Rakshit, S. Rindani, Int. J. Mod. Phys. A **16** (2001) 4891.

[40] U. Baur, E. L. Berger, Phys. Rev. D **47** (1993) 4889; U. Baur, T. Han, J. Ohnemus, Phys. Rev. D **57** (1998) 2823.

Acknowledgments

In this part I would like to thank all the persons who helped and supported me during my work on this thesis.

- I am very grateful to Dr. Ansgar Denner who suggested the topic of my thesis and guided me during my work. Without his professional support this work would not have been possible.
- I am very grateful to Prof. Daniel Wyler for his support and providing a lot of coffee at the Institute for Theoretical Physics.
- I am thankful to Stefano Pozzorini for introducing me into the great art of determining the right signs of the corrections he calculated.
- I would like to thank Markus Roth who provided most parts of the phase space generator.
- I am thankful to Elena Accomando for her remarkable endurance during our long terms of comparisons between our FORTRAN programs.
- I would like to thank all my colleagues at the Paul Scherrer Institut and at the Institute for Theoretical Physics for their support. Especially I am thankful to Christoph Meier and Lars Wieders for all the useful and not so useful discussions we had.